Manpower in the Electronics Industry

JUST over three years ago the Economic Development Committee for the Electronics Industry decided to set up a Working Group on Scientific and Technological Manpower. The main objective of the Working Group, which was under the chairmanship of Professor G. D. Sims (Fellow), Deputy Vice-Chancellor and Head of the Department of Electronics, University of Southampton, and included among its members Mr. G. D. Clifford, Director of the I.E.R.E., was to study the education, training and retraining of qualified scientists and engineers. (The abbreviation 'QSE' appears even in the terms of reference and is freely used throughout the report.) The Preliminary Report just issued by the Working Group confines its attention mainly to the electronics industry *per se*, and does not include consideration of the employment of electronics QSE in government organizations or in other industries.

One of the more unexpected conclusions is that the present numbers of QSE are just keeping pace with the steady growth of 10% per annum in demand by the industry. Nevertheless a further increase in overall numbers is suggested. The report suggests an increase in the proportion of engineers to scientists, at present about 2 : 1, and believes that this can be achieved both by 'conversion' at post-graduate stage and by encouraging a greater input to engineering courses from the schools.

The Working Group commented on two areas in which there were shortages of graduates. The first is that of production engineers qualified to work in the electronics industry. Universities and Polytechnics are urged to develop combined production engineering/electronics courses as a matter of priority. The second shortage is that of applied mathematicians able to work in the development of software and even more urgently in advanced theory which calls for greater mathematical ability than most specialist engineers possess. University mathematics departments can help here by developing their work in these directions in collaboration with their electronic engineering colleagues.

By far the most striking observation in the report concerns a group other than QSE, namely technicians. The ratio of technicians to QSE in the electronics industry is falling while in manufacturing industry as a whole it is rising. Unfilled vacancies for technicians in electronics are increasing whereas vacancies are decreasing for industry overall. The forecasts of growth of numbers of technicians over a four-year period by all sectors of the electronics industry have been consistently underestimated. These statistics, culled from independent sources, lead to the conclusion that not nearly enough school leavers embark on a career in technician engineering: improved awareness of the opportunities and educational routes must be given to schools. Wider knowledge of educational facilities is necessary both in industry and among potential students. The initiative taken by the I.E.R.E. in producing a comprehensive guide to courses is commended and advocated as a pattern for a single, well-publicized source, in a form suitable for frequent up-dating.

The Working Group finds that the joint university–industry 'Bosworth-type' courses in applied technology are not receiving the general support of industry despite the fact that the industry has been closely associated with the initiation of these courses. However, the Working Group's suggestion that industrial sponsorship of students be dropped as a requirement is controversial; it might be more satisfactory to bring recruitment officers more closely into contact with their colleagues concerned with the courses.

The impression gained from reading the report is that communication between the many separate bodies at present studying different aspects of the manpower problem must be made far more effective. The proposal to improve industry/university relations by regular conferences of both parties on a wide basis and with full and frank discussion seems realistic. This Institution would certainly welcome an invitation to sponsor and organize such conferences.

EMRYS WILLIAMS

The Physics Exhibition, 1971

The 1971 Physics Exhibition will be held in The Great Hall of Alexandra Palace, Wood Green, London, N.22. It will be open at the following times and admission, *except for those holding tickets*, will cost 25p.

Monday, 19th April	10.30 a.m.–6 p.m.
Tuesday, 20th April	10 a.m.–6 p.m.
Wednesday, 21st April	10 a.m.–7.30 p.m.
Thursday, 22nd April	10 a.m.–5 p.m.

Requests for season tickets should be sent to The Exhibitions Officer of The Institute of Physics, 47 Belgrave Square, London, S.W.1, enclosing a stamped addressed envelope, to take the tickets, which measure $3\frac{1}{4}$ in by $4\frac{7}{8}$ in. (Written requests enclosing such an envelope are likely to be dealt with more expeditiously than telephone requests.)

Italy has accepted an invitation to stage a large national contribution at this year's Exhibition. Italian Universities, Government Laboratories and Industrial Organizations will be represented in a collection of instruments and apparatus organized by FAST, the Federation of Scientific and Technical Associations of Italy, in collaboration with several other bodies (the Italian Physical Society, Lombard Physical Society, National Research Council and the National Committee for Nuclear Research). In addition to the modern instruments and apparatus on display, the Italian stand will incorporate as a special feature a historical/cultural section, illustrating the life and scientific work of a number of important Italian figures in the history of physics.

The Council has made a number of important changes in the regulations this year, including the introduction of a special 'B' Category of Exhibits which are good quality standard production items, as distinct from the novelties and innovations which normally compose the bulk of the Exhibition. The number of invitations issued to overseas concerns has also been increased, so that there will be exhibitors from France, Hungary and Israel, in addition to the special Italian stand.

During the Exhibition several meetings and lectures will be held in the Alexandra Room as follows:

Monday, 19th April   3.30 p.m.
'The Impact of Electronics on the Medical Field'
   by Professor Vito Svelto (University of Pavia)

Tuesday, 20th April   3.30 p.m.
'Science Teaching at the Open University'
   by Professor M. J. Pentz (Dean and Director
   of Studies in Science, The Open University)

Wednesday, 21st April   2.30–7.00 p.m.
'The Teaching of Electronics'
   (Joint meeting of the Education and Electronics
   Groups of the Institute of Physics)
'Electronics Teaching in Schools'
   by G. Foxcroft (Rugby School)
'Electronics Teaching in Universities'
   by Professor G. D. Sims (University of Southampton)
'Industry's Requirements of Electronics Teaching'
   by Dr. E. Eastwood (Hirst Research Centre)

Thursday, 22nd April   3.00 p.m.
'Holography, Industry and the Rebirth of Optics'
   by J. W. C. Gates, F.Inst.P. (Division of Optical
   Metrology, the National Physical Laboratory)

There will also be showings during the Exhibition of new educational films on physics subjects.

New I.Prod.E. Travelling Scholarship

The Institution of Production Engineers has established a Travelling Scholarship worth £2000 annually. This award has been made possible by a very generous grant from the Clarkson Foundation, which was created by Mr. F. H. Clarkson, who is the Chairman of Clarkson International Tools Limited, Nuneaton.

The Clarkson Travelling Scholarship, to be offered for the first time this year, is for the study of production engineering management in an industrial environment in other countries. It carries no age restrictions and is not confined to members of the Institution. It is hoped that its value will attract those of sufficient calibre not only to widen their own knowledge and to apply this to the needs of their firm, but who will eventually be able to contribute to the total field of production management knowledge.

The conditions of the Award and further information, including application forms, may be obtained from The Secretary, Institution of Production Engineers, 10 Chesterfield Street, London WIX 8DE. (Telephone 01-499 5254.)

Engineering '71 Exhibition and Technology for Profit Conference

A Conference on Technology for Profit has been arranged in conjunction with the Engineering '71 Exhibition and will be held in London from 21st to 29th April 1971. Industry in the 70s and 80s will undergo many changes and the theme recognizes the demands on future technology.

A day will be devoted to each of the following subjects:

'Materials for Tomorrow's Environment'
'Reinforcing the Future'
'Versatility of Powders'
'Fabrication Towards the 70s'
'Welding: Evaluation of Modern Techniques'
'Welding: New Horizons in Plant and Materials'
'New Engineering Techniques for Mechanical Handling
   Equipment and Systems'

Complimentary tickets for the Exhibition which is being held at Earls Court and Olympia are being circulated to all I.E.R.E. members. (For further information see 'Conferences, Courses and Exhibitions' on page (xv) in this issue.)

Corrections

The following corrections should be made to papers published in the February 1971 issue of *The Radio and Electronic Engineer*.

'Efficiency of the Two-Frequency M.T.I. System':

Page 78: In equation (13) the last term in the first line should read . . .

$$-4\{R_o^2(T)\cos\Delta\omega_e^D T$$

Page 79: In equation (20) the first term in the denominator should be

$$3R_z^2(0)$$

Page 80: Col. 1, line 12, should read 'speeds of 80 and 160 km/h (50 and 100 miles/h), respectively . . .'
   Figure 3 caption, the parentheses should read
   (R_e and R_z according to eqn. (22))

'Ultrasonic Imaging in Solids':

Page 93: Section 5, line 12 should read
   'Fig. 5 contains only the 5 MHz components . . .'

Speech Scrambling by the Re-ordering of Amplitude Samples

By

V. J. PHILLIPS,
Ph.D., B.Sc.(Eng.),†

M. H. LEE, M.Sc.‡

and

J. E. THOMAS, B.Sc.§

Many modern communication systems transmit amplitude samples of the original input signal, the sampling being carried out according to the well-known requirements of the Sampling Theorem. At the receiver the signal is reconstituted by low-pass filtering. This paper investigates the degree of privacy which can be introduced in a speech communication system by deliberate variation of the order of transmission of the samples. The distortion of the signal which results from the low-pass filtering of such 'scrambled' samples is investigated theoretically and practically, and intelligibility tests are used to assess the effectiveness of the system. Finally, some guidance is given as to the selection of the scramble sequence for maximum effectiveness.

Notation

N	size of block of samples used for interchange
q	position of individual sample within block; $(1, 2..q..N)$
n	the general integer
γ_q	displacement vector associated with qth sample in block
Γ	gamma number; equals sum of displacement vectors neglecting signs
Γ_{max}	maximum value of Γ for sequence of given size N
$u(t)$	train of rectangular pulses of unit height
k	duty cycle (on/off ratio) of sampling pulse train
f_c	sampling pulse frequency
$v(t)$	scrambled samples
$s(t)$	input signal
ω	angular frequency of input signal
A	amplitude of input signal

1. Introduction

Nowadays, pulse-modulation techniques are frequently used for the transmission of speech signals. The basis of all these techniques is the Sampling Theorem which states that if amplitude samples of a bandwidth-limited signal are taken at regular intervals of time, then these samples contain all the information necessary for the reconstruction of the signal provided that the sampling rate is greater than $2B$, where B is the bandwidth of the signal. Reconstruction of the signal may be accomplished by passing the samples through a low-pass filter of bandwidth B.

An interesting possibility now arises that these samples might be shuffled or reordered in time thereby creating a scrambling system which gives the users some degree of privacy. If these scrambled samples are low-pass filtered, one might expect the resulting signal to be of low intelligibility. It is clear that provided the samples can be replaced in their correct order according to a

known descrambling key, no information is lost by varying the order in which the samples are actually transmitted.

There will obviously be other factors to be taken into account in the practical realization of such a system. If the samples are to be transmitted by pulse-code techniques, scramble synchronization information will have to be added in some way. If, on the other hand, the scrambled signals are to be converted back into continuous signals for transmission in analogue form, such additional factors as the effects of phase (waveform) distortion and noise, and band-limitation by non-ideal filters will have to be considered. These transmission problems will not be treated in this paper; the purpose of the investigation reported here was solely to determine the effectiveness of the scramble itself. Unless the method of scrambling itself is shown to be effective, there is not much point in proceeding to consideration of a practical system.

Initially it will be considered that the scrambling of the samples will occur within a definite sequence pattern or block. Figure 1(a) shows a scramble of this sort occurring in a block length of five samples. Other types of scrambling are also possible, but these will be discussed later, and the analysis developed for the simple block-scramble can be extended to cover them. Block size, for which the symbol N will be used, may be formally defined as 'the number of samples within one complete re-ordering sequence'.

One method of achieving a re-ordering of this sort is to use a system of delay networks such as that shown in Figure 1(b). The selection of suitable delay times is discussed later, but it should be noted that samples may not be advanced in real time, and so an overall block delay is inherent in the process. A commutating switch directs the incoming samples into the appropriate delay networks in turn, and a synchronously rotating switch reassembles the delayed samples into the required order. For experimental purposes such an apparatus would be rather inflexible and would involve the construction of large numbers of delay networks. A serially-connected tapped delay-line would be somewhat better in this respect, the tapping points being varied to produce the various sequences. However, a digital computer can perform the necessary operations much more con-
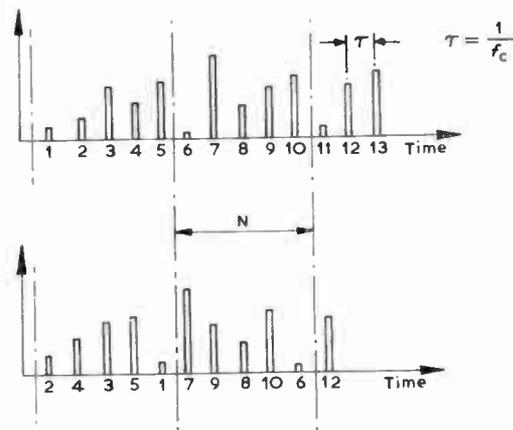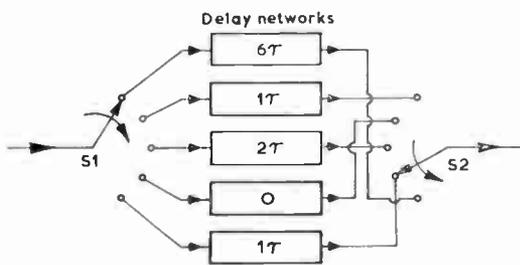

(a) Block 5 scrambling (2 4 3 5 1).

(b) Delay networks to achieve scramble shown in (a).

Fig. 1.

veniently. The sample values are converted to digital form and stored in the computer, being read out again in the required sequence under direct control of the program.

2. Theoretical Examination of Sample Re-ordering

If the samples occurring in the original unscrambled block are labelled $(1\ 2\ 3 \ldots N)$, then the scrambled sequence may be specified by repositioning the numbers within the bracket. If a block size of $N = 4$ is taken as an example then $(4\ 2\ 1\ 3)$ would designate one particular scramble out of the $N!$ different possibilities. The effectiveness of any given scrambling sequence (measured by the lack of intelligibility of the signal produced when the scrambled samples are passed through a low-pass filter) would, as a first estimate, seem to depend on various factors:

(a) The block size N.

(b) The number of samples re-ordered within the block. Sequences which involve a small amount of re-ordering would probably provide a poor effective scramble, whilst sequences which have a great number of changes in sample positions might be expected to produce greater destruction of intelligibility.

(c) The extent to which the samples are actually displaced within the block. In some sequences the samples would only be moved to adjacent or nearby positions; in others the samples would be moved considerable distances within the block.

A method of obtaining some measure of the various factors is desirable, and one obvious way is to subtract the original unscrambled sequence from the re-ordered sequence. For example, using the block-6 scrambled sequence $(5\ 3\ 6\ 4\ 2\ 1)$ would give

$$
\begin{array}{rrrrrr}
5 & 3 & 6 & 4 & 2 & 1 \\
1 & 2 & 3 & 4 & 5 & 6 \\
\hline
4 & 1 & 3 & 0 & -3 & -5
\end{array}
$$

The numbers which result are positive if the sample has been advanced from its previous position ($\leftarrow$) and negative if it has been delayed ($\rightarrow$). Since these numbers have signs associated with them they have been designated the 'gamma vectors'. Thus, for any scramble there will be a sequence of gamma vectors $(\gamma_1, \gamma_2 \ldots \gamma_N)$. It follows also that for scrambles of this type

$$
\sum_{q=1}^{N} \gamma_q = 0
$$

A measure of the extent of the shifting and re-ordering may be obtained by defining a 'gamma number'

$$
\Gamma = \sum_{q=1}^{N} |\gamma_q|
$$

where the signs are neglected. The unscrambled sequence may be referred to as the 'zero sequence' since its gamma number is 0.

The gamma vectors and gamma numbers are useful because they can be used not only as a measure of the degree of scrambling, but also because they show up certain phenomena which can occur. Consider for example the block-6 scrambled sequences $(3\ 1\ 2\ 6\ 4\ 5)$ and $(2\ 1\ 4\ 3\ 6\ 5)$. These sequences have gamma vectors of $(2\ -1\ -1\ 2\ -1\ -1)$ and $(1\ -1\ 1\ -1\ 1\ -1)$ showing that the block-6 scramble has degenerated into the lesser block-3 and block-2 scrambles. Assuming that the scramble effectiveness is proportional to block size N, then this degeneration is clearly to be avoided. Particularly with long block sizes, this is not easy to spot by inspection of the sequence itself.

Consider again the three block-4 sequences $(1\ 2\ 4\ 3)$, $(1\ 3\ 2\ 4)$ and $(2\ 1\ 3\ 4)$ which at first sight appear to be quite different. The gamma vectors for these sequences are $(0\ 0\ 1\ -1)$, $(0\ 1\ -1\ 0)$ and $(1\ -1\ 0\ 0)$. Long sequences of these blocks are obviously equivalent and would produce precisely the same scrambling effect. It is desirable to know whether two scrambles are equivalent, especially if the scramble sequences are being altered at intervals for secrecy, and the gamma vectors once again show up the effect much more clearly than the sample numbers, especially in large blocks. Another case where the gamma number Γ should be used with care is illustrated by the sequences $(6\ 1\ 2\ 3\ 4\ 5)$ and $(6\ 5\ 1\ 2\ 3\ 4)$ which have gamma vectors $(5\ -1\ -1\ -1\ -1\ -1)$ and $(5\ 3\ -2\ -2\ -2\ -2)$ respectively. These are cases where the gamma numbers produced are quite high (10 and 16), but the overall effect will be largely one of time delay. This can be seen quite easily

from the gamma vectors. Clearly therefore, the gamma number should be used *after* these obviously degenerate cases have been eliminated.

It is of some interest to determine what is the largest gamma number obtainable with a block of given size since this could well represent the best scramble. A simple way to demonstrate maximum gamma number is to split or partition the block of samples into two and interchange the half blocks:

$$
\begin{array}{cccccc}
(4 & 5 & 6 & 1 & 2 & 3) \\
(1 & 2 & 3 & 4 & 5 & 6) \quad \Gamma = 18 \\
\hline
3 & 3 & 3 & -3 & -3 & -3
\end{array}
$$

It can be seen that maximum gamma number has been achieved in this way since all samples have been displaced by the same amount, and if any sample is shifted to a greater extent another is bound to be reduced in displacement. Consider also the reverse sequence

$$
\begin{array}{cccccc}
(6 & 5 & 4 & 3 & 2 & 1) \\
(1 & 2 & 3 & 4 & 5 & 6) \quad \Gamma = 18 \\
\hline
5 & 3 & 1 & -1 & -3 & -5
\end{array}
$$

This also has maximum gamma number and since reverse sequences are easily and conveniently written it will be convenient to use them in determining maximum gamma number for any block size. The effects of odd and even block sizes will now be investigated, even blocks being considered first.

The reverse and original sequences may be written

$$
\begin{array}{cccccc}
(N & N-1 & N-2 & \ldots & 2 & 1) \\
(1 & 2 & 3 & \ldots & N-1 & N) \\
\hline
N-1 & N-3 & N-5 & \ldots & 3-N & 1-N
\end{array}
$$

For the gamma number, magnitudes only are required, and thus the second half of the gamma vector series is a repeat of the first half. Then

$$\Gamma = 2(N-1) + 2(N-3) + 2(N-5) \ldots + 2(1)$$

there being $N/2$ terms. The sum of the last and first terms is $2N$, and similarly for the other pairs of terms so that the expression becomes

$$\Gamma_{max} = 2N \cdot \frac{N}{4} = \frac{N^2}{2}$$

The case where N, the block size, is an odd number will be somewhat different, and will be found to reduce in a similar way to $(N-1)/2$ terms, each of value $(N+1)$ so that

$$\Gamma_{max} = \frac{(N-1)(N+1)}{2} = \frac{N^2-1}{2}$$

The reverse sequence is not the only one which yields maximum gamma number as noted above. Consider a reverse block 5 as an example

$$
\begin{array}{ccccc}
(5 & 4 & 3 & 2 & 1) \\
(1 & 2 & 3 & 4 & 5) \quad \Gamma = 12 = \Gamma_{max} \\
\hline
4 & 2 & 0 & -2 & -4
\end{array}
$$

Now let the fourth and fifth samples be interchanged

$$
\begin{array}{ccccc}
(4 & 5 & 3 & 2 & 1) \\
(1 & 2 & 3 & 4 & 5) \quad \Gamma = 12 = \Gamma_{max} \\
\hline
3 & 3 & 0 & -2 & -4
\end{array}
$$

Γ remains at 12.

A further shift of the 5th sample again produces a $\Gamma = 12$.

$$
\begin{array}{ccccc}
(4 & 3 & 5 & 2 & 1) \\
(1 & 2 & 3 & 4 & 5) \\
\hline
3 & 1 & 2 & -2 & -4
\end{array}
$$

The fifth sample has now reached the mid-point, and a further shift to the right will reduce the value of Γ.

$$
\begin{array}{ccccc}
(4 & 3 & 2 & 5 & 1) \\
(1 & 2 & 3 & 4 & 5) \quad \Gamma = 10 \\
\hline
3 & 1 & -1 & 1 & -4
\end{array}
$$

The condition for the gamma number to remain unchanged after a second shuffle may be stated as follows. 'For an undisturbed gamma number, exchanges can only be made between samples that have gamma vectors of the same sign initially; further, the signs of the changed gamma vectors must both be the same as that initial sign.' (A gamma vector of zero may count as having either sign.)

This may be alternatively expressed by considering a scrambled series given by

$$
\begin{array}{cccccc}
A & B & C & D & E & F \\
1 & 2 & 3 & 4 & 5 & 6 \\
\hline
U & V & W & X & Y & Z
\end{array}
$$

Now let the samples B and E be interchanged. Then if the gamma number is to remain unchanged we must have $B > 2$ and $E > 5$ (both same positive sign initially) and also $B > 5$ and $E > 2$ so that the resulting vectors are also positive; *or* we must have $B < 2$ and $E < 5$ (both negative initially) and $E < 2$ and $B < 5$.

3. Fourier Analysis of Scrambled Sequences

The most important consideration is to determine the type of distortion produced by the sample interchange process. Does it destroy completely the information content of the signal, or does it merely introduce terms of a harmonic or intermodulation nature into the spectrum? This question may be resolved by a Fourier analysis of the signal in the following manner. Consider first the unscrambled and unmodulated pulses. Each pulse within the scramble block, together with all the corresponding pulses in other blocks may be considered to constitute a separate pulse train. If a block of size $N = 4$ is taken as an example the pulses may be regarded as the sum of four constituent pulse trains:

$$u(t) = u_1(t) + u_2(t) + u_3(t) + u_4(t) \qquad \ldots\ldots(1)$$

Scrambling of the pulses in blocks may then be achieved by shifting each individual pulse train by the appropriate amount.

The Fourier expression for a train of pulses of unit height may be written

$$u(t) = k + 2k \sum_{n=1}^{\infty} \frac{\sin(n\pi k)}{n\pi k} \cdot \cos(2\pi n f t) \quad \ldots\ldots(2)$$

where f is the pulse frequency and k is the duty cycle. For a typical constituent pulse train of the pulses of frequency f_c and block size N

$$u_q(t) = \frac{k}{N} + \frac{2k}{N} \sum_{n=1}^{\infty} \frac{\sin\left(\frac{n\pi k}{N}\right)}{\frac{n\pi k}{N}} \cdot \cos\left(\frac{2\pi n f_c}{N}(t - T_q)\right) \ldots(3)$$

where q corresponds to the subscripts in (1).

Any required time delays or advances can be indicated by the term T_q. If the first component pulse train is taken as a datum (i.e. for $u_1(t)$ let $T_1 = 0$), then it is possible to express the other values of T_q in terms of multiples of the original sampling period $1/f_c$

$$u_q(t) = \frac{k}{N} + \frac{2k}{N} \sum_{n=1}^{\infty} \frac{\sin\left(\frac{n\pi k}{N}\right)}{\frac{n\pi k}{N}} \times$$

$$\times \cos\left(\frac{2\pi n f_c}{N}\left(t - \frac{[q-1]}{f_c}\right)\right) \quad \ldots(4)$$

Then

$$u(t) = \sum_{q=1}^{N} u_q(t) \quad \ldots\ldots(5)$$

Two methods of analysis are now possible. Samples of the input signal $s(t)$ may be generated by multiplying the pulses by $s(t)$, and introducing various delays to represent the scrambling. A somewhat neater analysis is however provided by the alternative method of multiplying each pulse train by a delayed or advanced version of the signal so that the scrambled signal is derived straight away. For example, let a particular scrambling sequence require that the fifth sample in the block be moved to the first position. The first pulse train $u_1(t)$ is then multiplied by the signal that occurs four sample periods ahead of the u_1 pulses, $s(t+4/f_c)$. Similar signal shifting is carried out for the other pulses so that the final scrambled signal is given by the general expression

$$v(t) = \sum_{q=1}^{N} u_q(t) \cdot s\left(t + \frac{\gamma_q}{f_c}\right) \quad \ldots\ldots(6)$$

where γ_q is the gamma number (as previously defined) which occurs in the qth place in the scramble block.

If the signal is the single tone

$$s(t) = A \cos \omega t$$

then from equation (6)

$$v(t) = \sum_{q=1}^{N} u_q(t) A \cos \omega \left(t + \frac{\gamma_q}{f_c}\right) \quad \ldots\ldots(7)$$

Assuming that $A = 1$ for simplicity, and substituting for u_q from equation (4),

$$v(t) = \sum_{q=1}^{N} \cos \omega \left(t + \frac{\gamma_q}{f_c}\right) \times$$

$$\times \left[\frac{k}{N} + \frac{2}{\pi} \sum_{n=1}^{\infty} \frac{\sin \frac{n\pi k}{N}}{n} \cdot \cos \frac{2n\pi}{N}(f_c t - q + 1) \right] \quad (8)$$

Multiplication yields a first term equal to

$$\frac{k}{N} \cos \omega \left(t + \frac{\gamma_q}{f_c}\right)$$

which on further expansion becomes

$$= \frac{k}{N} \left[\cos \omega t . \cos \frac{\gamma_q \omega}{f_c} - \sin \omega t . \sin \frac{\gamma_q \omega}{f_c} \right] \quad \ldots\ldots(9)$$

This represents a term in the scrambled spectrum which has the same frequency as the input signal $s(t)$. To compute the amplitude of this term it is necessary to perform the summation over all values of q, and to find the resultant of the orthogonal terms. Thus the amplitude of the term at ω is

$$\frac{k}{N} \sqrt{\left(\sum_{q=1}^{N} \cos \frac{\gamma_q \omega}{f_c} \right)^2 + \left(\sum_{q=1}^{N} \sin \frac{\gamma_q \omega}{f_c} \right)^2} \quad \ldots\ldots(10)$$

Further multiplication of the remaining terms in equation (8) shows that there are further terms present at frequencies $(n(f_c/N) \pm \omega)$, i.e. sideband terms around suppressed carriers at frequencies $n(f_c/N)$. The amplitudes of the upper and lower sidebands in each pair are equal and are given by the following series:

$$\frac{1}{\pi} \sum_{n=1}^{\infty} \frac{\sin\left(\frac{n\pi k}{N}\right)}{n} \cdot \sqrt{\left[\sum_{q=1}^{N} \cos\left(\frac{n2\pi}{N} \cdot (1-q) - \frac{\gamma_q \omega}{c}\right) \right]^2 +}$$

$$+ \left[\sum_{q=1}^{N} \sin\left(\frac{n2\pi}{N}(1-q) - \frac{\gamma_q \omega}{f_c}\right) \right]^2$$

It has therefore been established that the spectrum of the scrambled signal consists of a term of at ω, the original input frequency, together with the sideband terms described above. Each audio component in the signal $s(t)$ will result in similar sets of sidebands, and if $s(t)$ occupies a range of frequencies of, say, zero to 3.5 kHz, some of these sideband terms will fall within that range. In general, the larger the value of block size N the more terms will fall within the given range. The effectiveness of the scrambling is therefore seen to be a matter of the degree of masking of the original signal term by all the other sideband terms.

Expressions of the above type are easily evaluated by a digital computer, and a program was in fact written to do this, the results of typical computations being shown in Figs. 2 and 3. Sinusoidal input signals of unity amplitude are assumed; the sampling frequency is taken to be 7 kHz and k is 0.04. Figure 2 gives the amplitudes of the original component and the sideband terms for various input frequencies for a simple $N = 2$ sequence (2 1). In this simple case there is only one sideband component which falls within the signal range. For example, if the input sinusoid has a frequency of 1 kHz, the scrambled samples would contain a 0.025 V
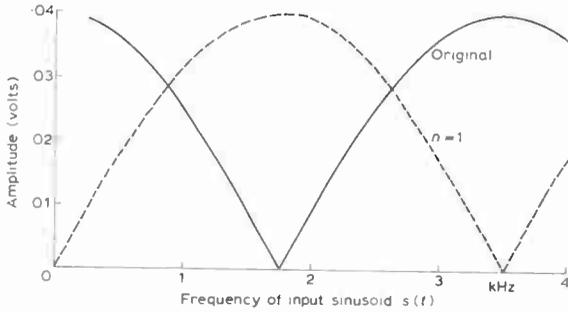
102

Fig. 2. Spectral amplitudes after scramble with $N = 2$.

component at this frequency, and components at $((1 \times 7/2) \pm 1)$ kHz of amplitude $0 \cdot 0315$ V. Only the lower of these would fall within the signal band.

Note that normally, in order to avoid violation of the regeneration requirements of the sampling theorem the input signal would be limited to a maximum frequency of $3 \cdot 5$ kHz. However, there is no physical reason why a 4 kHz signal should not be sampled at 7 kHz; it would merely mean that such a sampled signal would have a non-removable distortion component in the signal band before scrambling. The scrambling spectral analysis would still be correct. Many of the curves presented fall to zero at $3 \cdot 5$ kHz, so they have been extended to a slightly higher frequency for ease in labelling.

Figure 3 shows the amplitudes for three different block-4 exchanges (2 3 1 4), (3 1 4 2) and the reverse sequence (4 3 2 1). It will be seen from these figures that the amplitudes of the various terms vary considerably as the input frequency changes, and at certain frequencies the amplitude of the term at the original frequency ω falls to zero.

Thus far, the analysis has dealt with those scramble sequences which are confined to the simple interchange of samples within a defined block. There are, however, other possible sequences such as the 'running' exchange, an example of which is illustrated in Fig. 4(a). The samples are again divided into blocks, but this time exchanges are made between blocks as shown. Only one sample is moved in each block in this illustration for clarity, but similar moves are possible with some of the other samples of course. The analysis carried out above is directly applicable to this case since the sequence can again be broken down into component pulse trains, one of which is delayed by a time equal to 5 sample intervals. We have merely removed the restriction that

$$\sum_{q=1}^{N} \gamma_q = 0$$

as was the case for the simple block exchange.

A more complicated exchange such as that of Fig. 4(b) can also be envisaged. Here the samples move from one group to the next by jumps of varying size as shown. This leads to the formation of a 'super block' as indicated, and the previous analysis is still applicable. Now, however, the constituent pulse trains have a fundamental

period equal to that of the super-block so that sidebands are centred around the harmonic carriers $n(f_c/20)$ kHz as compared with $n(f_c/5)$ kHz in the previous case. If it were possible to imagine the limiting case of samples being exchanged in a truly random manner the harmonic carriers would have infinitesimal spacing as the super block would, in the limit, be infinitely long. This case is of course of no practical significance due to the practical difficulties in arranging a truly random exchange, and the even worse difficulty of de-scrambling such a sequence!
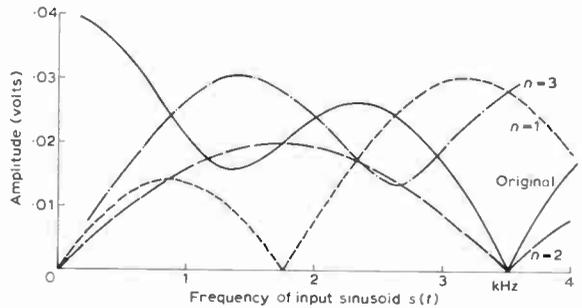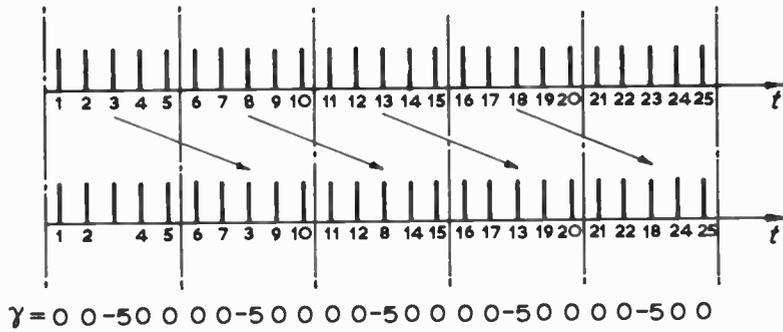

(a) (2 3 1 4) $\Gamma = 4$.
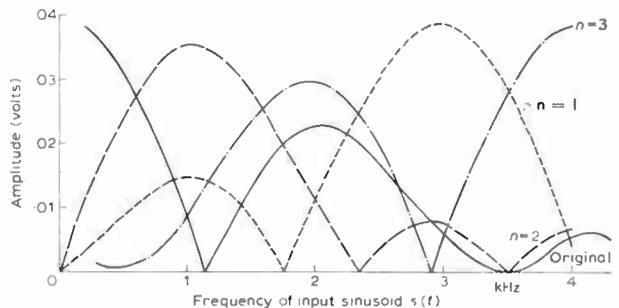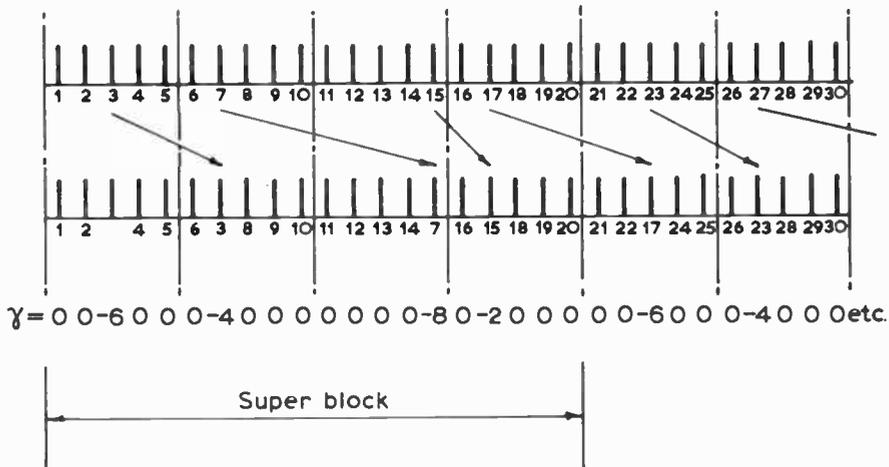

(b) (3 1 4 2) $\Gamma = 6$.
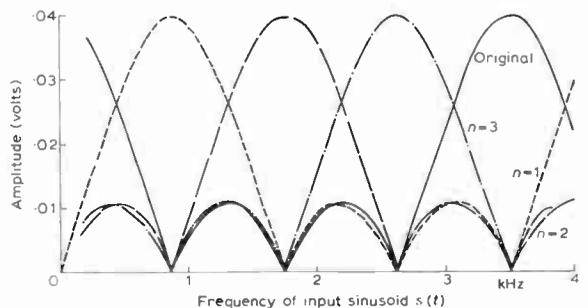
(c) (4 3 2 1)—reverse sequence $\Gamma = 8$.

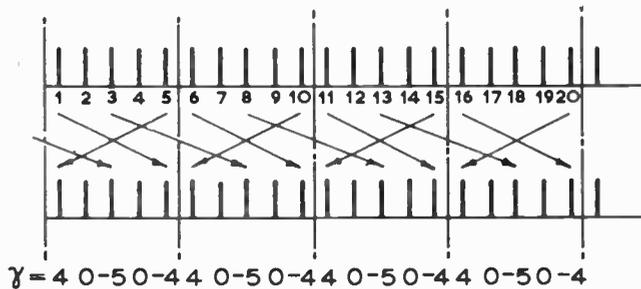Fig. 3. Spectral amplitudes after scramble with $N = 4$.

Combinations of simple block and running sequences are of course possible. Figure 4(b) is really such a case, all gamma vectors being negative, and Fig. 4(c) shows a more obvious example, with positive and negative vectors.

(a) Simple 'running' exchange.

(b) More complex 'running' exchange.

(c) Mixed block/running exchange.

Fig. 4. Sequences involving changes between blocks.

It is perhaps interesting to note the obvious point that where all values of γ are negative, no overall block delay is required since all time shifts are in fact delays and no samples have to be moved backwards in time. If this is not the case an overall gamma shift has to be applied to ensure that all values of γ are negative. In the example of Fig. 1(a) the gamma numbers are $(1\ 2\ 0\ 1\ -4)$. An overall gamma of -2 has to be added to each corresponding to the networks shown in Fig. 1(b) with delays $-1\ 0\ -2\ -1\ -6$.

4. Experimental Results

4.1 Apparatus

It was pointed out in Section 1 that the most flexible and convenient way of producing sample re-ordering is by means of a digital computer. A schematic diagram of the system used in this investigation is shown in Fig. 5. The input signal, derived from an audio oscillator or tape recorder is first passed through a low-pass filter in order to ensure that the signal is band-limited. The 12-bit analogue-to-digital converter of the computer used required about 56 µs to achieve each conversion, and thus a sample-and-hold circuit is provided to sample the signal and hold the converter input at this level for the required time. The system is timed by the recirculation time of the program within the computer, and one of the digital-to-analogue converters is used to provide a synchronizing pulse which tells the sampler when to operate. Another digital-to-analogue converter is used as the output channel, producing samples 6·8 µs in duration which are then passed to
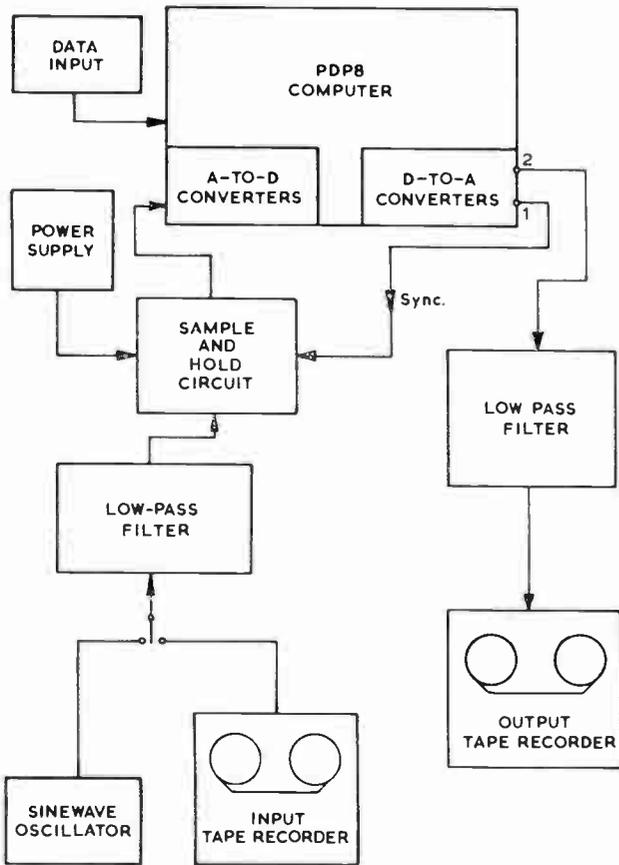
Fig. 5. Experimental system.

was found to be substantially flat over the audio range of 200 Hz to 3 kHz.
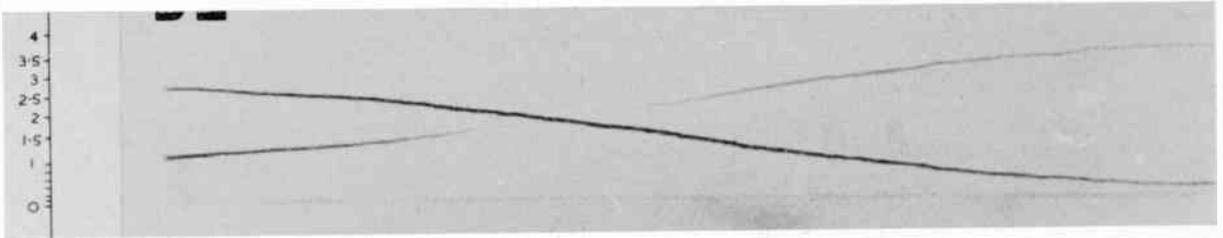
4.2 Spectral Analysis

The frequency spectra of the scrambled signals were investigated using the well-known Sonograph spectrum analyser.† This instrument produces a trace showing the frequencies present as a function of time, the intensity or amplitude of the various components being portrayed as varying blackness of the trace.

The results of this analysis for simple sinusoidal signals scrambled in various ways are shown in Fig. 6. (The large black figures which appear on some of these photographs were inserted for another purpose, and should be ignored.) The input signal for all these photographs except where otherwise stated consists of a sinusoid whose frequency is slowly varied in time from 1 kHz to 3·5 kHz. Figure 6(a) shows the output after a simple block 2 (2 1) scramble; the original component is seen as a line starting at the left-hand side at 1 kHz, and rising to 3·5 kHz at the right, and in accordance with what would be expected from Fig. 2 its amplitude diminishes to zero at 1·8 kHz. Only one sideband term is present in the signal band, namely the lower sideband about a carrier at 3·5 kHz, and this component reaches its maximum amplitude at 1·8 kHz.
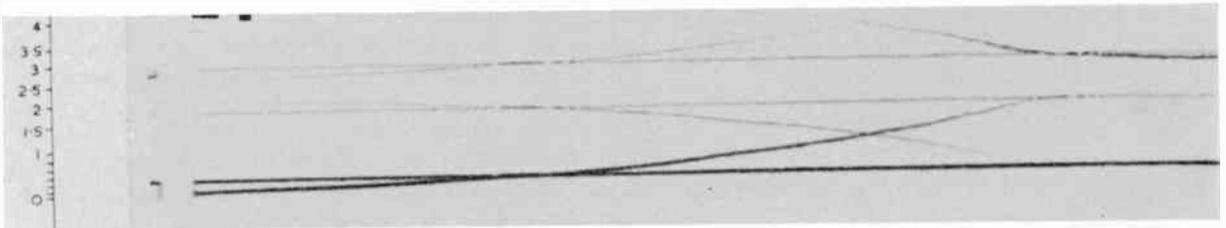
Figure 6(b) is a sonagram for a block 3 interchange (1 3 2) and for this photograph the input consists of a steady sinusoid at 500 Hz plus another which rises with time from 200 Hz to 2 kHz. There will be harmonic carriers at $n.2·33$ kHz, and the various sidebands due to the input components may be clearly seen, free from any other intermodulation tones showing that the spectra produced by the two input tones superimpose linearly.

The original 1 kHz to 3·5 kHz rising tone was used for Figs. 6(c) and (d) which show the spectra for two block 4 interchanges (2 3 1 4) and (3 1 4 2). These should be studied in comparison with the graphs of Figs. 3(a) and (b), and it should be remembered that negative frequencies double back and appear as positive frequencies. For example, the component which is at the original frequency ω in Fig. 6(d) vanishes when the frequency is just above 1 kHz, becomes quite strong at 2 kHz, and then decreases again to vanish at 3·5 kHz. The lower sideband component of the first carrier at 1·75 kHz starts at 0·75 kHz, falls to zero frequency and then 'doubles back' when it becomes a negative frequency and rises again. The curves of Fig. 3(b) predict that this component should be quite strong when the input frequency is 1 kHz, should fall to zero amplitude when $\omega = 1·75$ kHz, and should then become very strong for ω greater than about 2·5 kHz. Inspection of Fig. 6(d) will confirm this behaviour. Figures 6(e) and (f) show the results of (1 2 4 3) and (2 1 3 4) scrambles, and it will be seen that the resulting spectra are virtually identical. (The photographs are slightly different in that the input tone rises rather more quickly in Fig. 6(f), but the arrangements of null points are the same.) If the gamma vectors for these two sequences (0 0 1 −1)

the output low-pass filter which regenerates a continuous waveform. The properties of this waveform will be investigated. The sampling rate used in all experiments was 7·0 kHz/s and the filter cut-off frequencies were 3·1 kHz so that the requirements of the Sampling Theorem were met.

The computer works 'on line' in real time and is organized in the following way. Two stores, each capable of storing N sample values, are provided. N samples are read sequentially as they occur into store I, and at the same time N samples previously stored in store II are read out sequentially in the order which has been specified at the data input. The stores then interchange functions, the next block of samples being read into store II while others are read out of store I and so on. There is of course an overall delay equal to the time of occurrence of N samples.

To be certain that the experimental results would be free from spurious effects the system was checked carefully for correct operation. The linearities of the digital-to-analogue and analogue-to-digital converters were found to be perfectly satisfactory by simple d.c. tests. Further, a sinusoid was fed into the input and processed without re-ordering of the samples, and by comparison of input and output waveforms on an oscilloscope the linearity was again found to be excellent. Finally, an overall frequency response measurement was made for the case of no scrambling, and the frequency response

† Potter, R. K., Kopp. G. A. and Green. H. C., 'Visible Speech' (Van Nostrand, New York, 1942).
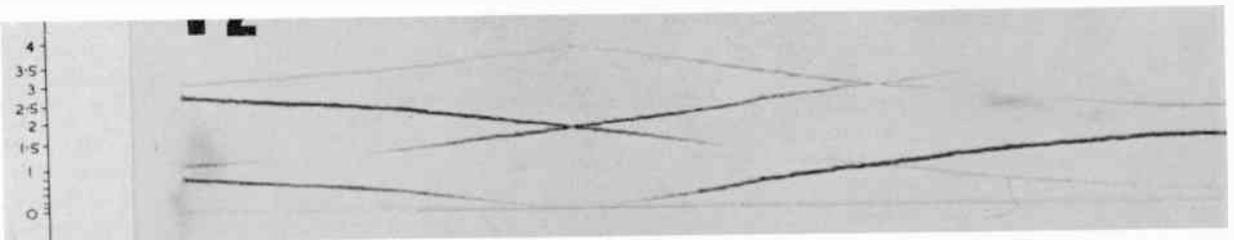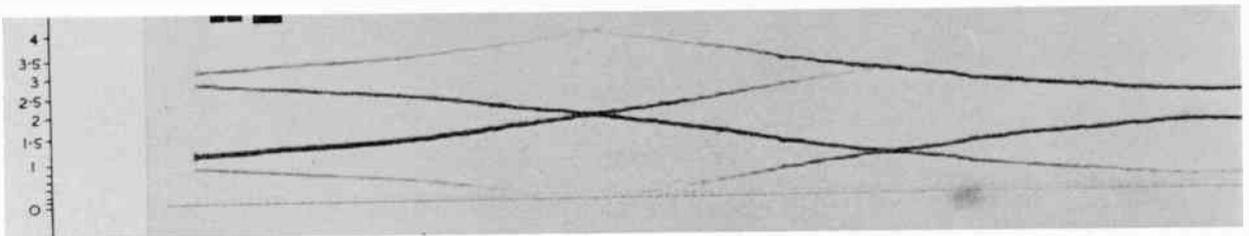
(a) Block 2 (2 1).
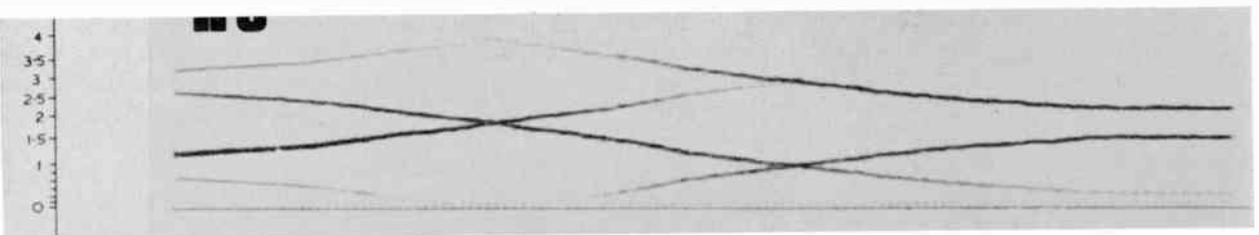
(b) Block 3 (1 3 2).
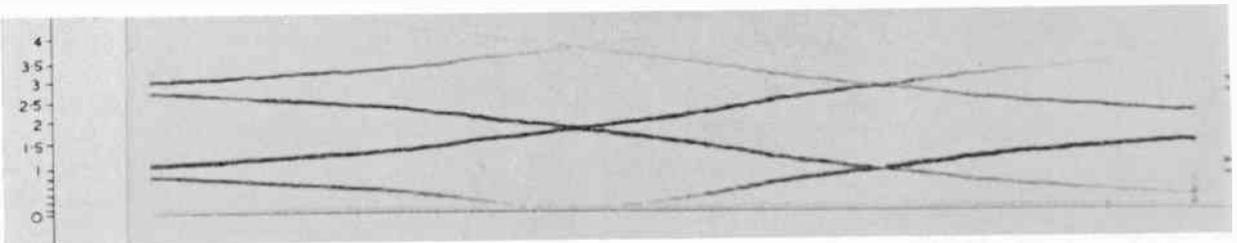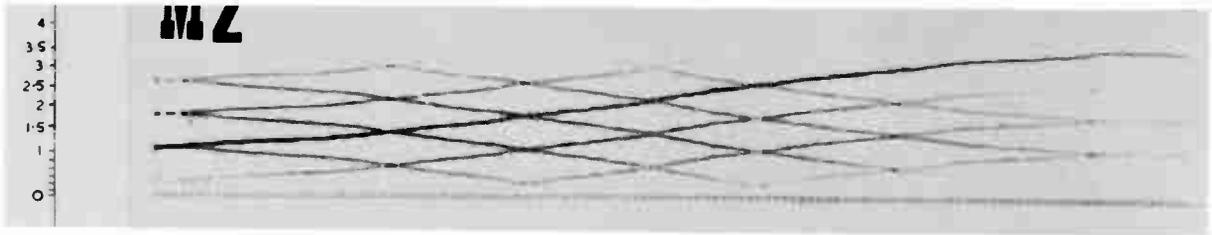
(c) Block 4 (2 3 1 4).

(d) Block 4 (3 1 4 2).

(e) Block 4 (1 2 4 3).

(f) Block 4 (2 1 3 4).

Fig. 6. Frequency spectra of scrambled sinusoidal signals. Vertical scales are in kHz.

(g) Block 10 (3 2 1 4 5 6 7 8 9 10).
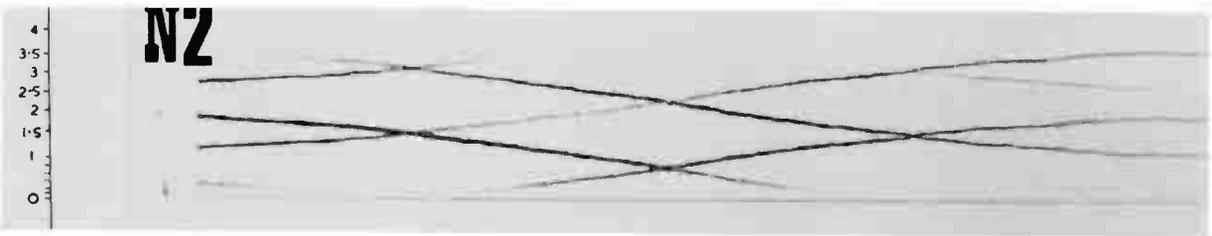
(h) Block 10 (3 2 1 4 5 8 7 6 9 10).

(i) Block 10; reverse sequence.

(j) Block 20; reverse sequence.

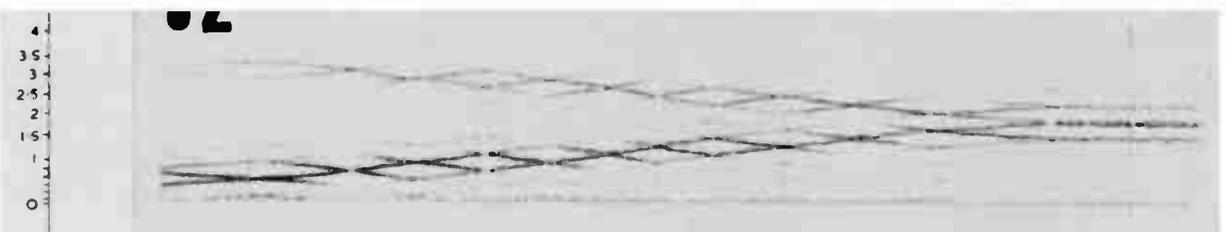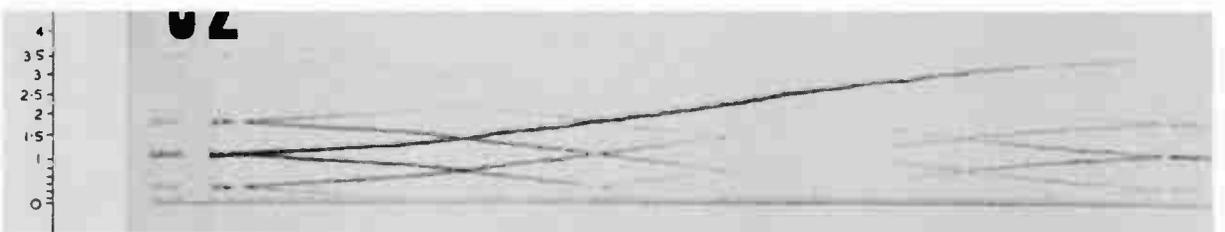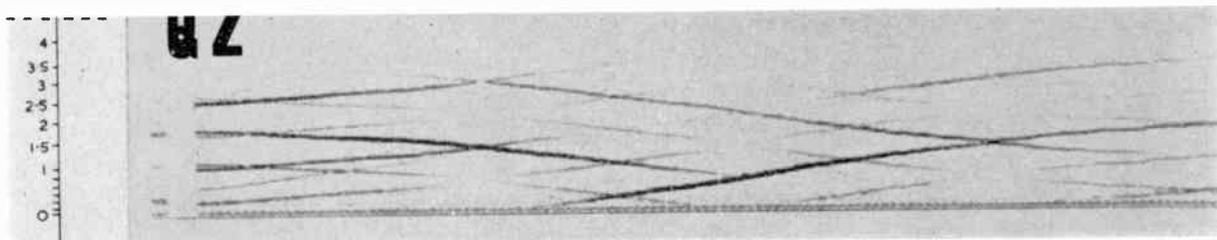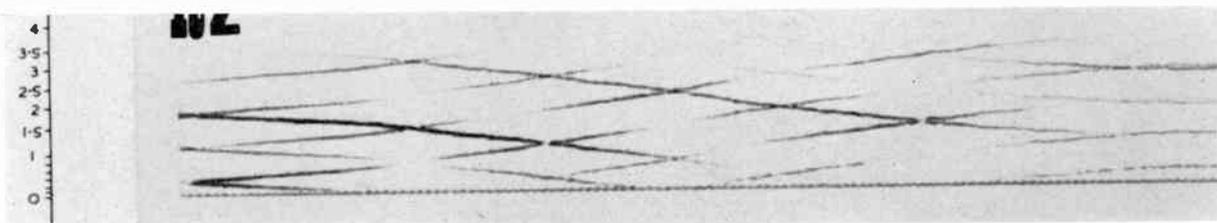(k) Block 20 (20 1 19 2 18 3 17 4 16 5 15 6 14 7 13 8 12 9 11 10).

(l) Block 10. $\Gamma = 6$.

Fig. 6. Frequency spectra of scrambled sinusoidal signals. Vertical scales are in kHz.

(m) Block 10. $\Gamma = 18$.

(n) Block 10. $\Gamma = 28$.

Fig. 6. Frequency spectra of scrambled sinusoidal signals. Vertical scales are in kHz.

$(+1\ -1\ 0\ 0)$ are compared, it will be seen that in fact these are two equivalent sequences.

Figures 6(g) and (h) show the spectrum resulting from a block 10 scramble, the sequences used being (3 2 1 4 5 6 7 8 9 10) and (3 2 1 4 5 8 7 6 9 10). The first of these shows the expected structure of sidebands around carriers of $n(f_c/10)$ but the second shows a much simpler structure. If the gamma vectors for the second sequence are examined it will be found that it has degenerated into a block 5 scramble.

Figures 6(i) and 10(j) show reverse sequences for block 10 and block 20 scrambling, and an interesting phenomenon appears here. The original rising tone appears in these spectra in 'shadow' form. When a particular sideband term has a frequency equal to that of the input signal at that time, then it has maximum amplitude. This effect can also be seen in Fig. 3(c) which shows the calculated spectra for a block-4 reverse sequence. For example, when the input frequency is 875 Hz, the first set of sidebands $(n = 1)$ occur at $7000/4 \pm 875$, the lower component of which occurs at 875 Hz. Under these conditions, this sideband component has maximum value. The spectra have also been computed for a block-10 reverse sequence and the same phenomenon appears. This effect is not really as surprising as it sounds, because if the samples in a block are reversed this is equivalent to cutting the input signal into sections and reversing each one. If there are several cycles of sinusoids per block, then it is only to be expected that the spectrum would have a strong component at signal frequency. Indeed, in certain cases when a block period contains an exact number of half cycles of the sinusoid there will be exact lining up of the half cycles and the scrambled signal will be a pure sinusoid. This occurs when the frequency of the signal is equal to $n(f_c/2N)$ as is easily proved by letting the integral number of half signal periods equal the block period. For the case illustrated in Fig. 6(i) this phenomenon occurs at frequencies $n.350$ Hz. For example, when the original

frequency is 1750 Hz other terms disappear leaving an undistorted sinusoid of this frequency. Five cycles of a 350 Hz signal occupy a time of 14 300 µs which is the duration of one block of ten samples. This effect is even more marked in the case of Fig. 6(j), the block-20 reverse sequence. It would thus appear likely that reverse sequences should be avoided for purposes of scrambling. Figure 6(k) shows the block-20 pattern (20 1 19 2 18 3 17 4 16 5 15 6 14 7 13 8 12 9 11 10) where half the samples are in reversed order interleaved with samples in the correct order. There is still some evidence of intensification of the pattern but it no longer simply follows the input rising signal.

Figures 6(l), (m) and (n) show block-10 scrambles with increasing values of gamma number ($\Gamma = 6, 18, 28$). These photographs show differing degrees of complexity in the occurrence of zero amplitudes in the sideband terms, and there is a general tendency to stronger overall levels of sideband amplitudes with increasing gamma number as shown by the darkness of the traces representing these terms. This effect can also be seen in the graphs of Fig. 3. In Fig. 3(a) ($\Gamma = 4$), over most of the range $\omega =$ zero to 3 kHz the original component is stronger than any of the other components. In Figs. 3(b) and (c) ($\Gamma = 6, 8$) this is certainly not the case.

All the tests described thus far have been made on simple sinusoidal input signals. The next series of photographs shows the effect of scrambling on the spectrum of speech signals. Figure 7(a) shows the spectrum of the unscrambled sentence 'an attempt to obtain money by false pretences'. Figures 7(b) to (e) show the same phrase after scrambling in a block-10 pattern, the gamma numbers being 14, 26, 44 and 50. The general conclusion to be drawn here is that the larger the value of the gamma number the stronger are the sideband components relative to the original signal.

Figure 7(f) shows the sonagram of the unscrambled phrase 'on where harsh brakings required'. Figure 7(g) shows the same phrase after scrambling with a block-60
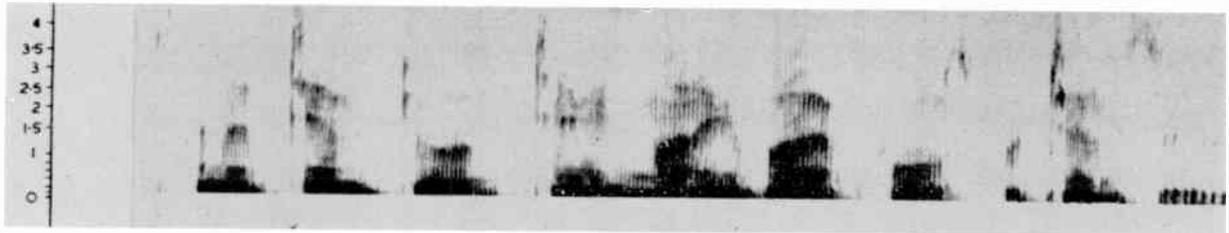
(a) Speech unscrambled.

(b) After block 10 scramble $\Gamma = 14$.
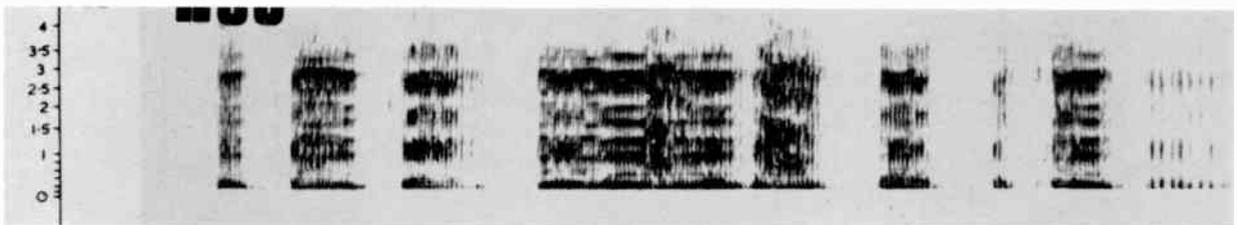
(c) After block 10 scramble $\Gamma = 26$.
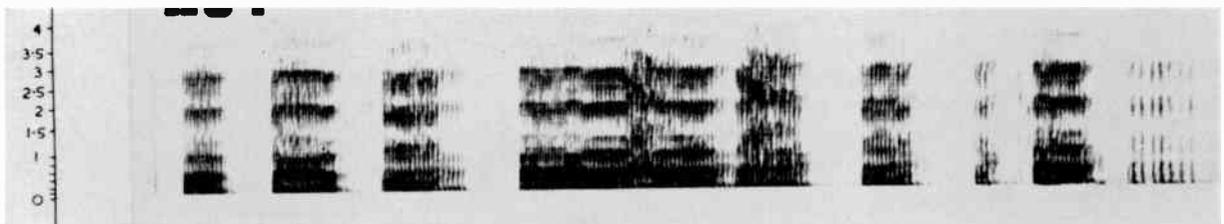
(d) After block 10 scramble $\Gamma = 44$.
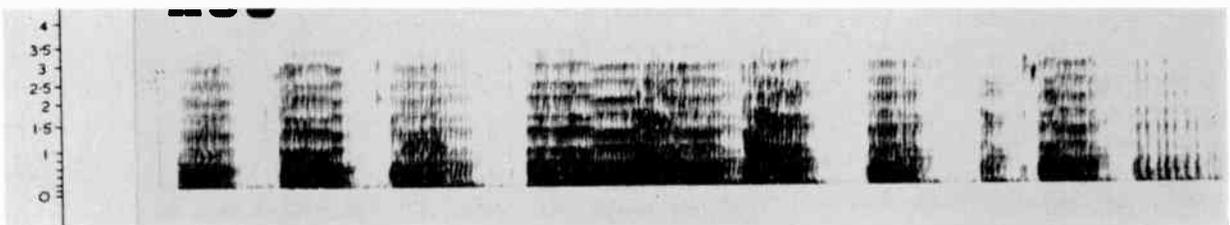
(e) After block 10 scramble $\Gamma = 50$.

Fig. 7. Frequency spectra of scrambled speech signals. Vertical scales are in kHz.

reverse sequence, and it will be seen that the original speech structure shows up with remarkable clarity confirming the remark made earlier, namely that the reverse sequence should be avoided. One block of 60 samples occupies a time of about 8·6 ms; this is short compared with the duration of the speech syllables so it is not surprising that much of the formant structure and the patterns of formant changes are preserved.

4.3 Intelligibility Tests

The analysis of the previous Sections has been concerned with examination of the spectra of the scrambled signals. Although this is valuable in that it illustrates the mechanism of production of the distortion terms, it is clearly very important to discover the effect of these distortions on the intelligibility of the scrambled speech. Some initial intelligibility tests were carried out using
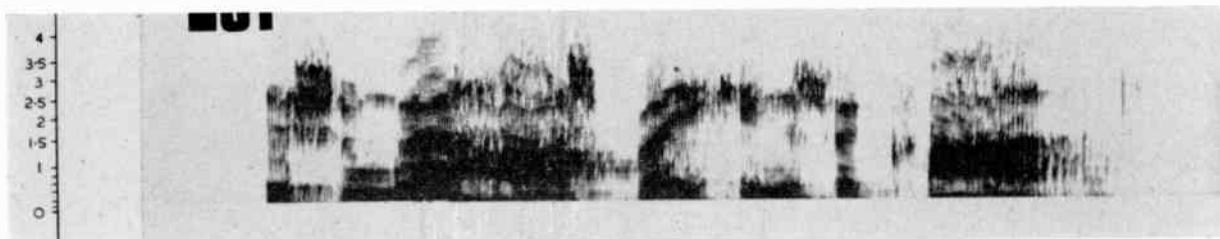
(f) Speech unscrambled.
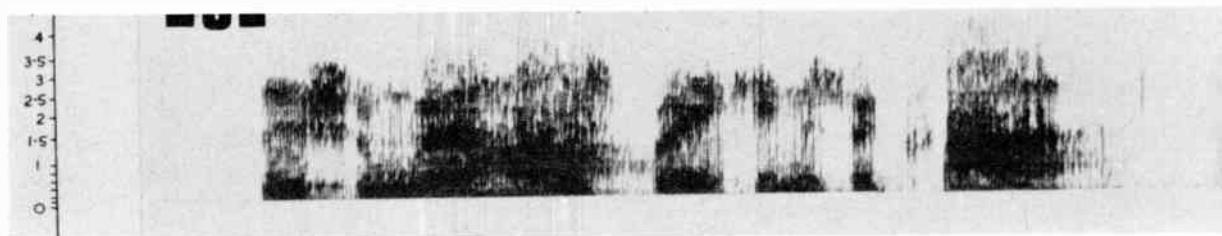
(g) After block 60 scramble; reverse sequence.

Fig. 7. Frequency spectra of scrambled speech signals. Vertical scales are in kHz.

seven different block-10 scrambles, each having a different gamma number. In addition, a block-10 reverse order scramble and a simple block-2 scramble were tested. A zero sequence was also used as a control for comparison purposes.

Lists of monosyllabic words were used as test material, four listeners being used for each scramble sequence. The usual precautions were observed to ensure that no listener heard any particular list more than once, and in addition a short passage of continuous scrambled speech was presented to the listener before each word list to accustom him to the type of distortion occurring, and to attempt to minimize learning effects during the hearing of the word list itself.

The results of these tests are summarized in Fig. 8, the intelligibility scores being plotted as a function of gamma number. The actual sequences used are listed in Appendix 1. Each point on the graph represents the average of four intelligibility scores, and the spreads of the individual scores are also indicated. Zero scramble produced a score of 92%. It is clear from this graph that, in general, the greater the value of the gamma number, the greater is the scrambling effect, and this is maintained up to a gamma number of about 40. The reverse sequence produced a significant increase in intelligibility as might have been expected from the foregoing discussion. A sequence having the maximum gamma number, but not being a reverse sequence gave a reduced, but non-zero score (2%). In order to produce maximum gamma as described previously, it is necessary to divide the block into two, and to change all samples into the other half block. This means that, in general terms, such a sequence must be tending to a reverse sequence.

The simple block-2 interchange gave a score of 22% which might be thought surprisingly low in view of the relatively simple type of distortion produced. However, it must be remembered that the distortion, although

simple in form, has an amplitude comparable with that of the original signal component (see Fig. 2), and signal components in the important 1·25 to 2·25 kHz range are much attenuated.

Further tests were then performed to determine the effect of varying the block size, and also to confirm the general form of the curve of Fig. 8. In this series of tests eight listeners were used in each scramble condition. The test lists were presented to four of them in order of increasing gamma number, and to the other four in order of decreasing gamma number. The results are presented in Figs. 9(a), (b) and (c), the spread of results being shown as in Fig. 8. The sequences used are given in Appendix 2.
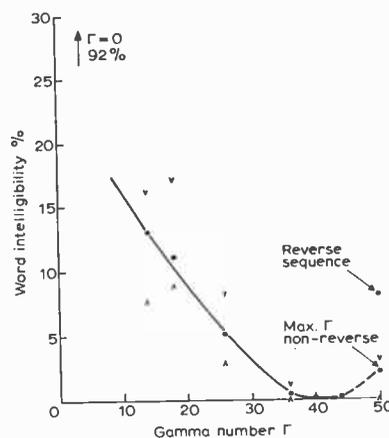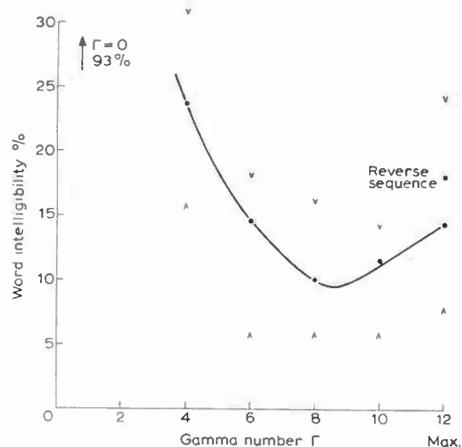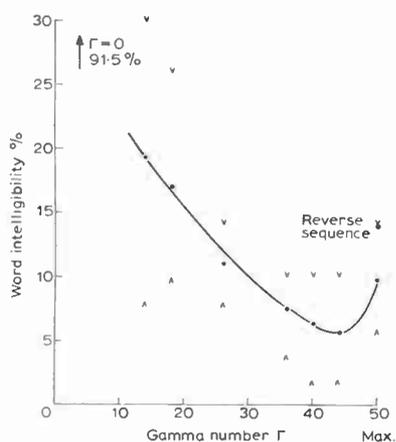

Fig. 8. Result of initial intelligibility tests.
Block size $N = 10$.

Although too much reliance cannot be placed on the precise shapes of curves in subjective experiments of this sort, it will be observed that the graphs all have the same general shape as that of Fig. 8. That is to say, the intelligibility decreases with increasing gamma

(a) Block size $N = 5$.

(b) Block size $N = 10$.
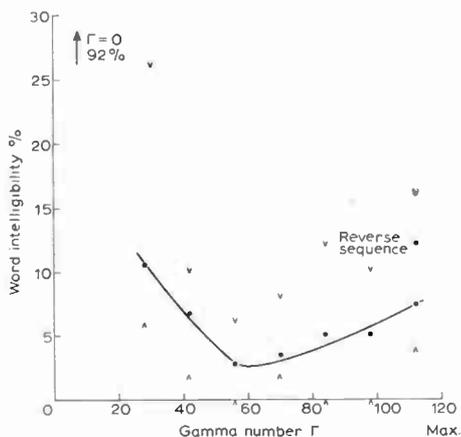
(c) Block size $N = 15$.

Fig. 9. Word intelligibility.

number, but tends to increase again at the higher gamma numbers.

In order to be able to compare the three graphs of Fig. 9 more directly, the average curves are replotted in Fig. 10, but this time as functions of normalized gamma,

which is defined as

$$\text{normalized gamma} = \frac{\text{gamma number}}{\text{maximum gamma number for that sequence}}$$

These curves indicate that for any given normalized gamma number the intelligibility decreases with increasing block size. Each point on these curves represents the average of eight scores. Since subjective results of this sort are invariably rather scattered, it is worth while pausing to consider the statistical significance of these curves. The points at a normalized gamma of 0·5 will be taken for purposes of comparison.

The means and standard deviations of the sets of eight readings here are:

	Mean	Standard deviation
Block-5	14·25	3·38
Block-10	11·0	2·65
Block-15	2·75	2·44

A Student's $-t$ test† of the confidence levels which can be assigned to these results shows that the probability that the block-5 and block-10 averages differ purely by chance is 6 parts in 100. The same probability for block-10 and block-15 averages is less than 1 part in 1000.

Bearing in mind the inevitable variability of subjective results such as these, too much reliance should not be placed on the precise positions of the minima of the curves. However, it is possible to state that for minimum intelligibility a normalized gamma in the range 0·5 to 0·8 should be selected.

Fig. 10. Word intelligibility results of Fig. 9 plotted as function of

$$\text{normalized } \Gamma = \frac{\Gamma}{\Gamma_{max}}$$

5. Conclusions

It must be concluded that the sample-exchange method is inherently inferior to the more usual speech scrambling method whereby the speech is split into various frequency

† Moroney, M. J., 'Facts from Figures', pp. 227ff (Penguin, London, 1956).

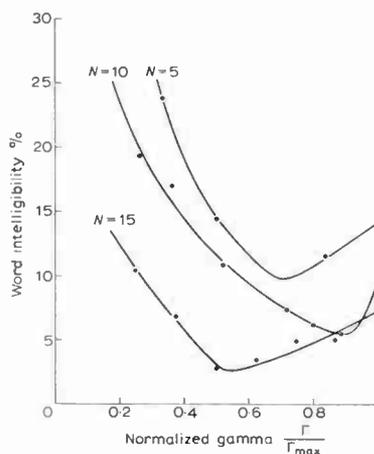bands, and these are interchanged. This is because the sample interchange leaves in the scrambled signal a component of the spectrum which, apart from a frequency weighting, is that of the original signal. The reduction in intelligibility relies on the masking and confusion of this original spectrum by the distortion components produced by the scrambling. In spite of this, the fact remains that low intelligibility figures are produced by suitable interchanges. Monosyllabic word lists were used as test material, and it is well known that sentence intelligibility will be somewhat higher for any given scramble condition. Listeners reported however that in those conditions where word intelligibility was almost zero, sentence intelligibility was negligible also. Thus the sample interchange method could be used to provide a reasonable degree of privacy against unauthorized eavesdropping in any communication system using amplitude samples. The selection of the scrambling sequence is obviously of considerable importance.

It is not possible to give a set of rules which can be used to calculate in a positive way the best sequences to use; rather one may provide a set of simple testing rules which can indicate whether a chosen sequence is an effective one, or whether it is best avoided.

Rules for Best Scramble

(a) Choose as large a value of block size N as is practicable so that many masking terms are produced in the speech band.

(b) Avoid the reverse sequence and those approaching it, including those with maximum or almost maximum gamma number.

(c) Avoid those sequences which approach the zero sequence—i.e. those which have very small values of gamma number.

(d) Avoid those sequences having long runs of equal gamma vectors indicating simple time delays.

(e) Avoid sequences which degenerate into subsequences, indicated by repetitive patterns in the gamma vectors. It would seem reasonable also to avoid those sequences which approach this condition.

(f) If sequences are to be changed at intervals for reasons of security, use the gamma numbers to ensure that sequences selected are not equivalents having identical long-term patterns of gamma vectors. It is possible that the use of these equivalents could make unauthorized decoding easier in some cases.

(g) Best scrambling is obtained with sequences having gamma numbers in the range approximately 0·5 to 0·8.

6. Appendix 1

Block-10 re-order sequences

Test	Gamma number	Sequences									
1	14	2	1	5	3	7	4	6	9	10	8
2	18	3	4	1	2	6	8	5	10	7	9
3	26	3	5	4	8	2	1	9	6	10	7
4	36	4	7	2	10	1	8	9	6	5	3
5	40	5	10	8	1	7	3	2	9	6	4
6	44	10	3	7	9	8	5	4	1	6	2
7	50	7	6	9	8	10	5	1	3	2	4
8	50	10	9	8	7	6	5	4	3	2	1

7. Appendix 2

Block-5 re-order sequences

Test	Gamma number	Sequence
1	4	13425
2	6	21534
3	8	24153
4	10	52413
5	12	35421
6	12	54321

Block-10 sequences are as in Appendix 1.

Block-15 re-order sequences

Test	Gamma number	Sequence														
1	28	2	6	1	5	3	7	4	12	11	9	8	10	14	13	15
2	42	6	4	9	1	7	2	5	3	8	15	10	12	14	11	13
3	56	7	2	6	12	1	4	9	15	3	10	11	14	5	8	13
4	70	4	1	7	12	15	3	11	2	6	14	13	8	5	10	9
5	84	6	14	3	12	8	1	10	13	15	5	2	7	4	9	11
6	98	9	7	15	10	11	8	2	13	14	6	5	3	1	4	12
7	112	11	12	9	13	10	8	15	14	2	6	4	1	7	5	3
8	112	15	14	13	12	11	10	9	8	7	6	5	4	3	2	1

Measurement Techniques in Television Studios and Outside Broadcasts

By

I. H. TEEAR†,

J. D. HUGHES†,
C.Eng., M.I.E.R.E.
and

M. E. HILL (Graduate) †

A review is given of some methods of measurement employed in colour television studios and outside broadcasts which are used for acceptance tests which are carried out when new equipment is commissioned. Line-up of major items of apparatus, and the assessment of performance of temporary line or radio link transmission circuits, are also considered.

1. Introduction

The advent of colour television has necessitated considerable improvements in the measuring techniques used in a television studio complex and in an outside broadcast mobile control room. Occasionally completely new techniques are required, but in most cases it has been possible to modify existing methods of measurement.

For example, the need to measure colour camera channel registration was a problem which had not been encountered before and for which new procedures were developed.

The precise adjustment of camera channel gain and contrast law has always been a problem, but the accuracy to which each of the channels in a colour camera has to be matched necessitated considerable modifications to the existing techniques.

Colour coder setting up entails accurate assessment of the amplitude of several signals, some of them at colour sub-carrier frequency. Providing that the response of the oscilloscope to colour sub-carrier can be checked, conventional methods of measurement may be used.

The colour sub-carrier frequency, and hence the chrominance band, is situated near the upper end of video spectrum. A $2T$ sine-squared pulse has insufficient components at these frequencies to enable an accurate assessment of circuit performance to be made. Consequently additional test signals are necessary which will provide the required information.

In addition to non-linearity distortion, equipment may exhibit level-dependent gain and phase variations to frequencies which are near the upper limit of the passband. These effects are known as differential gain and differential phase distortions respectively, and are not revealed by conventional line time non-linearity tests. Consequently additional test procedures are necessary to measure these distortions.

2. Acceptance Testing of Colour Camera Channels

Before a camera channel is put into operational service a series of tests and measurements is carried out to ensure that it is functioning according to its design specification.

† British Broadcasting Corporation, Television Operations and Maintenance Department, London, W1A 1AA.

In the first instance a line-up of the camera channel is carried out from initial gain setting to final grey scale balance. This line-up provides a check that all functions of the camera channel are operating correctly and should highlight any major deficiencies.

More specific measurements are then carried out, some of which are detailed below.

2.1 Registration

The linearity and geometry of the master channel are first measured according to established monochrome practice. The master channel is normally green, for both three- and four-tube colour cameras.

Of more vital significance in a colour camera is the accuracy to which the remaining channels can be registered to the master channel, as differential errors between channels may cause loss of definition and colour fringing effects on the reproduced pictures.

Horizontal mis-registration may be defined as a relative displacement in a horizontal direction of a point on a vertical line. Similarly vertical mis-registration may be defined as the relative displacement in a vertical direction of a point on a horizontal line.

Several methods of registering colour cameras have now been established, and for each, the camera is positioned to view a good quality registration chart. The one normally used consists of 22×22 squares horizontally and vertically, formed by white lines on a black background.

The simplest method requires that the master channel signal be added to that of the channel being registered, the resultant being displayed on a monochrome picture monitor. The horizontal and vertical scan controls are then adjusted to achieve registration. If the appropriate centering control is offset slightly to produce a series of very close parallel lines, any amplitude or linearity errors become more discernible on the monitor. Therefore amplitude, linearity and skew controls may be adjusted in this condition and the picture then re-centred for optimum registration.

The second method is a refinement of the above in that the master channel is reversed in polarity before being added to the channel being registered. Thus if perfect registration were attained and signal amplitudes were equal, complete cancellation of the signals would occur as viewed on the picture monitor.

A further means of effecting registration is provided by the camera line-up equipment (Sect. 3).

Having registered the camera channel it is necessary to measure the errors. Two methods have been used and both will be described. For each it is advisable to use the negative master channel type of display so that errors and the points of coincidence are easily visible.

2.1.1 Calibrated delay method

Two switchable delay lines are required, each having the delays of 10 ns, 20 ns, 40 ns, 80 ns, 160 ns available, enabling any delay to be selected to an accuracy of 10 ns up to a total of 310 ns. The accuracy of the delays may be checked by measurement of sub-carrier phase change. At PAL sub-carrier frequency 1 ns = 1·590°.

The two delay lines are then connected in series in the master channel signal chain, one having zero delay selected, and the other having sufficient delay inserted to enable measurement of the maximum error in the 'negative delay' direction.

Horizontal registration errors are measured by increasing or decreasing the delay in the master channel until there is no mis-registration at the point under consideration. The difference in settings of the delay networks is then noted.

Readings are normally taken at 25 points on the raster to obtain a complete picture of the registration accuracy and errors are expressed directly in nanoseconds of delay.

Vertical errors are measured at the same 25 points and are expressed in 'equivalent nanoseconds' so that horizontal and vertical errors may be compared directly. At any point under consideration the horizontal shift controls are used to make the horizontal error zero. The delay network is then adjusted to create a horizontal error of equal size to the vertical error and the difference in delay settings on the delay network then gives the vertical registration error in 'equivalent nanoseconds'.

This method has proved to be a quick and simple one but it has been found difficult to repeat results to the required accuracy especially for vertical errors and the second method to be described is recommended for greater accuracy.

2.1.2 Calibrated centering control method

The method described here is for a three-tube camera but may be used for other types.

As the picture centering produced by the scanning assembly is linearly related to the centering current and therefore to the d.c. centering voltage across the coils, it is possible to calibrate the centering controls in terms of 'effective nanoseconds'.

For greater accuracy a differential method of measurement is employed.

Assume that red to green horizontal mis-registration is to be measured. The slider of the red horizontal centering control is connected to one input of an oscilloscope d.c. difference amplifier and the slider of the blue horizontal centering control to the other. The blue centering control may then be used to centre the trace on the oscilloscope, this being the 'zero' condition.

In order to calibrate the oscilloscope in terms of nanoseconds the red centering control is adjusted to mis-register the red channel by one complete square of the registration chart as viewed on the picture monitor. The d.c. voltage change is then measured on the oscilloscope so that it is possible to calibrate this voltage swing in terms of 'effective nanoseconds':

$$\text{d.c. voltage change} = \frac{\text{line time (ns)}}{\substack{\text{no. of divisions per line} \\ \text{of registration chart}}} \quad (1)$$

As this swing will normally be much greater than the mis-registration to be measured, the sensitivities of both halves of the oscilloscope difference amplifier may be increased by equal amounts, and the corresponding multiplying factor introduced into the above equation for greater accuracy.

Registration errors are then measured at 25 points covering the raster, the red horizontal centering control being adjusted for coincidence at each point and readings in 'effective nanoseconds' being taken from the oscilloscope.

Vertical mis-registration may be measured in a similar manner, using the vertical centering controls. In this case when calibrating the oscilloscope, the distance between vertical divisions must be calculated in 'effective horizontal nanoseconds', i.e. with the chart normally used, the squares have a 4×3 aspect ratio and each vertical division is therefore equivalent to

$$\frac{(\frac{3}{4} \times \text{line time (ns)})}{\text{no. of divisions per line on chart}} \text{ effective nanoseconds}$$

The blue and luminance mis-registration may then be measured and, from the results, graphs may be drawn showing the registration errors, so that any suspected change in performance may be checked at a future date.

2.2 Noise and Sensitivity

Signal/noise ratio is measured according to standard monochrome practice, the instrument used being of the type which gates out a noise sample during the middle of the active line period.

It is desirable that a set of standard test conditions be specified, so that when a new camera is developed, its performance may be compared directly with earlier cameras.

When using a colour camera employing lead oxide tubes, the major sources of noise are the head amplifiers, and therefore in the first instance the performance of these amplifiers should be assessed. A suitable test signal such as a sawtooth waveform is fed through a high resistance to the head amplifier input circuit to simulate a tube signal current:

$$I_s = \frac{\text{test signal voltage}}{\text{high resistance}}$$

A value of 300 nA signal current is chosen as the standard. The camera channel gain controls are adjusted

114

for standard level output and the signal/noise ratio measured at linear gamma, with horizontal aperture correction, together with any linear matrixing and vertical aperture correction, switched out.

Secondly, a comprehensive figure for noise and sensitivity is required, so that the optical system of the camera is included in the test conditions.

The camera is set up to produce a standard 0·7 V output viewing a grey scale chart of 40 : 1 contrast ratio and 60% peak white reflectance. The incident illumination on the chart is adjusted to give 150 lumens/ft^2 (16·6 lm/m^2), at 3000° K colour temperature as measured towards the camera lens. The lens aperture is set to $f4$. The camera is then capped.

Signal/noise measurements are then taken of each channel separately at linear gamma with no frequency enhancement or linear matrixing and also for the luminance signal at the coder output with the chrominance switched off. A reading is then taken with any linear matrixing in circuit, so that its effect on noise performance may be checked.

The signal currents are then recorded for each channel, and from these the signal currents at any colour temperature and light level may be calculated to provide a guide to lag and noise performance under varying illuminations.

2.3 Frequency Response

Frequency response is checked using standard pulse and bar or sweep techniques. It has been found useful to check pulse and bar performance with the gamma correction set to 0·45, as any errors at or near black level are enhanced, giving an indication of streak performance at the base of the waveform.

2.4 Resolution

Resolution measurements are made using a test card containing sine-squared shape frequency gratings.

Aperture correction characteristics may be explored, together with the operation of any 'amplitude dependent correction' controls. It is often useful to utilize the grey scale wedge which is included in the test card.

2.5 Cable Length

Frequency response is checked at various cable lengths up to the design maximum. A check on registration and noise is also made at the maximum length.

Measurements are then made of crosstalk and spurious signals at this length.

2.6 Colour Temperature Variation

Most camera channels are provided with filter wheels in the optical path, in which colour temperature correction filters may be inserted, together with a range of neutral density filters. However, under outside broadcast conditions, situations can arise where it is not possible to use correction filters to balance the camera in different illuminants. This could occur

(a) under very low light conditions where the additional light loss due to the insertion of such a filter cannot be tolerated,

(b) on programmes necessitating rapid movement of the camera such that shots very close together in time are required, under both artificial and daylight illuminants, e.g. a shot inside a building followed by a shot looking out through a window.

Because of these restrictions, it is necessary to ensure that sufficient gain control is available at the camera control unit, to enable the camera to be balanced in both high and low colour temperature illuminants.

Measurements made on a three-tube RGB camera show that for a change of Illuminant from 3000°K to 6000°K, the red gain is required to increase by 3 dB, and the blue gain to decrease by 5 dB, relative to the green channel.

2.7 Subjective Evaluation

The final assessment carried out on the camera channel is the subjective evaluation of picture quality as viewed by a number of trained observers.

With the camera channel lined up for optimum, a number of colour fidelity tests are carried out, which include the viewing of a coloured flag made from fairly saturated coloured materials, and of a wide range of flesh tones. The effect of any linear matrixing in the channel is assessed at this stage.

The camera is then focused on a suitable scene and an appraisal is made of picture sharpness, which includes an evaluation of the effect of horizontal and vertical aperture correction, and any associated amplitude dependent or coring controls.

The operation of the camera under low light conditions is also investigated thoroughly as it has been found that the ultimate sensitivity of a camera at very low light levels is a combination of many factors which include noise visibility, lag, and the visibility of spurious signals.

3. Waveform Amplitude and Contrast Law Adjustments during Colour Camera Line-up

This Section reviews some of the methods employed for the setting up of signal levels and transfer characteristics in a colour camera channel. It is standard practice to align the master channel accurately and to use this as a reference for comparison in setting up the remaining channels in the camera.

3.1 Accurate Adjustment of Signal Level and Transfer Characteristic

The methods for accurately setting signal levels have become well established in monochrome practice.

One method, now used frequently, employs a low-frequency square wave of correct amplitude, upon which the signal to be adjusted is impressed. The technique is discussed more fully in Section 4.2. In order that the gamma correction control may be set to give the required transfer characteristic, a suitably engraved oscilloscope graticule may be used.

Alternatively a linear step waveform may be fed through an external gamma correction circuit, the law of which is the inverse of that required. This signal may then be fed to the camera test signal input and the

gamma controls adjusted to obtain a linear waveform output from the channel.

A third method requires an external gamma correction circuit having a pre-set law which is the same as that required by the camera channel. A linear sawtooth waveform is fed to this circuit and also to the camera channel test input. The output signals may then be compared in a difference amplifier, and the camera channel gamma controls adjusted for a null.

3.2 Methods of Matching Other Channels to Master Channel

Having aligned the master channel as above, the remaining requirement is to match the other channel gains and transfer characteristics to this as accurately as possible.

Firstly, a difference amplifier and waveform monitor may be used, one input being the master channel, the other being switchable to the remaining channels in turn.

Secondly, a superimposition method may be used, in which the master channel and any of the others may be superimposed on the waveform monitor. A refinement of this method utilizes an electronic switch operating at 12½ Hz. The switch cuts between the master channel and the channel under adjustment, the output of the switch being displayed on a waveform monitor. If signal levels are unequal at any point on the waveform, the displayed trace 'flickers' at 12½ Hz and thus camera channel controls may be adjusted to minimize this 'flicker'.

A further method for comparison of signal levels utilizes the camera line-up equipment (CLUE), a block diagram of which is shown in Fig. 1.

The master channel and the channel to be adjusted are again fed to the inputs of an electronic switch, the output of which is displayed on a monochrome picture monitor. The switching signal is obtained from a divide-by-four counter fed with line drive pulses.

Alternate blocks of four lines from each input signal are thus displayed on the picture monitor, and inequalities in signal levels at any point will result in horizontal bands of differing brightness. It has been found that a moving pattern provides a more sensitive indication of errors. Therefore the chosen switching frequency results in an upward movement of the pattern of one line per field.

When adjusting signal levels high-frequency response is not essential and it has been found useful on occasions to insert a 1 MHz low pass filter in series with the display device to reduce the noise on the signal and thus obtain a clearer display.
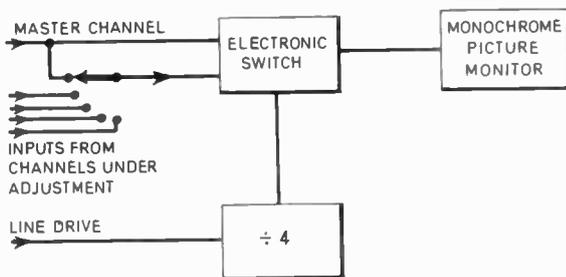

Fig. 1. Simplified diagram of camera line-up equipment (CLUE).

4. Coded Signal Amplitude and Phase Measurement

In this Section of the paper, practical working tolerances for some of the parameters of the coded signal which could be applied to apparatus inside a colour television studio complex are discussed. Details of methods of measurement involved in the line-up of the coder and other apparatus which carries the coded signal will also be given. Test signals particularly suited for continuous monitoring of the parameters of the signal, through all the operational processes of mixing and video-tape recording and replay, are also described.

4.1 Working Tolerances for Burst and Differential Phase

The performance parameters which affect burst and differential phase are those which are of particular interest here. The term 'burst phase' refers to the accuracy with which the burst axes are maintained with respect to the chrominance axes, during burst stabilization and reinsertion processes, in vision mixers and video-tape machines.

Much work has been done on the statistical analysis of measurements made on the diverse items of apparatus which comprise a vision distribution network, from the point at which the signal leaves a studio complex, through switching centres, to the transmitter aerials.
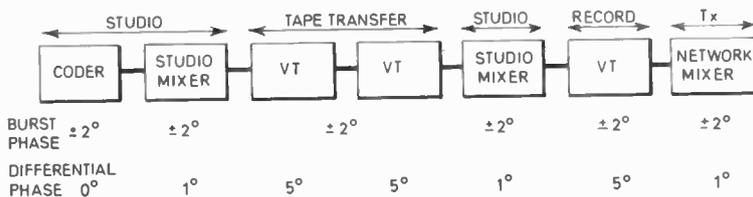
B.R.E.M.A. has recently published recommended maximum tolerances for the PAL colour signal as radiated from the transmitter aerial.†

Recently an analysis has been made of burst and differential phase errors in complete programme chains inside a television studio complex under operational conditions. The object of this analysis was to decide on provisional practical tolerances for the parameters mentioned which could be applied to the signals leaving the studio complex for distribution to the network. An allocation of this tolerance was made to each opera-

Fig. 2. The programme chain.

r.s.s. burst phase $= \sqrt{24} = 4.9$

r.s.s. differential phase $= \sqrt{78} = 8.8$

r.s.s. overall phase errors $= \sqrt{24 + 78} = \sqrt{102} \simeq 10$

†'Technical performance targets for a PAL colour television broadcasting chain', *The Radio and Electronic Engineer*, **38**, No. 4, pp. 201-16, October 1969.

	STUDIO		TAPE TRANSFER		STUDIO	RECORD	Tx
	CODER	STUDIO MIXER	VT	VT	STUDIO MIXER	VT	NETWORK MIXER
BURST PHASE	±2°	±2°	±2°		±2°	±2°	±2°
DIFFERENTIAL PHASE 0°		1°	5°	5°	1°	5°	1°

tional area in the complex, in order that the overall figure would not be exceeded.

The block diagram of the programme chain which was analysed and the tolerances which were allocated to each block in the chain are shown in Fig. 2.

The angular tolerances which are published for the coder are shown in Fig. 3. It will be seen that a maximum error of 2° is allowed, between the burst and chrominance axes.
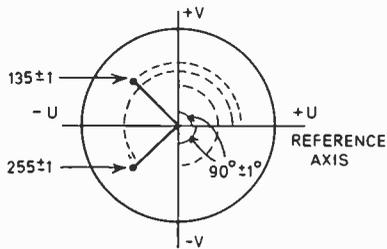

Fig. 3. Coder axis tolerances.

Referring again to Fig. 2 it can be seen that the burst phase of a signal at the output of the vision mixer can also be in error by up to 2°.

The action of burst stabilization incorporated in most vision mixers will reduce any angular error in burst to chrominance axis relationship which may exist on a video tape machine replay, providing that the machine is replaying synchronously, and is phased so that the chrominance axes are correct with respect to the burst axis at the mixer output. This will also apply to any synchronous remote source.

The differential phase errors shown in Fig. 2 are representative of those obtained in practice.

Emphasis was placed on the practical nature of the analysis and it was found that the root of the sum of the squares of the individual tolerances gave a very close approximation to the overall figure obtained in practice. No mathematical justification of this statement has been attempted.

4.2 Methods of Measurement used in Coder Line-up

4.2.1 Coder calibrator

The coder is lined up by means of voltage measurement of the components of a 100% colour bar test signal. The measurements are made differentially with reference to square waveforms of standard amplitude and of approximately 11 kHz frequency.

As the display oscilloscope is being used to compare the amplitudes of sub-carrier signal components with the amplitudes of low frequency square waveforms, it is essential that the amplitude response of the oscilloscope Y amplifier is the same at both frequencies. This is achieved by the use of a simple cable equalizer on the Y amplifier input to the oscilloscope.

The equalizer is set up by the use of a test signal which consists of a sine waveform of approximately sub-carrier frequency, and of precisely 0·5 V peak-to-peak amplitude. This waveform is mixed with the 11 kHz square wave also of precisely 0·5 V p–p amplitude.

The equalization must include compensation for the amplitude loss, at sub-carrier frequency, in any flying coaxial leads or tie lines which are used for connecting the coder output to the oscilloscope and other measuring apparatus. The coder outputs must be monitored at a point in the signal chain, ideally at a jackfield, from which the chrominance to luminance ratio is equalized in the installation.

The waveform as displayed on a correctly equalized oscilloscope is shown in Fig. 4(a).

If the response of the oscilloscope amplifier and associated leads at sub-carrier frequency is high, with respect to the 11 kHz square wave, then the display is as in Fig. 4(b) and conversely if it is low, it is as in Fig. 4(c).

The signals used for the alignment of the coder are generated in a coder calibrator unit which is part of the measuring equipment in every colour mobile control and studio apparatus room.

The reference waveforms from this unit are stable in amplitude to within ± 0·1 dB, over many months of
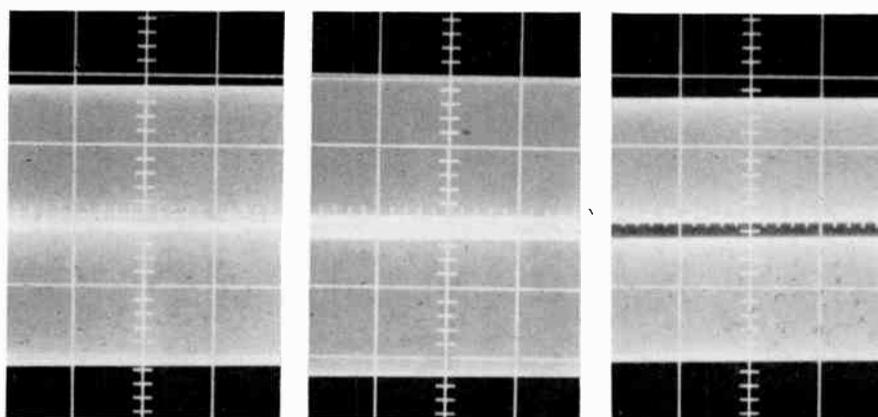
(a) Correct.   (b) High.   (c) Low.

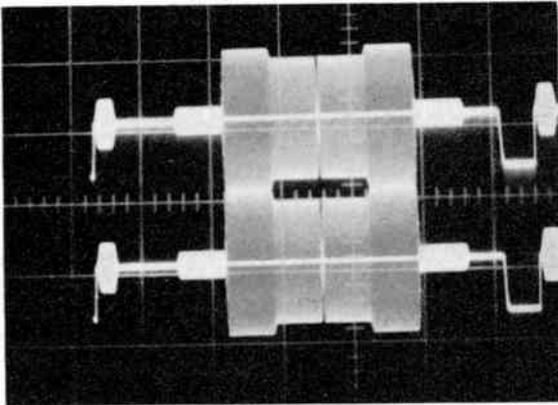Fig. 4. Responses of amplifier to 11 kHz square wave.

Fig. 5. Coder calibration display.

operation, in ambient temperatures between 5°C and 45°C.

The reference amplitudes available are:

(i) Luminance 0·7 V

(ii) Syncs. and burst 0·3 V

(iii) B–Y signal 0·612 V

(iv) R–Y signal 0·861 V

A photograph of the display produced when the R–Y signal is of the correct amplitude is shown in Fig. 5.

The 90° angle between the chrominance axes is set by the 'twitter' method. The coder output is viewed directly on the equalized oscilloscope which is triggered so that the display alternates between successive lines of the PAL waveform.

The 'twitter', which is a difference in amplitude of the waveform on alternate lines, is reduced as nearly as possible to zero by adjustment of the 'coder 90°' control.

The burst 90° angle is pre-set on initial test to an accuracy of 90° ± 1°, using a calibrated 90° delay line and vectorscope.

Carrier balances at black level and at peak white are carried out using the measuring oscilloscope at high gain, with the coder inputs shorted together.

4.2.2 Use of colour signal analyser, 'A-scan' display

The method of coder line-up described in the last section, although accurate in setting signal amplitudes, is not as sensitive as could be desired for the setting of burst and chrominance quadratures. An alternative arrangement is shown in Fig. 6. It will be seen that it consists basically of the circuitry of a conventional colour signal analyser.

It is intended that the four input waveforms that are required should be taken from the distribution to the coder being measured. The coded signal may be taken directly from the coder or via distribution amplifiers.

The signal is passed through a chrominance band-pass filter to an AND gate, the output of the gate being the signal input to the demodulator. The gate is operated by the output of a divide-by-two binary switch, which is triggered by the PAL ident. square wave. The signal into the demodulator thus consists of two lines of signal followed by two lines of no signal.

The oscilloscope trace in the 'no signal' condition is used as a zero reference for the measurements. The oscilloscope is set to give a single line display triggered by line syncs. The signal to the oscilloscope is fed via an IRE roll-off filter to eliminate noise and other spurious signals.

In order to make measurements of carrier balances, all chrominance signals in the coder are switched to 'off'. The demodulation axis in the measuring unit is set to coincide with the B–Y axis of the coder, by adjustment of the goniometer phase shift control. The B–Y axis is identified by the unswitched burst, the components of which, on the two lines displayed, lie over each other.

If a B–Y carrier balance error is present, the demodulator in the measuring apparatus will decode it as a d.c. voltage. As the reference gate switches the demodulator 'on' and 'off' at a two-line rate, the display on the oscilloscope will be that of the reference line (no signal), with a second line, representing the d.c. shift due to the demodulated carrier unbalance. The spacing indicates the amount of error and can be calibrated (Fig. 7(a)). The lines are overlaid when no error exists.

Differential carrier balance (crosstalk) is identified by separation of the two lines representing the period when the demodulator is switched 'on'. Figure 7(b) shows differential carrier balance errors only, Fig. 7(c) shows carrier balance and differential carrier balance errors together.

When the demodulation axis is brought into phase with the R–Y axis, because of the PAL switching action,

Fig. 6. Block diagram of measuring apparatus.

(a) B–Y carrier balance error. R–Y differential carrier balance error.

(b) B–Y differential carrier balance error. R–Y carrier balance error.

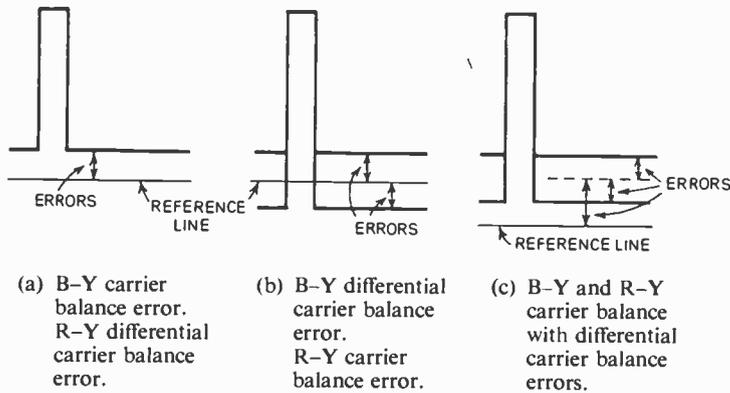(c) B–Y and R–Y carrier balance with differential carrier balance errors.
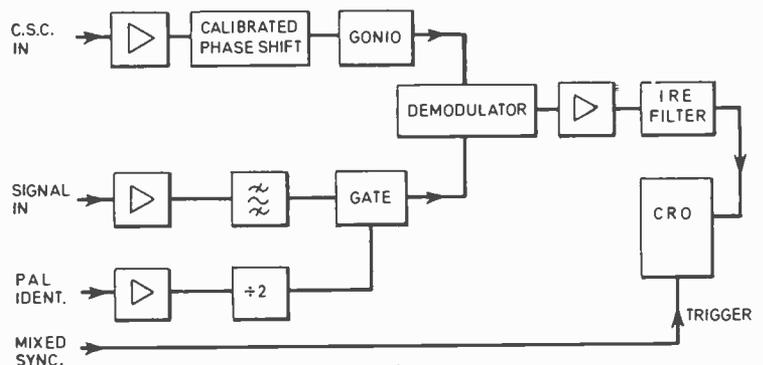
Fig. 7. Balance errors.

a carrier balance error will give a display as in Fig. 7(b) and a differential carrier balance error as in Fig. 7(a).

White balance is checked with the chrominance signals in the coder switched 'on', and with the inputs shorted. The axes are identified as for carrier balance, and the displacement of the trace from the reference line indicates the error which is present.

The quadrature of the chrominance and burst axes can be checked by direct measurement on the calibrated phase shifters.

4.3 Methods of Phasing Coded Sources on a Vision Mixer

4.3.1 Coder phasing and burst stabilization

The signals from the coder jackfield are connected by cables of equal length to the vision mixer inputs. The vision mixer consists of a series of 'cutting' and 'fading' amplifiers, and a 'split screen' effects unit.

The output of the selected amplifier is fed to an output stabilizing amplifier. This unit provides peak white clipping and clamping of the signal, together with sync. reinsertion and burst stabilization. The latter process is necessary in order that fades to black level and mixing can occur, without variation of the burst amplitude.

In the method of burst stabilization in current use, the burst on the input signal to the stabilizing amplifier is compared in amplitude with a reference burst. If an amplitude difference results from the comparison, then the error is fed back into the main signal chain of the stabilizing amplifier, in the appropriate phase, to correct the burst amplitude on the output of the vision mixer. In this particular system of amplitude stabilization, the phase and amplitude of the burst on the output of the vision mixer is always that of the reference burst.

Thus it is necessary that the sub-carrier phases of all coded sources be adjusted so they are coincident with the reference burst, at the point of comparison. The effect on a vectorscope display of colour bars from a burst stabilized vision mixer output when the selected coder phase control is adjusted is one of rotation of the colour bar display around the burst.

It is normally sufficiently accurate to set the burst on the appropriate part of the graticule of a high quality vectorscope, and phase each local coder, by setting the colour bar test waveform from each coder, to lie in the ± 2° 'boxes' on the vectorscope graticule.

Where remote synchronous sources are automatically controlled by a local phase comparator with a phase shifter at the remote site, the requisite accuracy of phasing is achieved by having available a small control of the phase of the reference sub-carrier into the phase comparator.

4.3.2 Test signals in the field interval for use in colour phasing of vision signals

In this paper so far, working tolerances for phasing have been discussed, and methods of measurement and line-up of apparatus have been described, which enable the tolerances to be met.

Consideration has also been given to the provision of a suitable test signal which could be inserted in the field blanking interval and would enable the phase parameters of the colour signal to be continuously monitored, through all the mixing, recording and replaying processes, before being fed to the network. Various forms of insertion test signal (i.t.s.) were considered.

The simplest form of test signal can be generated by the addition of two lines of inverted line-blanking to the burst gating pulse, on the appropriate lines in the field interval. The output of the coder during these two lines would be a block of sub-carrier, switched in phase on alternate lines and of 0·3 V peak amplitude. The amplitude would be at 0·3 V p-to-p, due to the in-built amplitude limiting action of the burst gating pulse input circuitry.

Figures 8(a), (b) and (c) show the waveform of the test signal and also diagrams of vectorscope displays, obtained when the signal is correctly and incorrectly phased, with respect to a stabilized burst.

From the operational point of view it is believed that this particular signal has several disadvantages. If the gain of the vectorscope has been set to give the correct saturation on a reference source of 100% colour bars, then the display of the burst is rather small to enable one to see small angular discrepancies between the stabilized burst and the i.t.s. The signal is of too low an amplitude to give any indication of differential phase
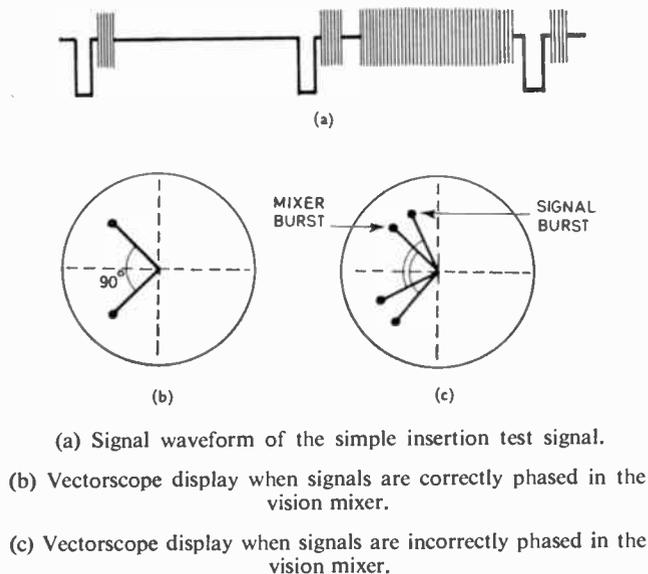
(a) Signal waveform of the simple insertion test signal.

(b) Vectorscope display when signals are correctly phased in the vision mixer.

(c) Vectorscope display when signals are incorrectly phased in the vision mixer.

Fig. 8.

distortion and likewise for absolute sub-carrier amplitude and differential gain.

It was considered that, to be of maximum use, the i.t.s. should be representative of the full excursion of the coded waveform, and that it should be inserted as early as possible in the vision chain. In this way the i.t.s. would indicate the performance of the vision chain in its entirety.

A full 100% colour bar signal is used in the installation to be described. The signal is injected into the coder RGB waveform on two consecutive lines during the field interval.

The method of insertion is shown in Fig. 9. It will be seen that a level raising amplifier is necessary to make up the 6 dB loss in the delta mixing pad. In many installations a distribution amplifier is used to distribute RGB waveforms. In the i.t.s. colour bar installation to be described, the distribution amplifiers were chosen to have 6 dB gain.

The resistors used in the pad are high stability resistors, and the 6 dB amplifier must have a very good gain stability performance. As the RGB signals are monitored, and distributed, after the distribution amplifiers, then any slight discrepancy in amplitudes due to the pads or amplifiers is taken up during line-up of the RGB source.

To avoid the necessity of two colour bar distribution systems in any studio or colour mobile control room that is equipped to use i.t.s. colour bars, one colour bar generator is used for both purposes. Full colour bars are only available when i.t.s. colour bars are not required.

A diagram to show the basis of the modified colour bar distribution system is shown in Fig. 10.

The colour bar generator is normally triggered by mixed blanking to give a full colour bar display. The i.t.s. pulse generator produces line blanking on the two lines chosen for the i.t.s. A relay mounted in the rear

connection panel of the colour bar generator selects either normal mixed blanking or the output of the i.t.s. trigger pulse generator. Thus the colour bar generator can give either full colour bars, or two lines of colour bars in the vertical interval.

The standard colour bar distribution is used, the cabling to the coders being intercepted in order to include the switching unit.

When the control switch is operated to select 'full colour bars', relay RLT is at rest and RLT 1 allows the colour bar generator to be triggered for full colour bars. Relays RLA, RLB, and RLC are also at rest and full colour bars are passed to the colour bar input of the coder for normal use.

The colour bar inputs to the delta mixing pads are terminated with a 75 $\Omega \pm 0.1\%$ resistor. The camera signals are attenuated by 6 dB in the pad, and the loss is made up by the 6 dB amplifiers which are used for RGB signal distribution.
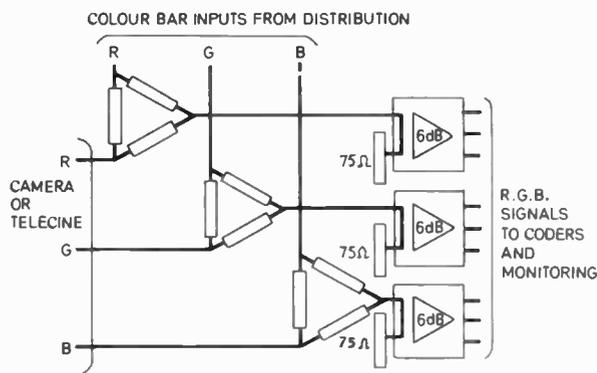

Fig. 9. Insertion of i.t.s. bars.

When the control switch is operated to select 'i.t.s. colour bars', contact RLT 1 makes, to trigger the colour bar generator from the i.t.s. trigger pulse generator, and relays RLA, RLB, and RLC also operate.

The colour bar input to the delta mixing pads is now fed from the output of the colour bar distribution amplifiers which have a 75 $\Omega \pm 0.1\%$ sending impedance. These distribution amplifiers now distribute i.t.s. colour bars, which are mixed with the camera outputs.

This system can be applied to any RGB originating source, cameras, telecine machines or caption scanners.

It will be seen that when i.t.s. colour bars are selected, they are present on all local sources, and full colour bars are not available. It has been shown in studio and outside broadcast operation that full colour bars are not required once the main line-up and vision link tests are completed.

4.3.3 The uses and advantages of interval test signals under operational conditions

It has become an operational requirement to have in the field interval of each signal an indication of some of the main parameters of the signal. This has become necessary in order that, in major network operations, where many telecine and video-tape machines, and remote
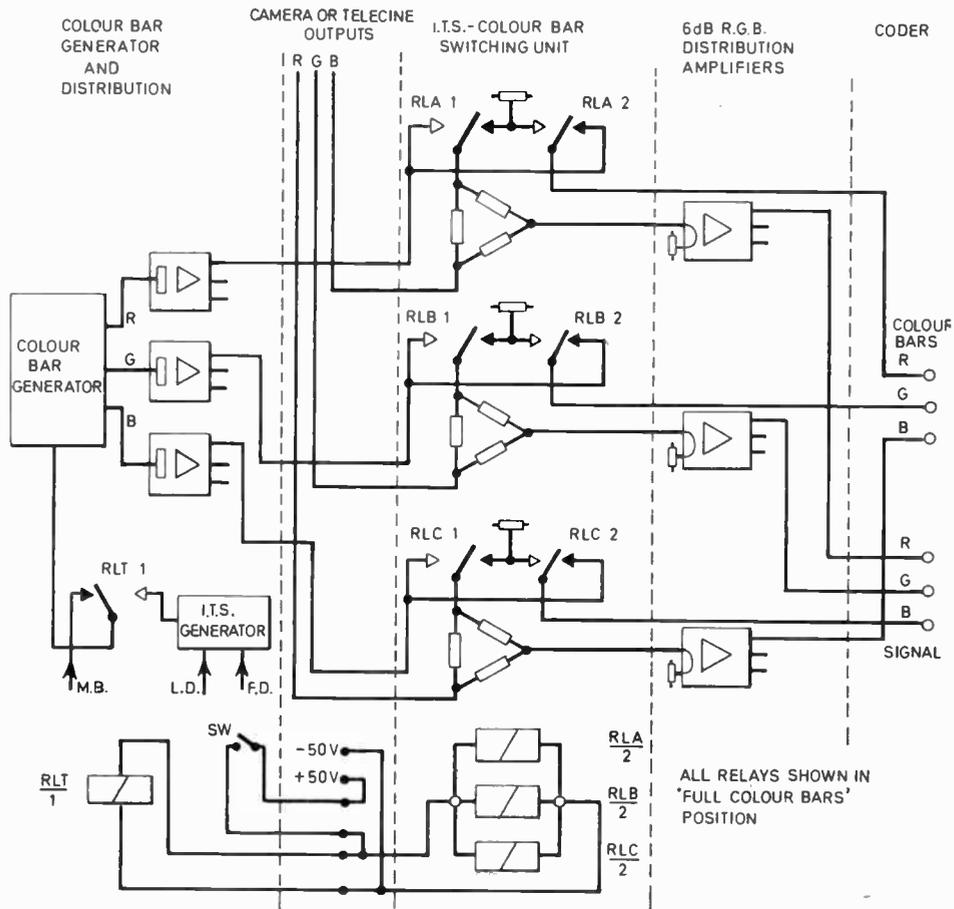
Fig. 10. I.t.s.-colour bar distribution.

outside broadcasts, contribute to a programme, the main signal parameters can be monitored to maintain prescribed tolerances.

Operational experience to date has indicated that the following parameters require to be checked on each contributory source to a programme: chrominance to luminance gain inequality, differential phase and gain errors, absolute phasing of the chrominance axes of the signal (with reference to the colour burst on the output of the main vision mixer).

The i.t.s. 100% colour bar signal enables the checks to be made to a first order by the use of high grade waveform monitors and vectorscopes which have been designed to monitor interval test signals.

The check and any resulting adjustments can be made whilst the signals are in use for rehearsal purposes. Equalization and phasing of the signals on the main vision mixer can be appraised. Signal amplitude adjustments can be made to the complete vision chain and the line-up of decoders can be carried out.

It is believed that with further experience in the use of interval test signals it might be possible to make an improvement in the efficiency of the operation of the service, as some engineering line-up processes could take place whilst signal carrying equipment is in use for operational purposes.

5. Some Waveform Distortion Measurements

Waveform distortion may be introduced not only by the major pieces of equipment such as camera channels, vision mixers, video-tape recorders and micro-wave links, but also by the less complex stages such as distribution and line sending amplifiers, routing devices, etc. In view of the large number of this type of unit through which a vision signal may pass between the source and the transmitter, the amount of distortion introduced by each must be very small. Consequently, it is desirable that methods of measuring waveform distortion should be extremely sensitive.

5.1 Linear Waveform Distortion
5.1.1 Pulse-and-bar methods

The use of a sine-squared pulse and a bar with integrated sine-squared transitions is now well established as a means of assessing the gain/frequency and phase/frequency response of equipment which is used to handle monochrome television signals. For equipment which is to be used with coded colour signals, additional test signals are necessary which are more sensitive to those distortions occurring over the chrominance passband. Consequently variations of the 'pulse and bar' waveform are required.

The process used to transmit the chrominance signal is a double sideband suppressed carrier modulation of a
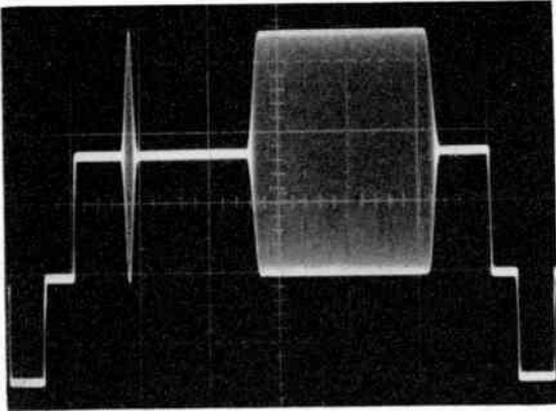
Fig. 11. Colour pulse and bar. Used for assessing linear waveform distortion in the chrominance band and sub-carrier rectification.
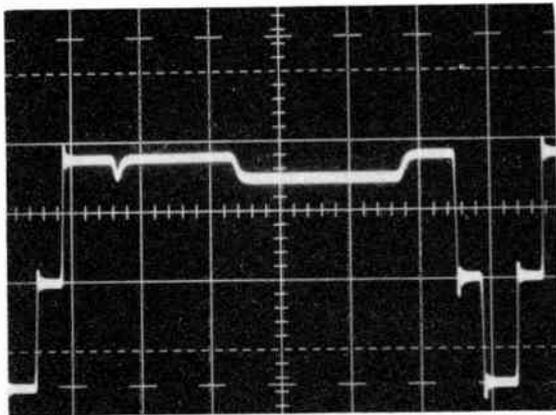

Fig. 12. Colour pulse and bar after the sub-carrier has been removed by filters. The variations in the height of the pedestal are the results of sub-carrier rectification.

sub-carrier whose frequency is approximately 4·43 MHz. Since the chrominance signal has a bandwidth of 1 MHz the chrominance circuit is required to pass signals between 3·4 MHz and 5·4 MHz.

The signal used to assess linear waveform distortion over this band consists of a 4·3 MHz carrier which is suitably modulated with a sine-squared pulse and bar whose bandwidth is sensibly 1 MHz, i.e. the half amplitude duration of the pulse is 1 μs. The modulated pulse and bar are symmetrical about a mean level and they are superimposed on a pedestal of half their peak-to-peak value.

Distortion occurring over the chrominance passband may be assessed by matching the received waveform to an engraved graticule in the usual way. K-factors may thus be assigned.

If equipment is unable to handle high amplitudes of colour sub-carrier, or if there is any degree of non-linearity, partial sub-carrier rectification may take place. This introduces a component which causes a change in the luminance signal amplitude, i.e. chrominance to luminance 'crosstalk' occurs.

To detect and measure sub-carrier rectification the modulated bar is used. At the receiving terminal the sub-carrier is removed by means of a band-stop filter.

Sub-carrier crosstalk will produce a change in the amplitude of the pedestal which can be seen easily by comparison with the pedestal on either side of the bar. The variation in pedestal height expressed as a percentage of the chrominance amplitude is the amount of chrominance/luminance crosstalk.

5.1.2 Sine-squared pulse method

Generally the variations in transfer characteristic which produce distortion of the pulse shape are smooth, and loss of one sideband with respect to sub-carrier frequency may be compensated by relative boost to the other sideband. This, however, may result in an overall loss or increase of the chrominance signal amplitude with respect to the luminance signal amplitude. Similarly, errors in chrominance to luminance timing may occur.

For accurate comparison of chrominance/luminance gain and delay it is desirable that both the modulated chrominance pulse and the original modulating waveform are available at the measuring point. The waveform used is formed by the linear addition of a modulated sine-squared pulse of half-amplitude duration 1 μs and the modulating pulse. The resulting waveforms are shown in Fig. 13.

The base of the waveform is normally flat (Fig. 13(a)). Chrominance/luminance gain inequality will cause the base of the waveform to bow upwards for chrominance loss (Fig. 13(b)), and downwards for chrominance boost (Fig. 13(c)).

Chrominance/luminance delay inequalities cause the base of the waveform to become S-shaped (Fig. 13(d) and (e)).

To measure these gain and delay inequalities special test equipment is used (Fig. 14). At the receiving point the distorted signal is split into two chains (chrominance and luminance) by band-pass and band-stop filters. One chain contains a variable gain and a variable delay stage. The other has a fixed gain and delay which is equal to half that of the variable gain and delay stages.
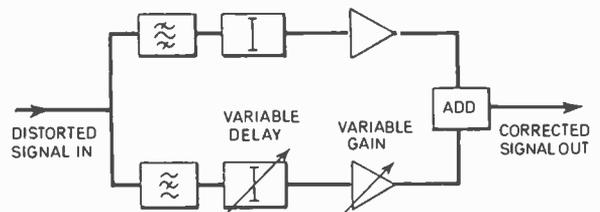
Fig. 14. Simplified diagram of colour gain and delay tester.

The controls are adjusted to produce gain and delay inequalities of the same magnitude but in the opposite sense to those present on the received signal and thus reproduce the original waveshape. The additional signals required are combined with the existing ones to produce the chrominance/luminance pulse and bar waveform (Fig. 15).

This consists of

(i) A sine-squared pulse of half amplitude duration 0·1 μs or 0·2 μs.

(ii) A chrominance pulse.

(iii) A 10 μs pedestal with a 7 μs block of colour sub-carrier.

(iv) A 22 μs bar with transitions corresponding to the selected pulse.

(v) Line synchronizing pulses 0·3 V peak-to-peak negative-going.

5.2 Non-linearity Distortion

Assessment of the non-linearity distortion introduced by circuits which are to be used for monochrome signals is usually made with a five-step staircase waveform. The received signal is differentiated, and the resulting pulses are filtered to give them an approximate sine-squared shape. Incremental gain variations are revealed as variations in the height of the pulses.

In order to measure differential gain and phase distortion colour sub-carrier is added to each of the levels of the staircase. Synchronizing pulses and a reference burst are also included (Fig. 16).

(a) Normal pulse.

(b) Chrominance loss.

(c) Chrominance boost.

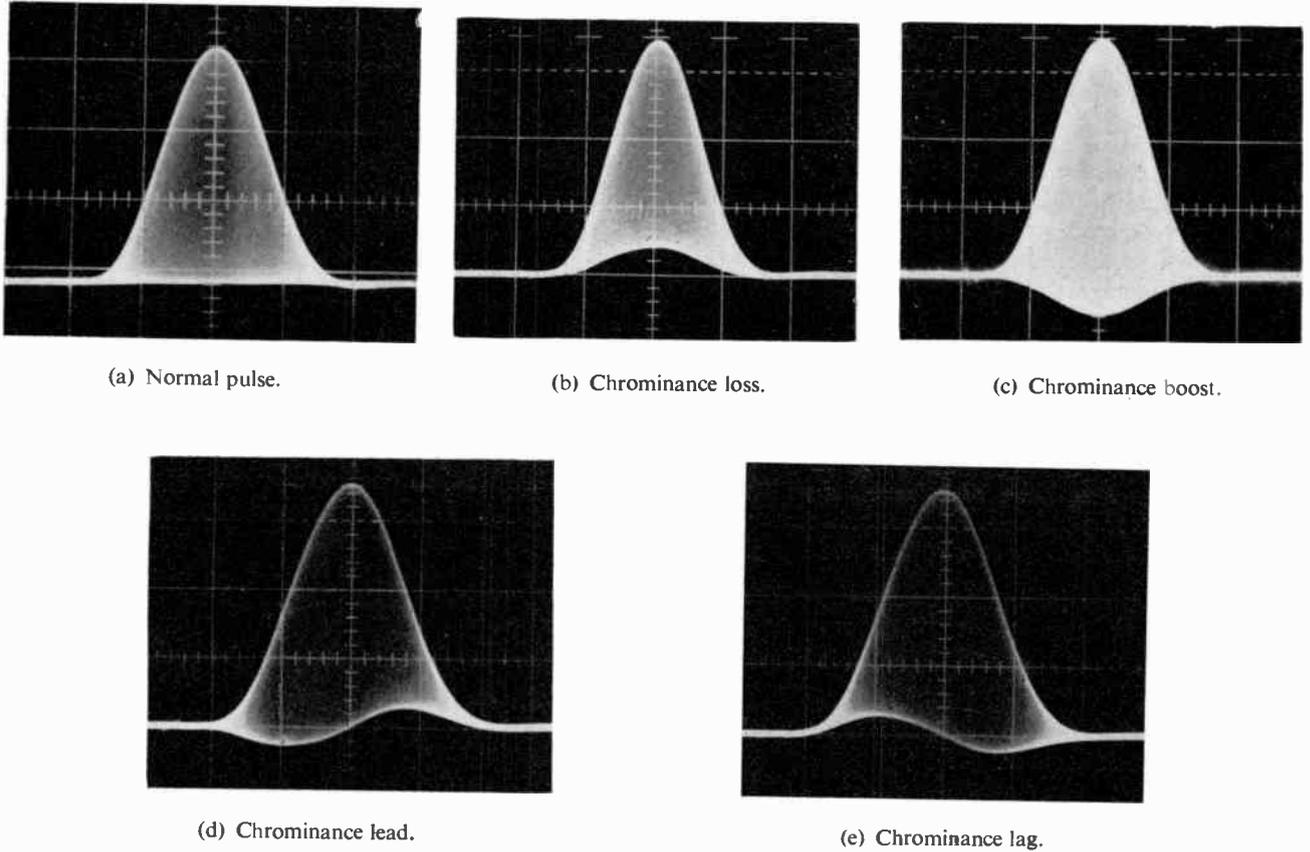(d) Chrominance lead.

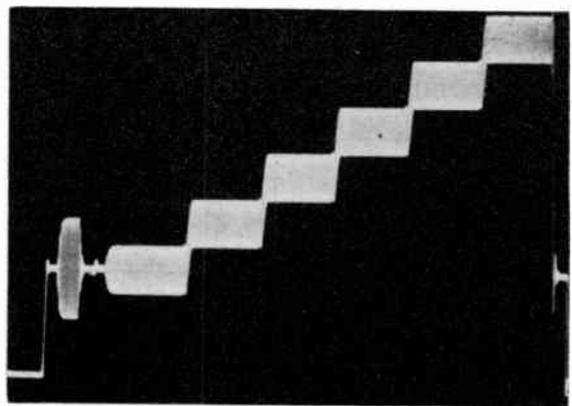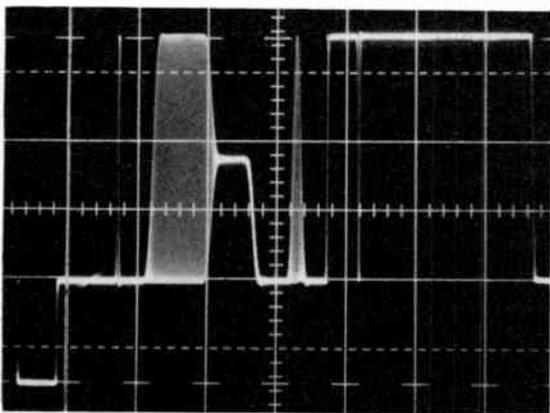(e) Chrominance lag.

Fig. 13. Chrominance pulse waveforms.

Fig. 15. The chrominance/luminance pulse-and-bar waveform.

Fig. 16. Staircase with added sub-carrier for measurement of differential gain and phase distortions.
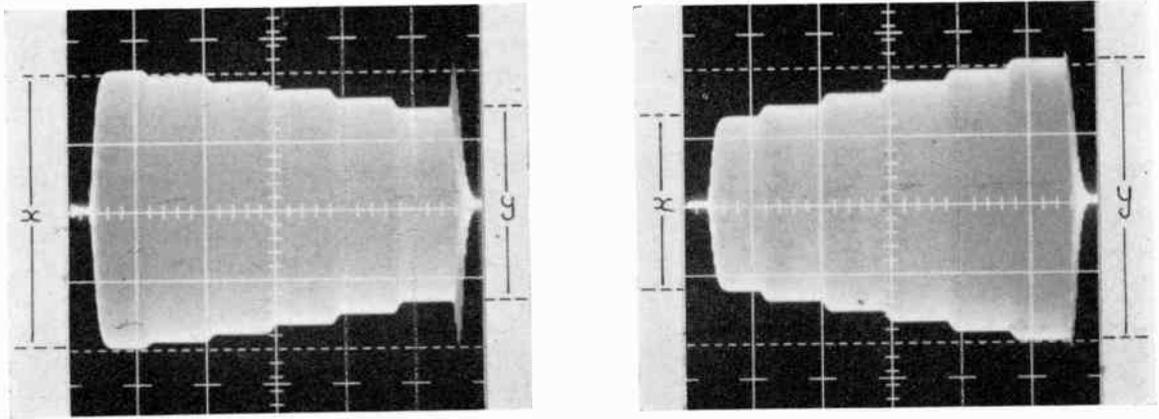
Fig. 17. Sub-carrier extracted from distorted waveform showing differential gain.

Differential gain distortions will cause the amplitude of the superimposed sub-carrier to vary from step to step. These amplitude variations are more easily seen if the signal is passed through a band-pass filter which rejects all but the sub-carrier (Fig. 17).

Differential gain is expressed as

$$\frac{x \sim y}{x} \times 100\%$$

where y is the amplitude of sub-carrier which differs most from the amplitude of the sub-carrier which occupied the black level period of the test signal x.

Differential phase distortion causes the phase of the superimposed sub-carrier to change from step to step. It is of course almost impossible to detect these phase changes with an oscilloscope.

The equipment used to measure differential phase distortion (Fig. 18) consists of:

(i) A burst locked oscillator which will regenerate sub-carrier at the same frequency as that on the test signal.

(ii) A calibrated phase shifting network.

(iii) A synchronous phase demodulator.

(iv) A suitable display device.

The output from the phase demodulator will vary in amplitude as the phase between the signal being measured and the regenerated sub-carrier varies. During the line blanking interval the demodulator output is zero, and this is used as reference level. The display is easier to read if this reference level is clamped to zero volts (Fig. 19(a)).

The controls of the calibrated phase shift network may be adjusted to position any part of the display on the reference. It is thus possible to measure the phase difference between the sub-carrier at black level, and that on any other step (Fig. 19(b) and (c)). The largest of these phase differences is quoted as the differential phase distortion.
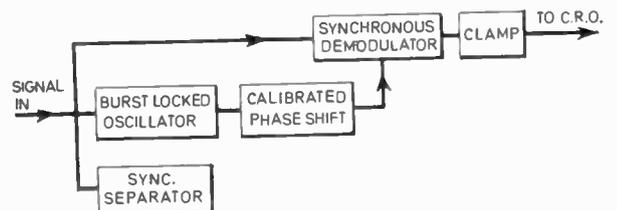

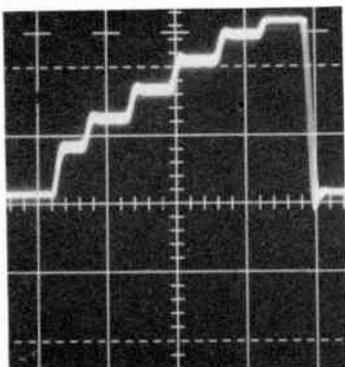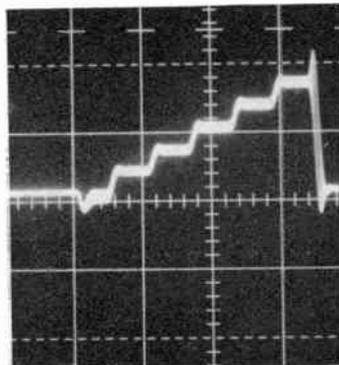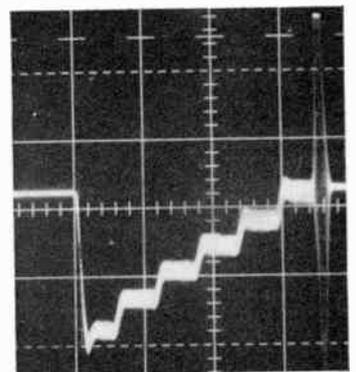Fig. 18. Simplified diagram of a signal analyser.

Fig. 19. (a) Demodulator output showing differential phase distortion.

(b) The step which corresponds to sub-carrier at black level is positioned beside the reference.

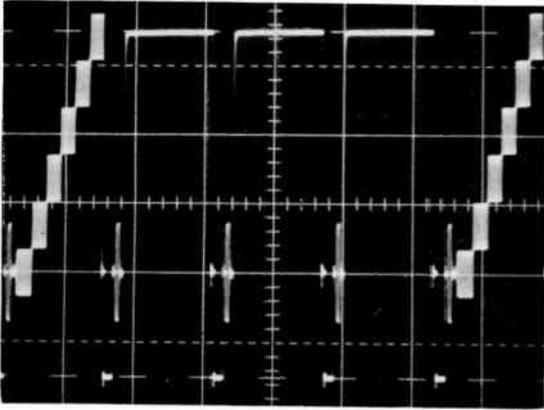(c) Calibrated control adjusted to position white step opposite reference.

Fig. 20. Staircase waveform on one line in four. The other lines may be white level or black level.

The output from the demodulator produced by the reference burst is suppressed.

The test signals may be generated at standard line-up level (1 V peak-to-peak) and also at +3 dB. To produce a change in mean level of the test signal the staircase waveform may be generated on one line only out of each successive four lines. The remaining three may be either at peak white level or at black level (Fig. 20).

5.3 Noise Measurement

It is well known that the subjective annoyance of noise on a picture decreases as the noise frequency increases. A weighting network may be used to attenuate the higher frequencies when making measurements of the signal-to-noise ratio.

With colour signals the noise which occurs in the chrominance band will be demodulated in the decoder, and appear on the displayed picture as low frequency noise. It is therefore necessary to be able to measure the noise introduced in the chrominance band.

This is done with the aid of a 2 MHz band pass filter centered about 4·43 MHz. The transfer characteristic of the filter gives the same weighting to noise components up to 1 MHz on either side of the centre of the passband as is given to noise up to 1 MHz by a luminance weighting network.

6. Acknowledgments

The authors wish to thank the Director of Engineering of the British Broadcasting Corporation for giving his permission to publish the paper and their colleagues in the Television Operations and Maintenance Department for assistance in the preparation of material.

The Authors

Mr. I. H. Teear joined the B.B.C. in 1943 at their Receiving Station at Tatsfield, Surrey. After a period in the Royal Navy Air Service as an air radar mechanic, he returned to the B.B.C. in 1952 as a junior engineer with the Television Service. He joined the B.B.C.'s experimental colour television team in 1960 and since 1967 has headed the technical investigations section in the television operations and maintenance department. He is now concerned with the detailed investigation of technical problems that occur in the operation of the Television Service.

Mr. J. D. Hughes (Member 1967; Graduate 1960) served a student apprenticeship with the Marconi Co. Ltd. and was subsequently employed as an engineer in the television development group. In 1961 he joined B.B.C. Television Outside Broadcasts and in 1967 transferred to the Television Services Department. At present, as an assistant to the Head of Engineering, Television Services, he is engaged on the investigation of operational and technical problems in colour television.

Mr. M. E. Hill (Graduate 1962) joined the B.B.C. as a technical assistant in the Television Service in 1959. In 1962 he was appointed to the Engineering Training Department as an assistant lecturer and he later transferred to Television Outside Broadcasts as the on-station instructor. At present he is with the technical investigations section and is engaged in the detailed investigation of the technical and operational problems of outside broadcasts.

Relationship between F.M. Noise and Current Noise in a Cavity-controlled Gunn Effect Oscillator

By

M. L. MEADE, B.Sc. Tech.†

A theory is developed to account for the observed ratio of f.m. noise and current noise in a cavity-controlled Gunn effect oscillator. The noise processes are assumed to have their origin in spontaneous fluctuations in the carrier concentration of the GaAs layer which give rise to a modulation of the Gunn diode impedance. The principal parameters of interest in the study are device current and domain capacitance both of which are functions of the carrier concentration n and the internal field F of the GaAs layer.

In order to estimate the relative contribution of the two terms in the expression derived for fluctuation in the device an analysis is made of the fluctuation mechanisms in terms of the zero-diffusion model of a propagating domain. It is concluded that the term representing the effect of internal field fluctuations makes only a minor contribution to the f.m. noise and current noise. Experimental evidence is produced in support of the theoretical study and an estimate is made of the carrier concentration fluctuation.

1. Introduction

Gunn effect oscillators have become established as a convenient and reliable means of microwave power generation and they are now finding application as klystron replacements in a variety of systems where cost and size are at a premium. A great deal of effort has gone into improving the frequency stability of Gunn effect oscillators for applications where oscillator noise determines the ultimate sensitivity of the system, and Hobson[1] has proposed a fundamental limit to the frequency stability. The limit is governed by the time jitter of the current waveform at the point of domain triggering, and is essentially a thermal noise restriction, requiring that the fluctuation in the instantaneous frequency of the oscillator (f.m. noise) is a white-noise process. Unfortunately, as is often the case with semiconductor devices, the thermal noise processes are masked at low frequencies by excess noise which has a $1/f$ power spectrum and which is usually sufficiently strong to be dominant at modulation frequencies greater than 1 MHz. Because of the steady roll-off in f.m. noise power it is possible to have the situation where a Gunn effect oscillator compares unfavourably with a klystron for audio-frequency fluctuations, but is superior to the klystron in a higher frequency band. For a carefully designed Gunn effect oscillator and an average local oscillator klystron the cross-over point usually occurs at noise modulation frequencies between 1 kHz and 10 kHz.

When a Gunn effect oscillator is operated under constant-voltage conditions the device current is found to exhibit fluctuations which have the characteristics of $1/f$ noise. It has been shown[2] that the f.m. noise and the current noise have a reasonably high index of correlation (typically 0·6–0·8) and that the f.m. noise remains unchanged when the oscillator is supplied from a constant-current source.[3] In this case correlation exists between the f.m. noise and the $1/f$ noise voltage appearing at the diode terminals.

† Physics Department, J. J. Thomson Laboratory, University of Reading, Whiteknights, Reading RG6 2AF.

The $1/f$ nature of the correlated noise processes suggests that they have a common, non-thermal, origin and it is consistent with the experimental evidence to attribute these observable fluctuations to non-thermal variations of the carrier concentration in the active GaAs layer.

Carrier concentration fluctuations have the effect of modulating the Gunn diode impedance as viewed from both the d.c. bias and microwave circuits. Under constant-voltage conditions the resulting fluctuations in the diode bias current and in the frequency (and amplitude) of microwave oscillation may be regarded as linearly scaled versions of the original fluctuation in carrier concentration, provided of course that the percentage fluctuations are sufficiently small. In practice the linearity of the modulation is emphasized by the fact that the current noise and f.m. noise have similar spectral characteristics and exhibit an appreciable degree of correlation.

The purpose of this paper is to account for the ratio of f.m. noise to current noise which we have measured recently in a large batch of Gunn oscillators in terms of the domain theory of Butcher, Fawcett and Hilsum[4] and the small-signal equivalent circuit theory of Hobson.[5]

2. Method of Analysis

When assessing the effect of carrier concentration fluctuations on the impedance of the Gunn diode the principal parameters of interest are device current and domain capacitance which can generally be written in terms of both carrier concentration, n, and the internal field, F, of the GaAs layer. We calculate the fluctuation in a device parameter γ from an expression of the form

$$\Delta\gamma(t) = \left[\frac{\partial\gamma}{\partial n} + \frac{\partial\gamma}{\partial F}\frac{\mathrm{d}F}{\mathrm{d}n}\right]\Delta n(t) \qquad \text{......(1)}$$

where $\Delta n(t)$ is the non-thermal fluctuation in carrier concentration, measured from the mean value $n = n_0$.

In writing (1) we have assumed that the derivatives are sensibly constant for small deviations from the selected operating conditions but we have included no bandwidth

limitation in the formulation. Now in practice there will always be a finite time-constant which limits the rate at which the domain structure can fluctuate, following variations in the carrier concentration. When operating in a transit-time mode the effective time-constant is determined by the domain capacitance and the bulk resistance of the GaAs layer, whilst in cavity-controlled operation the time-constant is much larger and is approximately equal to the decay-time of the resonant structure. In either case the effective bandwidth is large compared with the low-rate fluctuations which are of interest and we can include fluctuation-modulation frequencies of several megahertz in our calculations.

The second term on the right-hand side of equation (1) represents the contribution made by fluctuations in the internal field configuration of the GaAs layer and these in turn can be related to velocity fluctuations of the domain in transit. Matsuno[6] has used these fluctuations in his description of a Gunn oscillator noise model but has relied upon the experimental determination of some of the important differential coefficients. Now it is very difficult to make small static changes in the operating conditions of a Gunn oscillator without introducing spurious thermal effects due to heating of the sample, also the results obtained are not explicitly related to the dimensions of the Gunn diode structure. In view of these difficulties there is an obvious need to supplement the work of Matsuno by a theoretical study of the fluctuation mechanisms in the Gunn effect; this would enable us to interpret noise data without the need for poorly-defined supplementary measurements and give an indication of the relative contribution of the two terms in equation (1).

We have accordingly carried out an analysis based on the zero-diffusion model of a stable propagating domain described by Butcher, Fawcett and Hilsum.[4] This is the only domain description which lends itself to analysis without resort to digital computing techniques and many of the calculations can be resolved by means of simple geometric constructions. Despite the simplifications inherent in the zero-diffusion theory a number of important features emerge which are applicable to more complicated domain structures. This is particularly the case when the domain area is considered rather than the specific shape of the domain.

3. The Domain Model

With the short sample length of an X-band Gunn diode and bias fields not more than a few times threshold, the electric field within the GaAs layer, in the limit of zero diffusion, has the form of a propagating triangular domain region surrounded by neutral material. The uniform field within this external region is denoted by F_R and is less than the threshold field F_T. The peak domain field is F_D, the domain width is d and the zero-diffusion approximation requires that the domain velocity, v_D, is equal to the drift velocity, v_R, of the electrons in the neutral low-field region. Figure 1 shows the domain structure and Fig. 2 shows the fields F_R and F_D in relation to a three-line static velocity-field characteristic for GaAs.[4]
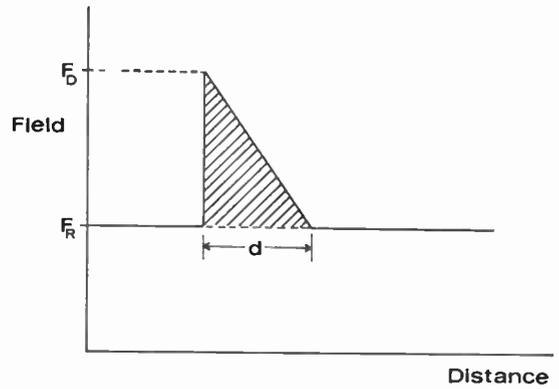
Fig. 1. Internal field distribution in the limit of zero diffusion.

The domain potential ϕ_D is defined as the area under the field plot above the field F_R in Fig. 1. We have

$$\phi_D = \tfrac{1}{2}d(F_D - F_R) \qquad \ldots\ldots(2)$$

where the domain-width is[4]

$$d = \frac{\varepsilon_0\,\varepsilon_r}{en}(F_D - F_R) \qquad \ldots\ldots(3)$$

Here n is the carrier concentration and ε_r is the relative permittivity of bulk GaAs. Combining equations (2) and (3) we obtain

$$\phi_D = \frac{\varepsilon_0\,\varepsilon_r}{2en}(F_D - F_R)^2 \qquad \ldots\ldots(4)$$

Equation (4) can be rewritten to eliminate the peak domain field F_D. To do this we make use of the 'equal areas rule'[4] which relates F_D, F_R and the domain velocity and requires that the areas shown shaded in Fig. 2 are equal in magnitude. The domain potential can now be written as

$$\phi_D = \frac{\varepsilon_0\,\varepsilon_r}{2en}(1+\alpha)^2(F_T - F_R)^2 \qquad \ldots\ldots(5)$$

α is a constant of the material given by

$$\alpha = \frac{F_V - F_T}{F_T - F_{RV}} \qquad \ldots\ldots(6)$$

Fig. 2. Three-line approximation to the static velocity-field characteristic showing the fields F_T, F_R and F_D. The shaded areas are equal in magnitude.

F_V is the valley field and F_{RV} is defined in terms of the low- and high-field mobilities μ_1 and μ_2.[4]
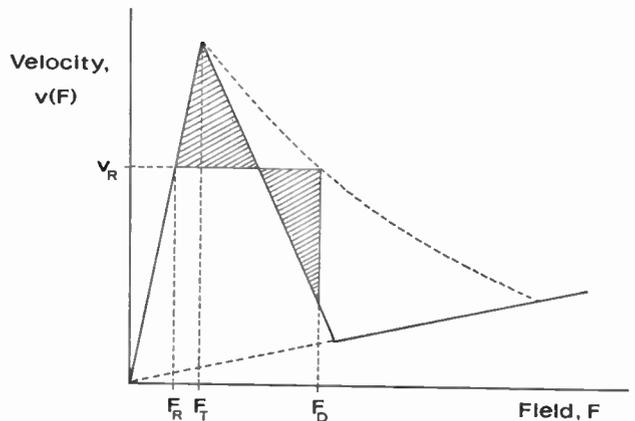
A further relationship between ϕ_D and the 'outside-field' F_R arises from the external bias condition obtained by integrating the field distribution in Fig. 1 over the length l of the GaAs layer. If the applied bias voltage is ϕ_B, then

$$\phi_B = \phi_D + F_R l \qquad \ldots\ldots(7)$$

Because ϕ_D is defined in terms of the domain area, (7) is a general result which does not depend upon the specific shape of the domain. We see that if ϕ_D is fluctuating as a result of fluctuations in carrier concentration then there must be a compensating variation in F_R to maintain the bias condition (7). Differentiating equation (7) with the bias voltage held constant we obtain,

$$\frac{d\phi_D}{dn} + l\frac{dF_R}{dn} = 0 \qquad \ldots\ldots(8)$$

We now have sufficient information to specify the domain parameters in terms of the GaAs constants and to calculate the derivatives $d\phi_D/dn$ and dF_R/dn for use in following sections. We obtain

$$\left.\begin{array}{l} \dfrac{dF_R}{dn} = \dfrac{-\phi_D}{n}\left[\dfrac{(F_T - F_R)}{2\phi_D - l(F_T - F_R)}\right] \\[2mm] \dfrac{d\phi_D}{dn} = -l\dfrac{dF_R}{dn} \end{array}\right\} \qquad \ldots\ldots(9)$$

4. Current Noise

From a physical viewpoint the neutral region with uniform field F_R and the domain region are series connected. Whilst the domain is in transit, therefore, the current in the external circuit can be made equal to either the conduction current outside the domain or to the displacement current within the domain. The conduction current density is

$$J = nev_R = ne\mu_1 F_R \qquad \ldots\ldots(10)$$

where the drift velocity is determined by the low-field mobility μ_1 and the outside field F_R.

Measurements show that both above and below threshold thermal noise and shot noise in the Gunn diode current are masked by a $1/f$ process. Let us now suppose that when a domain is in transit the carrier concentration has a non-thermal fluctuation $\Delta n(t)$ measured about the mean value n_0, and calculate the resulting fluctuation in current density $\Delta J(t)$, when thermal noise and shot noise are negligible. We obtain

$$\Delta J(t) = \left[\frac{\partial J}{\partial n} + \frac{\partial J}{\partial F_R}\frac{dF_R}{dn}\right]\Delta n(t) \qquad \ldots\ldots(11)$$

$$= e\mu_1\left[F_R + n\frac{dF_R}{dn}\right]\Delta n(t) \qquad \ldots\ldots(12)$$

Both equation (12) and the subsequent relation (13) (below) are quite general in form and are applicable to any domain model.

Now the collapse and nucleation of a domain are governed by a very short time-constant, so that the noise current-density is given by equation (12) for the greater part of a transit cycle. Low-pass filtering in the bias current monitor circuit will result in an output proportional to a smoothed version of $\Delta J(t)$ with an upper cut-off frequency determined by the monitor circuit— this may be well into the u.h.f. region. If the device area is A_0 then the current fluctuation for frequencies within the monitor circuit bandwidth is

$$\Delta i(t) = A_0 e\mu_1\left[F_R + n\frac{dF_R}{dn}\right]\Delta n(t) \qquad \ldots\ldots(13)$$

The derivative dF_R/dn has been given by equation (9). Combining (9) and (13) we obtain,

$$\Delta i(t) = A_0 e\mu_1\left[F_R - \frac{\phi_D(F_T - F_R)}{2\phi_D - l(F_T - F_R)}\right]\Delta n(t) \qquad \ldots\ldots(14)$$

5. F. M. Noise in Cavity-controlled Oscillators

When a cavity-controlled Gunn oscillator is in stable oscillation the reactance of the active device is balanced by an equal and opposite component from the external circuit. Fluctuations in the device reactance must now be compensated by variations in the frequency of oscillation, ω_0, and a first-order analysis shows how the frequency fluctuations (f.m. noise) can be reduced by the use of an external circuit with high Q-factor.

If we assume that the cavity control mechanism has a simple phenomenological description such as the delayed transit-time mode[7] or the 'quenched' domain mode of operation,[8] then the choice of a moderately high bias voltage ensures that the domain is in transit for the greater part of a microwave cycle. The average reactance of the Gunn diode over a microwave period now approaches a value appropriate to a device containing a domain which is perturbed by an r.f. field. A rigorous analysis of the true experimental situation can only be carried out by a computer simulation; however we would hope to gain some physical insight into the fluctuation mechanisms by using Hobson's results[5] for the small-signal Gunn diode impedance, calculated by considering the response of the device to an r.f. signal perturbation. This shows that the diode reactance can be approximated by the small-signal capacitive reactance of the dipole domain which has net charge q_D given by the integral

$$q_D = \int_0^\infty [N(x) - n]e\,dx \qquad \ldots\ldots(15)$$

where $N(x)$ is the electron density as a function of position within the sample and n is the carrier concentration of the GaAs layer. Referring to the triangular domain structure shown in Fig. 1, the spatial origin is at the position of peak domain field F_D and the integration is taken in either the positive or negative direction. Using Poisson's equation, (15) may be evaluated to give,

$$\left.\begin{array}{l} q_D = \varepsilon_0\varepsilon_r(F_D - F_R) \\[1mm] = [2\varepsilon_0\varepsilon_r ne\phi_D]^{\frac{1}{2}} \end{array}\right\} \qquad \ldots\ldots(16)$$

Equation (16) refers to unit cross-sectional area. The small-signal domain capacitance for a device of area A_0 is given by

$$C_D = A_0\left[\frac{\partial q_D}{\partial \phi_D}\right] = A_0\left[\frac{ne\varepsilon_0\varepsilon_r}{2\phi_D}\right]^{\frac{1}{2}} \qquad \ldots\ldots(17)$$

Let us now suppose that the carrier concentration in the GaAs layer has a non-thermal fluctuation $\Delta n(t)$ about a mean value n_0. The resulting fluctuation in domain capacitance is now

$$\Delta C_D(t) = \left[\frac{\partial C_D}{\partial n} + \frac{\partial C_D}{\partial \phi_D} \cdot \frac{d\phi_D}{dn}\right] \Delta n(t) \qquad \ldots\ldots(18)$$

Using equations (9) and (17) we obtain

$$\Delta C_D(t) = \frac{C_D}{n}\left[\frac{\phi_D - l(F_T - F_R)}{2\phi_D - l(F_T - F_R)}\right]\Delta n(t) \qquad \ldots\ldots(19)$$

If the Gunn diode is coupled to a microwave circuit with net reactance X_0, then it can be shown that the fluctuation $\Delta\omega(t)$ in the oscillation frequency ω_0 required to compensate the above changes in domain capacitance is approximately

$$\Delta\omega(t) = \frac{\Delta C_D(t)}{\omega_0\left[\dfrac{dX_0}{d\omega}\right]C_D^2} \qquad \ldots\ldots(20)$$

This formulation is valid for fluctuations well within the bandwidth of the microwave circuit.

We can convert equation (20) to a more useful form by noting that the loaded Q-factor of any resonant structure is given by

$$Q_L = \frac{\omega_0}{2R_L}\left[\frac{dX_0}{d\omega}\right] \qquad \ldots\ldots(21)$$

where R_L is the total circuit loss. In the case of a negative resistance oscillator the amplitude of oscillation builds up until R_L is cancelled by an equal and opposite component from the active part of the circuit.

6. F. M. Noise to Current Noise Ratio

The purpose of this Section is to derive an expression for the ratio of f.m. noise and current noise in a Gunn effect oscillator on the assumption that the oscillator is delivering maximum power at a bias field of approximately three times threshold. We shall further assume that the product of carrier concentration and length of the GaAs layer, $n_0 l$, is approximately 10^{16} m^{-2}; this condition is appropriate for both X-band and Q-band operation and ensures that the domain width is much less than the layer length.

We shall use the GaAs parameters of reference 4 which gives a small but finite value for μ_2, the high field mobility. The final results are found to be substantially independent of the precise value of μ_2, provided that the ratio μ_1/μ_2 is sufficiently high (> 100). Solving equations (5) and (7) simultaneously for a bias voltage of $3F_T l$, and an $n_0 l$ product of approximately 10^{16} m^{-2}, the domain potential and outside field are, to a close approximation,

$$\phi_D/l = 6\cdot5 \times 10^5 \text{ V/m}, \quad F_R = 2\cdot5 \times 10^5 \text{ V/m} \quad \ldots\ldots(22)$$

Calculating first of all the current noise from equation (14) we obtain

$$\Delta i(t) = 2\cdot2 \times 10^{-14} A_0 \Delta n(t) \qquad \ldots\ldots(23)$$

The internal field fluctuation is accounted for by the second term in equation (14) which makes only a 10% contribution at the selected bias voltage; the result is not significantly affected by a $\pm10\%$ change from the

bias voltage of $3F_T l$ (±1 V at X-band). For progressively higher bias voltages however, the second term makes a larger contribution whilst F_R is reduced. The net result is a reduction in current noise because dF_R/dn is negative. Examination of equation (14) for large bias voltages shows that the current noise cannot fall to zero as long as the sample supports a triangular domain.

Turning now to f.m. noise (Section 5), we make use of the following expression for domain capacitance calculated from equation (17):

$$C_D = 3\cdot7 \times 10^{-18} A_0 \left(\frac{n_0}{l}\right)^{\frac{1}{2}} \qquad \ldots\ldots(24)$$

For $0\cdot01$ Ωm material with active length 10 μm, C_D has a value of about $0\cdot3$ pF.

Inserting the internal field values from (22) into equation (19) we calculate the following value for the capacitance fluctuation

$$\Delta C_D(t) = 0\cdot48 \frac{C_D}{n}\Delta n(t) \qquad \ldots\ldots(25)$$

Now the value obtained when the second term in equation (18), involving $d\phi_D/dn$, is neglected is

$$\Delta C_D(t) = \frac{C_D}{2n}\Delta n(t) \qquad \ldots\ldots(26)$$

Comparison of these two results shows that on the basis of the zero-diffusion model the fluctuations of the internal field do not have a significant effect on the variation of domain capacitance with respect to carrier concentration. These remarks apply for bias voltages such that $2\phi_D \gg (F_T - F_R)l$.

The frequency fluctuation corresponding to a carrier concentration fluctuation $\Delta n(t)$ may now be calculated from equation (20) using (19) and (24); we obtain

$$\Delta\omega(t) = \frac{6\cdot3 \times 10^{16}}{A_0 Q_L R_L}\left(\frac{l}{n_0^3}\right)^{\frac{1}{2}}\Delta n(t) \qquad \ldots\ldots(27)$$

$\Delta\omega(t)$ represents the deviation of the oscillator frequency from the mean value ω_0. Let us define the r.m.s. frequency deviation in hertz by

$$\Delta f_{r.m.s.} = \frac{1}{2\pi}\left[\overline{\Delta\omega^2(t)}\right]^{\frac{1}{2}} \qquad \ldots\ldots(28)$$

Similarly the r.m.s. values of the current fluctuation and the concentration fluctuation are respectively $\Delta i_{r.m.s.}$ and $\Delta n_{r.m.s.}$.

The ratio of f.m. noise to current noise may now be calculated from equations (23) and (27), the result being

$$\frac{\Delta f_{r.m.s.}}{\Delta i_{r.m.s.}} = \frac{4\cdot55 \times 10^{29}}{A_0^2 Q_L R_L}\left(\frac{l}{n_0^3}\right)^{\frac{1}{2}} \qquad \ldots\ldots(29)$$

For the purpose of comparison with experiment it is desirable to include in the formulation as many measurable quantities as possible. Accordingly we may eliminate the device area from equation (29) by introducing the low-field resistance, R_0, of the GaAs layer defined by

$$R_0 = \frac{\rho_0 l}{A_0} = \frac{l}{ne\mu_1 A_0} \qquad \ldots\ldots(30)$$

By using (30) we can express the ratio of f.m. noise to current noise in terms of the low-field resistance, carrier concentration and length of the device, together with the loaded Q-factor and circuit loss of the microwave circuit. The result is

$$\frac{\Delta f_{\text{r.m.s.}}}{\Delta i_{\text{r.m.s.}}} = \frac{4 \cdot 55 \times 10^{-9}}{Q_L R_L} \left(\frac{n_0}{l^3}\right)^{\frac{1}{2}} R_0^2 \qquad \ldots\ldots(31)$$

7. Experimental Results

A large number of Gunn diodes were available for the measurement of frequency-modulation noise and current noise. The devices were prepared from three different slices of epitaxial GaAs and each had the following nominal characteristics for X-band operation:

length of active layer, l . . . $10\ \mu m$
resistivity, ρ_0 . . . . $0 \cdot 01\ \Omega m$
contact diameter . . . . $100\ \mu m$

The low field resistance R_0 is about $13\ \Omega$ for these dimensions.

The diodes were mounted in a waveguide 16 cavity of the type described by Court et al.[9] and oscillations were obtained at a frequency of 9·5 GHz with the short-circuit plunger approximately one half-wavelength behind the diode. In all cases maximum power output occurred in the bias voltage range $9\ V \pm 1\ V$.

From reference 9 we have the following value for the rate of change of mount reactance with frequency.

$$\omega_0 \left[\frac{dX_0}{d\omega}\right] = 2Q_L R_L \simeq 2\pi Z_0 \qquad \ldots\ldots(32)$$

where Z_0 is the characteristic impedance of the waveguide. Scanlan and Kodali[10] have shown that for this type of mount it is appropriate to define Z_0 on a power/voltage basis.

F.m. noise was measured using a wideband microwave discriminator operating on the interferometer principle, and current noise was measured by means of a monitor resistor included in series with the Gunn diode.

The noise voltages so produced had the characteristics of $1/f$ noise and it was therefore quite impracticable to measure the total r.m.s. value as assumed in previous Sections. To overcome this difficulty the noise voltages were filtered using a narrow-band tracking filter tuned to 1 kHz and the filter output was then taken to a wide-band analogue multiplier connected as a true mean-square indicator. The filter had a bandwidth of 50 Hz with a fourth-order band-pass response to reduce the effect of large low-rate deviations and a good long-term average of the filter output was obtained without difficulty.

7.1 F.M. Noise/Current Noise Ratio

The ratio $\Delta f_{\text{r.m.s.}}/\Delta i_{\text{r.m.s.}}$ was measured for each diode together with the low-field resistance R_0. A plot of the measured ratio versus R_0 is shown on log–log scales in Fig. 3. The error bars represent an estimated accuracy of $\pm 10\%$ from the combined noise measurements and the diodes corresponding to the three batches are identified by different symbols.

The solid lines in Fig. 3 are drawn from equation (31) with the value of $Q_L R_L$ given by (32), using device length as a parameter and assuming that the carrier concentration has a value of $10^{21}\ m^{-3}$ for all the diodes.

The agreement between the theoretical curves and the experimental data is very encouraging and it can be seen that the spread in experimental results might be explained by a variation in individual sample lengths of about $\pm 2\ \mu m$ from the nominal sample length of $10\ \mu m$. Examination of Fig. 3 shows that the devices from batches 1 and 2 exhibited a range of more than 2 to 1 in low-field resistance and that the majority of these are grouped about the theoretical line for a length of $8\ \mu m$. The batch 3 devices did not display such a large range of low-field resistance and so do not provide such a good test of equation (31); a rather longer sample length $(12\ \mu m)$ is indicated for this batch. Batch variations in carrier concentration will also contribute to the spread of the experimental results.
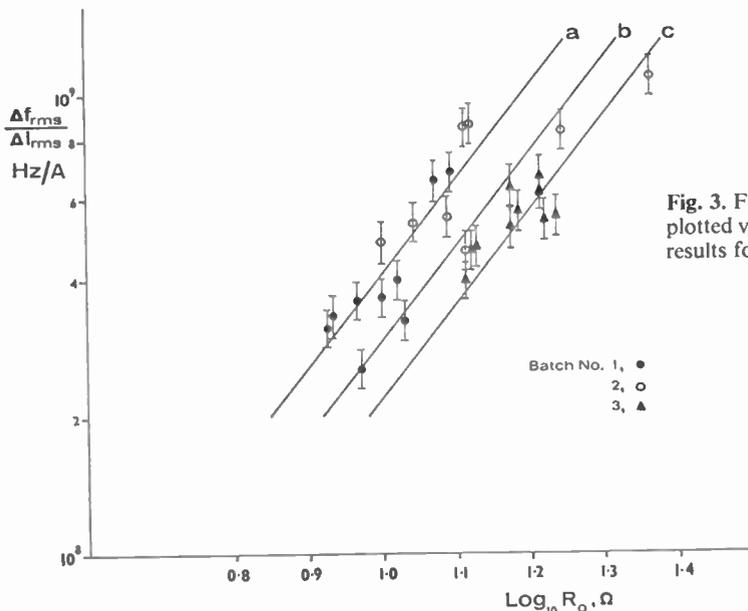

Fig. 3. F.m. noise/current noise ratio for diodes from three batches plotted versus low-field resistance. The solid lines are the theoretical results for different sample lengths.

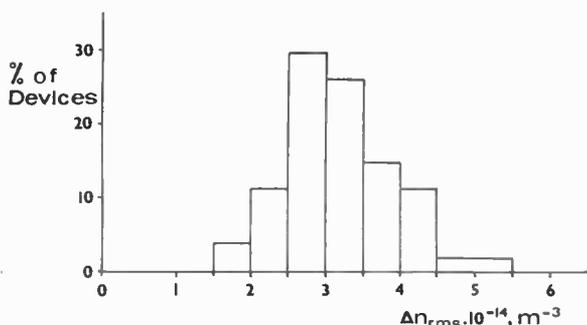(a) $l = 8\ \mu m$, (b) $l = 10\ \mu m$, (c) $l = 12\ \mu m$.

Fig. 4. Histogram of the measured values of $\Delta n_{r.m.s.}$ referred to 50 Hz bandwidth at 1 kHz.

A correction factor was originally calculated for each diode to allow for the slightly different bias voltage required in each case for maximum power output, but in the absence of precise information about the individual sample lengths the corrections cannot be applied with any confidence. On the basis of a length of 10 μm the average correction was found to be less than 5% and had no effect on the general trend of the results which have been plotted without modification.

7.2 Carrier Concentration Fluctuation

Equation (23) may be rewritten to express the r.m.s. carrier concentration fluctuation in terms of the r.m.s. current noise. Using (30) we obtain

$$\Delta n_{r.m.s.} = \frac{4 \cdot 55 \times 10^{13} R_0}{\rho_0 l} \Delta i_{r.m.s.} \qquad \ldots\ldots(33)$$

$\Delta n_{r.m.s.}$ has been calculated for each diode using the measured value of $\Delta i_{r.m.s.}$ together with $l = 8$, 10 or 12 μm crudely estimated for each device from Fig. 3. The results for about 30 devices are shown in histogram form in Fig. 4. It is seen that more than 50% of the devices have an r.m.s. fluctuation in the range

$$\Delta n_{r.m.s.} = (3 \pm 0 \cdot 5)10^{14} \text{ m}^{-3} \qquad \ldots\ldots(34)$$

measured in a 50 Hz bandwidth at a frequency of 1 kHz.

With a carrier concentration of 10^{21} m^{-3} the relative fluctuation, referred now to unit bandwidth at 1 kHz, is

$$\frac{\Delta n_{r.m.s.}}{n_0} \simeq 4 \cdot 5 \times 10^{-8} \text{ (Hz)}^{-\frac{1}{2}} \qquad \ldots\ldots(35)$$

Above threshold the current noise was found to be substantially independent of whether the Gunn diode was mounted in the microwave cavity or operating in a transit-time mode. The general behaviour of the noise above threshold was similar to that discussed in Section 4, but it was not possible to use very high bias voltages without exceeding the d.c. dissipation limit. Below threshold the current noise increased linearly with applied field which is consistent with $\Delta n(t)$ being independent of field; however the noise increased more rapidly as the applied field approached threshold. The above-threshold noise is generally much higher than the below-threshold noise measured at approximately the same average current which suggests that the non-thermal fluctuation mechanism is modified when the GaAs layer contains a high-field region. Similar observations have been reported by Matsuno.[6]

The values of carrier concentration fluctuation given here are for the GaAs layer biased above threshold and the non-ohmic behaviour of the specimen makes it very difficult to compare the relative fluctuation with published data from other sources. Hooge[11] has reviewed $1/f$-noise results from a large number of materials, selecting only those results which were not modified by field effects or specimen deformation, and has proposed that the fractional fluctuation in specimen conductivity obeys the following empirical law for all materials

$$\left(\frac{\Delta \sigma_{r.m.s}}{\sigma}\right)^2 = \frac{2 \times 10^3}{n_0} \frac{\Delta f}{f} \qquad \ldots\ldots(36)$$

where n_0 is the carrier concentration. Now for ohmic specimens in which the concentration fluctuation makes a much greater contribution to the measured noise than thermal (velocity) fluctuations we have,

$$\frac{\Delta \sigma_{r.m.s.}}{\sigma} = \frac{\Delta n_{r.m.s.}}{n_0} \qquad \ldots\ldots(37)$$

If we express our results in a form similar to (36) we obtain

$$\left(\frac{\Delta n_{r.m.s.}}{n_0}\right)^2 \simeq \frac{2 \times 10^9 \Delta f}{n_0} \frac{}{f} \qquad \ldots\ldots(38)$$

showing that the fractional fluctuation in the Gunn diodes is several orders of magnitude greater than the average value proposed by Hooge for ohmic specimens.

8. Conclusions

A theory based on the zero-diffusion model of a stable propagating domain has been developed to relate f.m. noise and current noise in a cavity-controlled Gunn effect oscillator. The observable fluctuations are assumed to have their origin in non-thermal fluctuations of the carrier concentration of the GaAs layer. The important results of the analysis are as follows:

(i) It is shown that for moderate bias voltages ($\simeq 3F_T l$) fluctuations of the field within the GaAs layer make a relatively small contribution to the measured noise processes.

(ii) An expression for the f.m. noise/current noise ratio has been obtained in terms of the oscillator design parameters.

Experimental evidence from a large batch of Gunn diodes has been produced in support of the theoretical study and an estimate has been made of the carrier concentration fluctuation.

9. Acknowledgments

10. References

1. Hobson, G. S., 'Source of f.m. noise in cavity-controlled Gunn-effect oscillators', *Electronics Letters*, **3**, No. 2, pp. 63–4, February 1967.

2. Faulkner, E. A. and Meade, M. L., 'Flicker-noise in Gunn diodes', *ibid*, **4**, No. 11, pp. 226–7, 31st May 1968.

3. Meade, M. L., 'Investigation of current-noise and frequency modulation noise in Gunn oscillators', I.P.P.S. Conference on Physical Aspects of Noise in Electrical Devices, Nottingham University, 1968, pp. 314–8.

4. Butcher, P. N., Fawcett, W. and Hilsum, C., 'A simple analysis of stable domain propagation in the Gunn effect', *Brit. J. Appl. Phys.*, **17**, No. 7, pp. 841–50, July 1966.

5. Hobson, G. S., 'The equivalent circuit of a Gunn effect device', 6th International Conference on Microwave and Optical Generation and Amplification, Cambridge, England, September 1966.

6. Matsuno, K., 'F.m. noise in a Gunn effect oscillator', *I.E.E.E. Trans. on Electron Devices*, **ED-16**, No. 12, pp. 1025–35, December 1969.

7. Warner, F. L., 'Extension of the Gunn-effect theory given by Robson and Mahrous', *Electronics Letters*, **2**, pp. 260–1, July 1966.

8. Carroll, J. E., 'Mechanisms in Gunn-effect microwave oscillators', *The Radio and Electronic Engineer*, **34**, No. 1, pp. 17–30, July 1967.

9. Court, W. P. N., Horman, P., Hilsum, C., Holliday, H. R. and Warner, F. L., 'Reduction of frequency-modulation noise from Gunn oscillators', *Electronics Letters*, **3**, No. 12, pp. 567–9, December 1967.

10. Scanlan, J. O. and Kodali, V. P., 'Characterisation of wave-guide-mounted tunnel diodes', *Proc. Instn Elect. Engrs*, **114**, No. 12, pp. 1844–9, December 1967.

11. Hooge, F. N., '1/f noise is no surface effect', *Physics Letters*, (*Netherlands*), **29A**, No. 3, pp. 139–40, 21st April 1969.

Avalanche Diodes as Transfer Noise Standards for Microwave Radiometers

By

N. J. KEEN,
B.Sc., C.Eng., F.I.E.R.E.†

Transfer calibrations of radiometers are performed by injecting noise via a directional coupler. The avalanche diode appears to have all of the physical attributes of the plasma noise tube, except for a reasonably predictable absolute noise level. Its saving in space, weight, cost and power consumption render it an attractive proposition for transfer noise calibrations. Results of measurements at three frequencies between 1 GHz and 3 GHz are given.

1. Introduction

In radio telescopes, the noise calibration at microwave frequencies has normally been provided by cold-cathode plasma noise sources.[1] The stability of these devices for very precise transfer standards has been called into question, and measurements at the Max-Planck-Institut für Radioastronomie have been performed to compare the stability of commercially available cold-cathode plasma noise tubes with that of avalanche noise diodes. The laboratory performance of the avalanche devices has been sufficiently encouraging to permit them to be used as transfer calibration sources on the 25-metre radio telescope at Stockert, some 30 miles west of Bonn. Furthermore, due to the satisfactory performance under operational conditions, it is proposed to utilize avalanche sources on the Institute's new 100-metre radio telescope at Effelsberg, some 30 miles south-west of Bonn. Hot-cathode plasma noise tubes, despite good reported long-term stability,[3] have been rejected for reasons of cost, size, weight, power dissipation and relatively low excess noise ratio (e.n.r.).

2. Device Requirements

Up to the present, the only commercially available semiconductor noise source operating up to X-band is the avalanche diode. Although at least four firms now manufacture these devices, references to avalanche diode noise sources in the literature are extremely sparse. Point-contact diodes were used as microwave noise generators some 25 years ago, but with only limited success and low noise level.[3] Measurements on avalanche noise sources were reported by Haitz and Voltmer,[4] who also considered the physical conditions for noise generation, but do not consider certain characteristics of

fundamental importance to radio astronomical systems. The three major requirements are:

1. e.n.r. > 15 dB, so that a 20 dB directional coupler would give > 100°K noise calibration;
2. long-term stability and reliability;
3. relatively flat spectrum, with no significant 'fine structure'.

The e.n.r. presents no problem; avalanche noise sources can provide 30 dB of e.n.r. up to X-band. The stability and reliability of the semiconductor sources has been studied continuously over a period of 15 months: the results are reviewed in the next section. The spectrum of the avalanche sources is considered subsequently. For purposes of comparison, results on reputable commercially available cold-cathode plasma tubes are included. All measurements were made with the noise sources running continuously, the mode of operation producing the best repeatability.

3. Stability and Reliability

Two test-methods were employed. The first was the 'total power' method, where the energy output was measured directly with a quadratic detector: the measuring system is shown in Fig. 1, the purpose of the two switches being to compare the avalanche source noise with plasma tube noise and with noise from the mixer-preamplifier alone. The second method uses the Dicke-switched system, where the difference between two signals is continuously measured: this method is particularly suited to measurements where heated and cooled terminations provide noise levels well below that of the receiver.

Tests were performed on several cold-cathode noise tubes at frequencies from 1·4 to 2·7 GHz. Inferior tubes
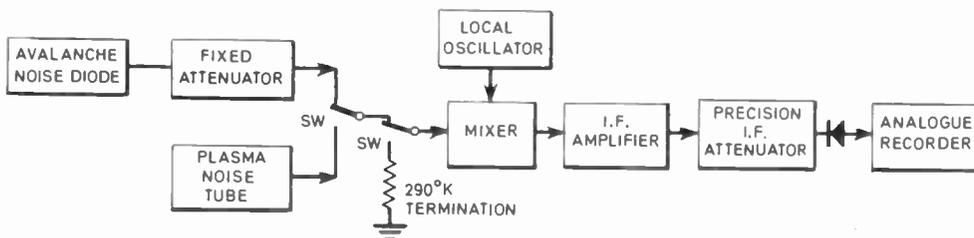

Fig. 1. System for total power noise measurements. SW is a coaxial switch (Hewlett Packard type 8761A).

† Max-Planck-Institut für Radioastronomie, Argelanderstrasse 3, 53, Bonn, Germany.
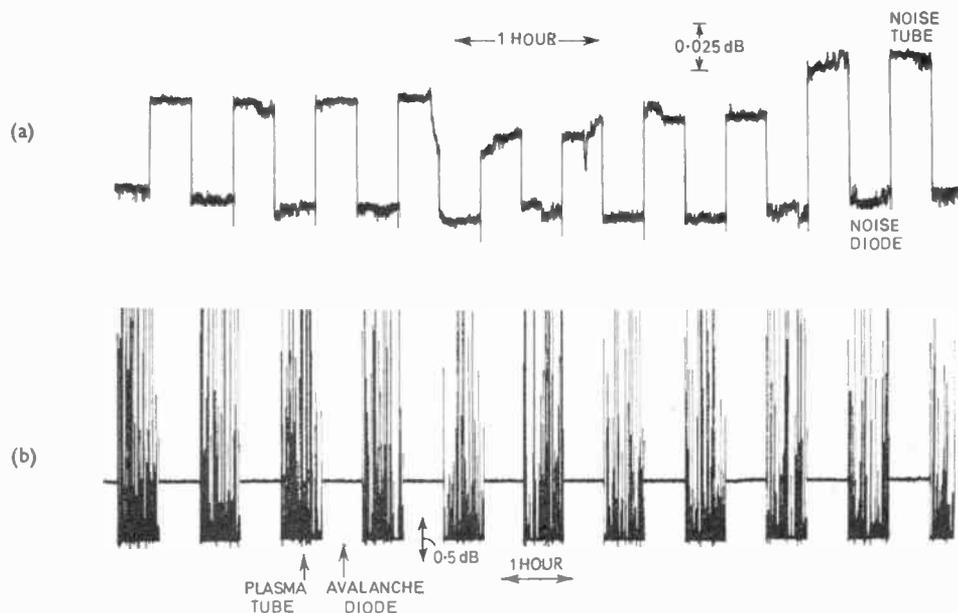
Fig. 2. Comparison of plasma and avalanche noise sources:
(a) Nore diode and best plasma tube; (b) Nore diode and worst
plasma tube. Source noise approximately 10 dB above mixer-
preamplifier noise.

Table 1. Stability tests

Test applied	Worst plasma tubes	Best plasma tubes	Solitron avalanche diode (Model RFN/25-4, S.N. 101)	Nore avalanche diode (Model NS 23NO2, S.N. 19)
Long term instabilities over >3 months: total power measurements with d.s.b. mixer	Several dB peaks, otherwise approximately as best plasma tube $f_{LO} = 1635$ MHz 2665 MHz	Jumps of up to 0·05 dB during otherwise stable operation; apparent 0·1 dB gradual drop in level over measuring period. The jumps and long-term drift are *not* usually associated with current changes $f_{LO} = 1390$ MHz 1635 MHz 2665 MHz	Level remained within a 0·05 dB range during each week of measuring (3 month stability not measured) $f_{LO} = 1635$ MHz 2665 MHz	Level remained within a 0·04 dB range during 3 periods of approximately one month $f_{LO} = 2665$ MHz
Long term instabilities over >3 months: switched measurements with s.s.b. parametric amplifier system at 1·4 GHz	—	Measurements on the 25 m radio telescope. Day-to-day variations of noise source output are in both cases masked by the non-statistical variations of the troposphere and the receiver system (total range of variations 0·06 dB). Calibrated against extra-galactic sources		$<0·05$ dB: Measurements in laboratory with 373°K and 80°K terminations are limited by 3 degK cycling of the hot termination
Behaviour after switch-on	15 minutes to drop $>0·5$ dB to a stable level		<5 seconds settling time	Settling time <1 s. One 0·7 dB jump shortly after turning on for the first time
Excess noise ratio (e.n.r.)	15 dB	15 dB	>28 dB at all frequencies below 3 GHz	>23 dB at all frequencies below 3 GHz
Effects of temperature	Not measurable during periods when tube current remained stable		Device case-temperature variations from 22°C to 35°C never brought the noise output outside the stability range for total power measurements	
Current stability	Variations of >5 mA occur several times per day (noise output varies approximately 0·01 dB per mA change). The associated noise variations are apart from those previously mentioned, which are *not* associated with current changes		No detectable variations over the total period	

with commercial power supplies have shown noise 'spikes' of many dB, which are invariably accompanied by jumps in tube current. Figure 2 shows records of noise tube outputs, alternated with avalanche noise diode outputs; the noise tube on the first record is the best of those tested, whilst that on the second record is the worst. It is noteworthy that the nature of the commercial power supplies is such that the higher supply voltage requirements of aged tubes results in inferior current stabilization: the best tubes were invariably those with the least hours of operation. Fortuitously the best plasma tube had very stable current a few minutes after firing, despite a reduction in noise output during the first 15 minutes.

For tests on avalanche noise sources, two different devices were tested. Test results on plasma and avalanche sources are summarized in Table 1.

Since all 'total-power' measurements were performed with very stable mixer-preamplifiers, the Dicke-switched measurements were only of academic interest. However, the long-term performance on the 100 m antenna will yield much more precise switched measurements, due to the higher level noise calibration required for sources of only moderate flux density.
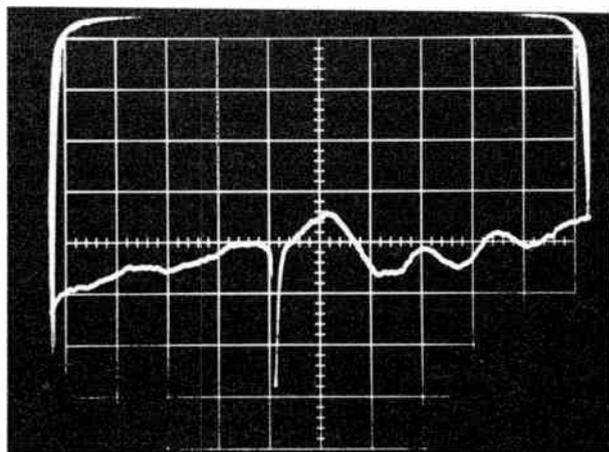
4. Spectrum

In an attempt to measure the spectral properties of the noise output, two types of measurement were performed on the Nore Electric diode in the region of 2·7 GHz:

(1) Direct spectral measurements were performed using a swept local oscillator frequency, and a selective voltmeter at intermediate frequency.

(2) The statistical fluctuations were observed with various post-detection time constants (τ), to determine that the noise fluctuation amplitude varied with $\tau^{-1/2}$.

Figure 3(a) shows the noise spectrum of the plasma tube and low-noise mixer-preamplifier (9·98 dB above mixer-preamp. alone), Fig. 3(b) shows the spectrum of the avalanche source and mixer-preamplifier when avalanche source current is 4 mA (13·2 dB above mixer-preamp. alone), and Fig. 3(c) shows the spectrum of avalanche source and mixer-preamplifier when the avalanche source current is 10 mA (10·10 dB above mixer-preamp. alone). In Fig. 3(c) the spectrum is displaced 0·2 dB to evaluate spectral variations, and the fainter trace is the spectrum of the mixer-preamplifier alone. The contribution of the avalanche diode includes a noise reduction due to an additional 6 dB attenuator to improve matching and to bring the noise level nearer to that of the plasma tube.

The spectra in Fig. 3 correspond to a local oscillator frequency sweep from 2·5 GHz to 3·0 GHz with the marker at 2·7 GHz; the double sideband intermediate frequency bandwidth is about 2 MHz. The vertical scale is 0·25 dB per division. Using a selective voltmeter with a 5 kHz band-width, very slow sweeps were required to reduce the statistical noise fluctuations; superposing many of these slow sweeps revealed essentially identical spectra to those shown in Fig. 3.

(a)
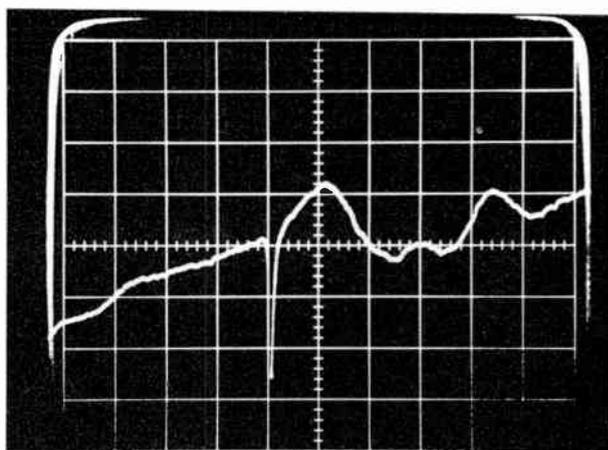
(b)
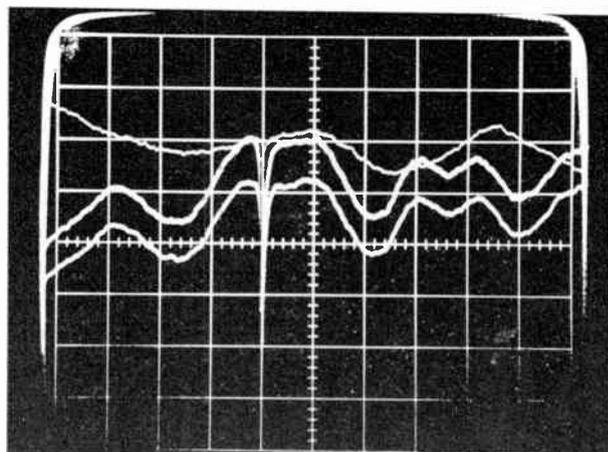
(c)

Fig. 3. Noise source spectra—2·5 to 3·0 GHz: (a) plasma tube (b) avalanche diode with $I = 4$ mA; (c) avalanche diode with $I = 10$ mA, and second spectrum displaced 0·2 dB from first. Vertical scales = 0·25 dB per division.

Theoretically, the r.m.s. fluctuation level of Gaussian noise should vary with $\tau^{-1/2}$ (provided $\Delta f . \tau \gg 1$). This was found to hold for values of τ from 10 s to 0·1 ms, insofar as a fixed relationship between r.m.s. and peak-to-peak noise is valid over this range. With a τ of 10 µs, the detected plasma tube noise appears to have peak amplitudes approximately 25% higher than those of avalanche sources with the same mean square noise intensity. However, quantitative conclusions are hard to draw without a statistical analysis of data recorded at $> 10\,000$ points per second.

5. Conclusions

Up to the present, the decision to dispense with plasma tubes for high-level noise transfer calibrations appears to be justifiable, although low-level absolute calibrations will still be obtained by switching between terminations at different temperatures. A more precise test of avalanche source stability will be possible when they are used on a radio telescope for beam-switching measurements or for spectral applications with frequency switching, since atmospheric contributions will cancel. For the present, the semiconductor noise source appears to be at least a practical alternative to cold cathode plasma tubes up to X-band.

6. Acknowledgments

7. References

1. Mumford, W. W., 'A broad band microwave noise source', *Bell Syst. Tech. J.*, **28**, pp. 608–18, October 1949.

2. Denson, C. I. and Halford, G. J., 'Plasma noise sources of improved accuracy', *I.E.E.E. Trans. on Microwave Theory and Techniques*, **MTT-16**, pp. 655–63, September 1968.

3. Montgomery, C. G., 'Technique of Microwave Measurements', pp. 270–281, Radiation Laboratory Series No. 11. (Boston Technical Publishers, 1964.)

4. Haitz, R. H. and Voltmer, F. W., 'Noise of a self-sustaining avalanche discharge in silicon: studies at microwave frequencies', *J. Appl. Phys.*, **39**, pp. 3379–84, June 1968.

Automatic Measurement of Insertion Test Signals

By

I. J. SHELLEY,
C.Eng., M.I.E.E., M.I.E.R.E.†

and

G. E. WILLIAMSON-NOBLE,
M.A.†

Reprinted from the Proceedings of the Conference on Television Measuring Techniques held in London from 12th to 14th May 1970.

This paper describes some of the problems and constraints associated with the measurement of insertion test signals and outlines various techniques which are either being used or under investigation for the automatic measurement of the various elements in the signals.

1. Introduction

During the past ten years the technique of inserting special test signals in the field-blanking interval of a television waveform has developed rapidly. Until 1967 a single line was used for simple test signals which provided an easy method of indicating on an oscilloscope whether, during programme transmission, the essential monochrome characteristics were satisfactory.

The introduction of colour television has imposed more stringent requirements on the performance of networks and transmitters, and automatic monitoring at strategic points in the transmission chain between the studio and the viewer is desirable. At certain points control devices, in the form of automatic correctors, have also been introduced.

For routine measurements the conventional line-repetitive test signals have been almost totally replaced by insertion test signals (i.t.s.), primarily because the latter allow measurements to be made during programme transmission. This is an important advantage as the time available for out-of-service testing is diminishing rapidly. To meet these requirements and in anticipation of the future automation of many elements in the broadcasting chain, a comprehensive insertion test signal for colour has been developed and full details of this are given in a companion paper.[1]

Concurrently with the development of the comprehensive i.t.s. major advances were being made in integrated circuit technology. Modern integrated circuit devices can now be assembled to perform sophisticated measurements to a high degree of accuracy. However, for the routine measurement of i.t.s. a somewhat lower standard of accuracy will usually be acceptable and, if measuring apparatus is to be placed at many points in the overall transmission chain, the major considerations determining its complexity are those of reliability and cost.

2. Measured Characteristics

Savage and Carter[1] list the following distortions and impairments as those which need to be measured for the routine assessment of transmission chain performance.

It should be noted that for the assessment of television transmitter performance additional measurements must

† British Broadcasting Corporation, Designs Department, London, W1A 1AA.

Distortion or impairment	Obtained from measurement of
Luminance gain	Peak-white bar amplitude
Luminance K-rating	(i) Tilt on peak-white bar top (excluding approximately the first and last 600 ns) (ii) 2T pulse amplitude (iii) Amplitude of lobes of 2T pulse
Chrominance–luminance gain inequality	Chrominance bar amplitude
Chrominance–luminance delay inequality	10T composite pulse: timing of the luminance component and the envelope-demodulated chrominance component
Luminance non-linearity	5-riser staircase: height of pulses obtained by differentiating and shaping staircase waveform
Differential gain	5-riser staircase with superimposed sub-carrier: amplitude of sub-carrier at black level and amplitude of sub-carrier on other treads of staircase
Differential phase	5-riser staircase with superimposed sub-carrier: phase of sub-carrier at black level and phase of sub-carrier on other treads of staircase
Chrominance–luminance crosstalk	Mean value of chrominance bar and amplitude of luminance pedestal
Signal/unweighted random noise ratio	Quasi-peak-noise on a single 'noise measuring' line in the field-blanking interval

be made to guard against non-linearity distortion of the synchronizing signal, the introduction of power-supply hum or the failure of black-level clamping. These measurements do not rely on i.t.s. and are not dealt with in this paper.

We can now consider how the measurements listed above can be obtained from the various elements in the insertion test signal as this will serve as a guide to the overall form and complexity of an automatic measuring system. It will be appreciated that several of the distortions may be measured in a variety of ways and the following represents the authors' choice based on previous experience with automatic measuring systems.

It should be noted that some of these measurements do not provide information directly in the manner required, e.g. the assessment of luminance non-linearity distortion involves a simple arithmetic calculation using the measured maximum and minimum pulse amplitudes. Techniques for performing arithmetic operations are

I. J. SHELLEY and G. E. WILLIAMSON-NOBLE

well known and therefore are not discussed in this paper.

3. Problems Associated with I.T.S. Measurements

The most fundamental problem associated with the measurement of i.t.s. arises from the fact that these signals only appear once in each field. 625-line television systems have a field-frequency of 50 Hz and the time between successive i.t.s. measurements, is, therefore, 20 ms. As most of the sampling periods are of a few microseconds or less duration conventional methods of measurement are not entirely satisfactory and new techniques are necessary.

When a picture signal, other than a test pattern or still picture, is transmitted over a network the distortion introduced will vary with time in a complicated manner dependent upon average picture level, the non-linear transfer characteristic and the long-term transient response of the network. Therefore the amount of integration which can be applied in the measurement process must be a compromise between the requirement for maintaining measurement accuracy under normal operational conditions (including periods when the signal/noise ratio is sub-standard) and the need to detect distortions which are dependent upon picture content. A 'time-constant' of about 2 s would appear to be the practical minimum but it should be noted that the normal concept of 'time-constant' is not particularly appropriate to the measuring techniques to be described later.

4. Line Selection

Because the test signals are confined to one or two lines in each field of the television waveform, the correct identification and selection of these lines is of considerable importance, particularly when measurements are required for automatic correction purposes. In general,

the operating time-constants used in correctors tend to be much shorter than those used in monitoring equipment and any errors in line selection can result in a serious misoperation of the corrector. The complexity of a line-selector will depend upon the degree of protection required from the various disturbances, such as an 'a.c. cut'† between picture sources or impulsive interference, which may occur occasionally on the signal waveform. The arrangement shown in Fig. 1 has been developed primarily for use in automatic correctors.

The incoming video waveform is filtered to remove chrominance information and high-frequency noise and, after amplification, mixed synchronizing pulses are obtained by means of a sync. separator incorporating a black-level clamp to improve operation under conditions of varying average picture level, etc. Breaks or impulsive interference in the input signal will cause a disturbance to the mixed sync. waveform from the separator and it is necessary to include suitable protection in order to obtain interference-free line and field trigger pulses.

Field pulses are derived from the mixed-sync. waveform by means of a conventional integrator circuit. These field pulses trigger a monostable with a quasi-stable period of 19·5 ms. At the end of this period, during which the monostable is insensitive to further input signals, it returns to its stable state and triggers a 1 ms gate-pulse generator. The signal from the field pulse generator and the 1 ms gate-pulse generator are applied to a coincidence gate, the output from which therefore consists of the required field trigger pulses free from extraneous interference. A similar protection circuit is used for the extraction of the line trigger information.

† An 'a.c. cut' is the term used for a switching operation between two picture sources which introduces a discontinuity in the blanking level potential.
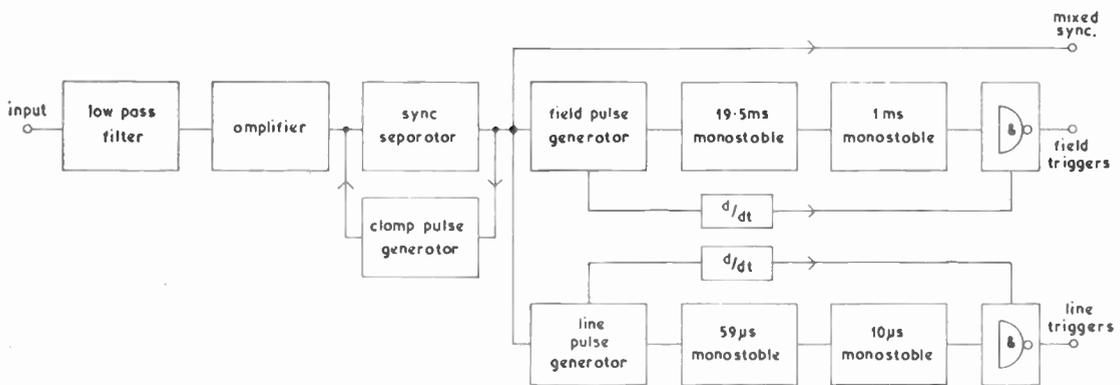

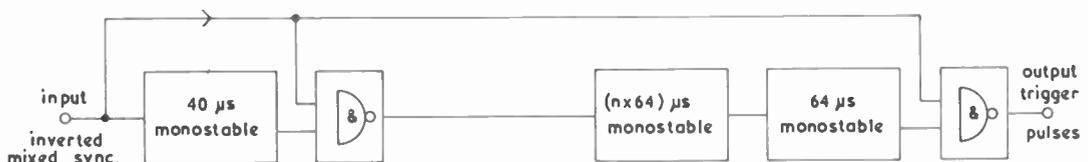Fig. 1. Line and field trigger pulse generators.

Fig. 2. Simplified line-selector.

Having derived line and field trigger pulses, the generation of gating pulses for the selection of the required lines is relatively straightforward. Where a large number of consecutive lines have to be identified, say four or more in each field, for insertion switching, data and test signal purposes, a shift register, started by a suitably delayed field trigger pulse and driven by line trigger pulses, may be used.

For applications where a less stringent performance specification is acceptable the simpler arrangement, shown in Fig. 2, will suffice. A 40 µs monostable and a logic gate are fed with inverted mixed syncs., whose trailing edges trigger the monostable. The output of the monostable is also applied to the gate whose output thus consists of pulses in the middle of lines, coincident with the equalizing pulses.

The first of these pulses, which is a constant time before the i.t.s. on all fields, is used to trigger a monostable delay circuit. The trailing edge of the output pulse is arranged to occur near the middle of the line before the first line to be selected and triggers a one-line monostable circuit which opens a gate and lets through the next synchronizing pulse, to act as a trigger for the required line. This trigger pulse can also be used to trigger a chain of similar circuits and produce pulses for other lines.

5. Waveform Gating

The composite video signal is first amplified by a straightforward 4× feedback pair: its blanking-level is then clamped accurately to zero volts by a shunt field-effect transistor (fed with clamping pulses from the synchronizing pulse separator). The clamped video signal is directly connected to a series of analogue gates, which dissect the i.t.s. into its component parts and direct them to the relevant detectors. Each of these gates consists of a series and a shunt field-effect transistor. The use of f.e.t.s for both clamping and gating avoids the effects of thermal drifts and offset voltages in these circuits, an important factor as the accuracy of amplitude measurement is directly dependent upon black-level stability. The pulses which drive the gates are derived from a chain of monostable circuits which is triggered by pulses from the line selector.

6. Measuring Techniques

The measuring techniques described in this Section have been devised as part of a development programme

aimed at the production of a fully automatic monitoring and control system for unattended operation. The most important consideration in the overall system design was the requirement that the measurements obtained should be capable of being compared directly with measurements made by conventional line-by-line methods or by direct observation of the i.t.s. waveform on an oscilloscope.

6.1 *Amplitude*

Several amplitude measuring techniques for i.t.s. have been investigated and although the circuits differ considerably from each other they have one factor in common; they all have to produce a continuous output voltage from an input signal whose duty ratio is very small but which is repetitive. The 2T pulse, for example, remains within 1% of its peak value for only about 25 ns. For this purpose any simple peak detector is inadequate. The arrangement finally preferred is a type of pumping slide-back voltmeter (Fig. 3).

The gated video signal, after suitable processing, is applied to one input of an integrated circuit comparator. The other input is a fed-back voltage derived from the final d.c. output. If the video input signal exceeds this voltage the comparator produces an output pulse. This is used to trigger a monostable circuit which provides a pulse of suitable duration to operate a diode-pump circuit whose output, after passing through a buffer amplifier, becomes the detector output. This process will cease as soon as the fed-back voltage exceeds the peak amplitude of the video input signal and it will then hover about this level.

The only places where errors can occur are in the input circuits of the comparator and in the feed-back resistors. These errors can be kept very small and an overall measurement accuracy of better than 1% is easily achieved. Further, by suitable choice of the pumping components, it can be arranged that the mean rate of rise of d.c. output voltage, when pumping, is equal to the rate of fall when not pumping. This enables the effect of noise in the input signal to be averaged out over many samples.

To measure bar amplitude the gated signal is applied, via a low-pass shaping network to remove overshoots, to an amplitude detector of the type described. For pulse amplitude measurement the gated pulse is applied directly to the detector. Chrominance amplitude is measured on the gated chrominance bar. The chrominance component is selected by an acceptor circuit and
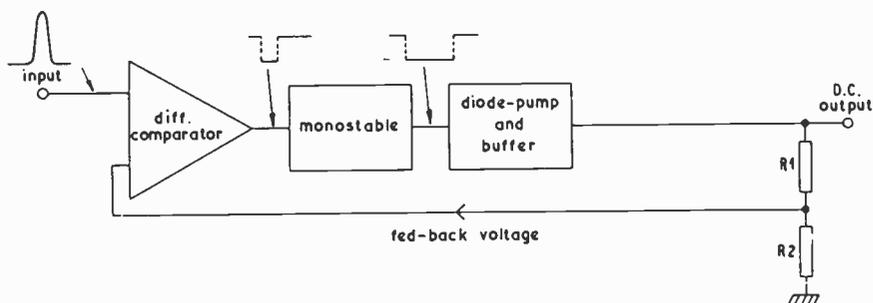

Fig. 3. Basic amplitude detector circuit.

applied to the detector which responds to the peak amplitude of the filtered subcarrier signal.

6.2 Bar and Pulse Waveform Distortion

Techniques for the measurement of bar and pulse waveform distortions are still being evaluated. High-speed waveform sampling coupled with computer analysis of the ordinates so obtained could be used but this method is considered to be too elaborate and costly for routine applications and an analysis of distortions likely to occur in practice has suggested that a somewhat simpler approach may be satisfactory. The method now under evaluation would be restricted to a measurement of:

(a) the tilt on the peak-white bar top (excluding approximately the first and last 600 ns)

and

(b) the amplitude of the 2T pulse at approximately ± 250 ns relative to the occurrence of the peak of the pulse.

Tilt on the bar top is measured by sampling the amplitude of the waveform at two points, 8·5 μs apart and approximately 0·8 μs from the half-amplitude point of each edge of the bar. A pulse proportional to the

difference between the two sampled voltages is then produced and the polarity will depend upon whether the bar tilt is positive or negative. This polarity difference is overcome by using a delay line to produce a delayed and inverted replica of the difference pulse. The two pulses are then passed to an amplitude detector which responds only to the positive-going signal and produces an output voltage directly related to bar tilt.

Work on 2T pulse waveform distortion is still in the early experimental stage and no definite conclusions have yet been reached.

6.3 Chrominance-luminance Delay Inequality

If the luminance and chrominance components of the 10T pulse are separated in a splitting filter, the chrominance component can be demodulated and smoothed to produce a 10T sine squared pulse, similar to the luminance pulse (Fig. 4). The time difference between these two pulses, measured at the 50% amplitude point, is taken as a measure of the luminance–chrominance delay. (The delay of approximately 300 ns which occurs mainly in the low-pass filter following the chrominance demodulator enables measurements to be taken for both chrominance delay and chrominance advance.) Each pulse is passed to a pulse amplitude detector and a voltage
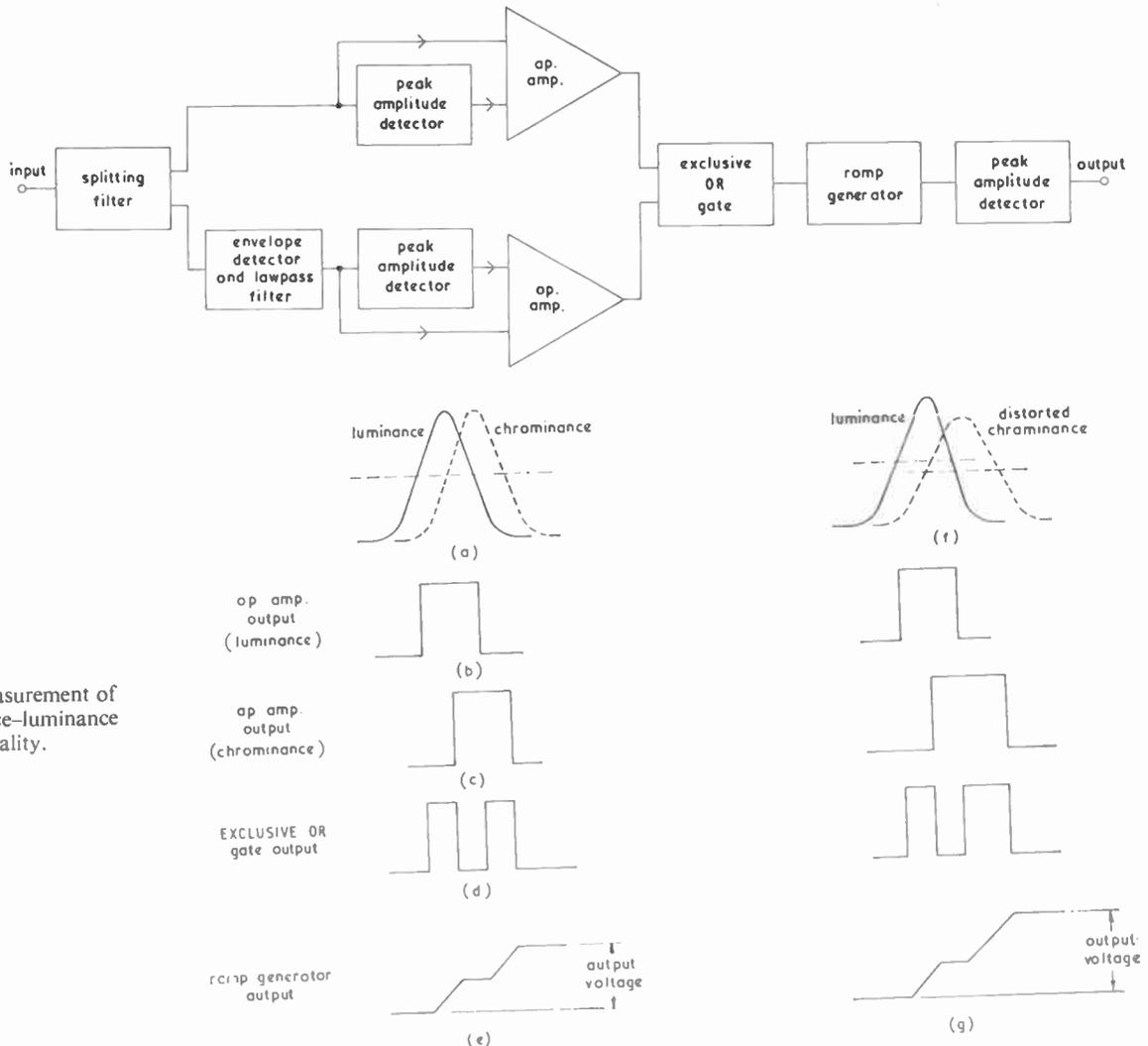

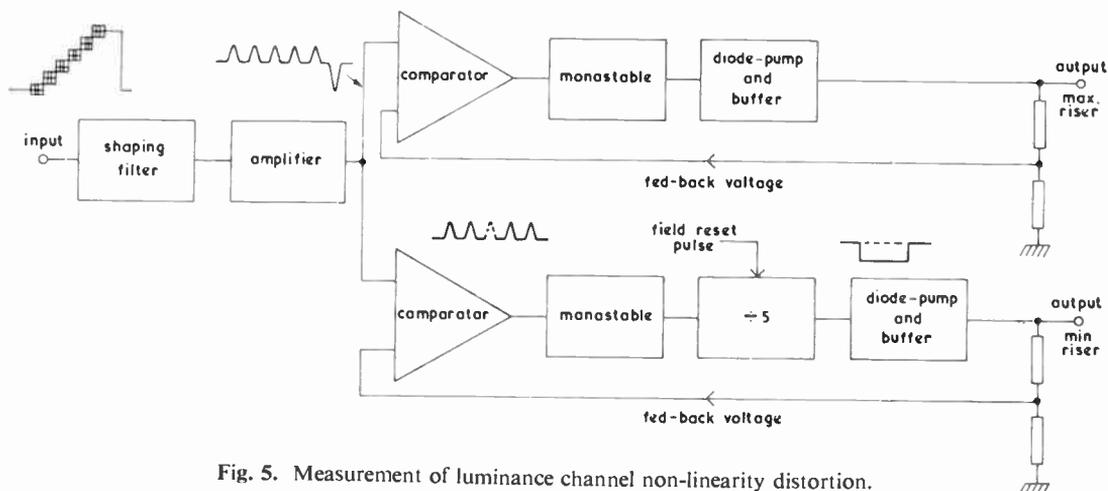Fig. 4. Measurement of chrominance–luminance delay inequality.

Fig. 5. Measurement of luminance channel non-linearity distortion.

which is 50% of the pulse height fed to the 'inverting' input of an operational amplifier (Fig. 4(a)). The pulses are also fed to the 'normal' inputs so that the outputs of the two operational amplifiers are square pulses whose leading and trailing edges are coincident with the half-amplitude points of leading and trailing edges of the luminance and demodulated chrominance pulses respectively (Fig. 4(b) and (c)). The two square pulses are fed to an exclusive OR gate and the output of this drives a ramp generator. The output from the OR gate consists of two pulses the first of which has a width equal to the timing difference between the leading edges, and the second, that between trailing edges (Fig. 4(d)). The ramp generator is designed to hold the first ramp voltage and add the second ramp to it, so that the output, which is the total ramp height (measured by a standard amplitude detector), is therefore proportional to the mean of the timing difference measured at the leading and trailing edges. This gives results which are in close agreement with those obtained by conventional measuring methods[2,3] even when the video signal has suffered a distortion such as band limiting, which can produce non-linear effects in the demodulated chrominance signal (Fig. 4(f)–(g)). Phase non-linearity over the chrominance band can also produce similar effects. With a signal/weighted-noise ratio of 52 dB or better, an accuracy of ± 5 ns is obtained.

6.4 Non-linearity Distortion, Luminance Channel

Non-linearity distortion in the luminance channel is measured by passing the gated staircase signal through a chrominance sub-carrier rejector and a band-pass filter to effect differentiation and shaping. The output consists of five pulses proportional in height to the heights of the risers of the staircase and these are applied to two separate detectors which measure the amplitude of the maximum- and minimum-height pulses (Fig. 5).

The maximum-height pulse detector is of the type already described. For minimum-height pulse detection a resettable counter and decoding gate are interposed between the monostable circuit and the pump. This combination only delivers a pump pulse if at least five pulses are delivered to it by the monostable circuit.

Pumping will therefore cease when the fed-back voltage exceeds the peak amplitude of the smallest of the input pulses and it will then hover about this level.

6.5 Non-linearity Distortion, Chrominance Channel

The measurement of non-linearity distortion in the chrominance channel requires more complex measuring apparatus.

6.5.1 Differential gain

The sub-carrier component of the staircase signal is selected by an acceptor and, after amplification, applied to two detectors which measure the maximum and minimum amplitude of the sub-carrier respectively. The maximum amplitude detector is of the type already described. In the minimum amplitude detector additional circuitry as shown in Fig. 6 is included between the comparator and the monostable-pump circuit.

The output of the comparator is fed to one input of the logic gate G1 and, via a 24 μs monostable circuit to the other input of G1. The output, after smoothing to reduce the amplitude of the sub-carrier, is passed via a 100 μs monostable circuit to one input of the gate G2. The other input is the inverted and differentiated output of the first monostable circuit. The output of G2 is applied to a monostable-pump whose output is fed back to the comparator.

To describe the method of operation of this detector consider an input in which the sub-carrier amplitude on one of the steps of the staircase is less than that on any of the others. Initially the sub-carrier amplitude will exceed the fed-back voltage for the whole duration of the staircase and the comparator will produce negative-going pulses during this time. The first of these will trigger the 24 μs monostable which will hold one side of G1 'high'. The other side will, however, be repeatedly driven 'low' by the sub-carrier pulses with the result that the smoothed output from G1 will remain high and the 100 μs monostable will not be triggered. Its output will remain 'high' and allow the inverted and differentiated pulses from the 24 μs monostable to pass through the gate G2 and pump up the output and fed-back voltages. After a time a state will be reached in which the minimum sub-carrier amplitude fails to exceed the
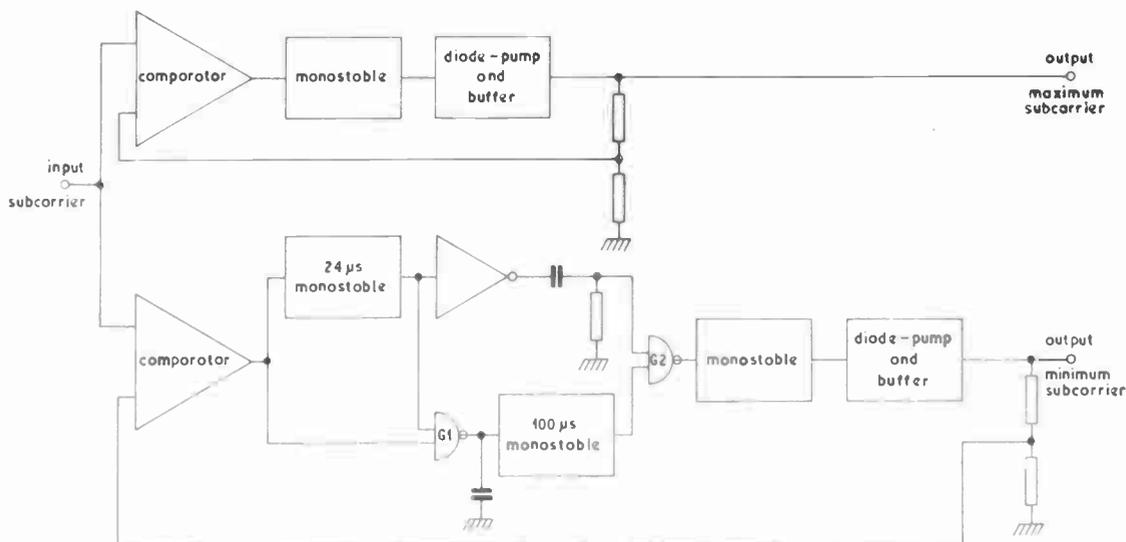
Fig. 6. Measurement of maximum and minimum sub-carrier amplitudes.

fed-back voltage. There will be a gap in the sub-carrier pulses from the comparator and the output of G1 will fall and trigger the 100 µs monostable. Its output will disable the gate G2 thus blocking the pulse from the 24 µs monostable and pumping will cease. The output will then hover about a level corresponding to the smallest sub-carrier amplitude.

To measure differential gain, as internationally defined, a further detector can be added to measure the sub-carrier amplitude at blanking level: its output is then fed to two difference amplifiers, together with each of the other two signals and the greater difference is the output required.

6.5.2 Differential phase

Several methods have been proposed for the automatic measurement of differential phase and all give results with a $\pm 2°$ accuracy which is sufficient for routine purposes.

All the systems utilize a phase-sensitive detector and they differ only in the way in which a reference sub-carrier is obtained. The simple arrangement using a conventional burst-locked oscillator is not particularly suitable for automatic operation and also suffers from the disadvantage that the sub-carrier bursts, transmitted during the line-blanking interval, are not an integral part of the test signal.

The sub-carrier reference can be transmitted as an extended burst on the line subsequent to the one containing the test signal and this is the function of the extended chrominance burst in the i.t.s. now in use in the U.K. As the test and reference signals are transmitted in a time-sequential manner a standard 64 µs delay line is used to restore the time-coincidence of the two signals, at the receiving end. The signals can then be applied to the phase-detector.

A further possibility, which does not require the use of a separate reference signal has been proposed and details of this are given in another Conference paper.[4]

6.6 Chrominance-luminance Crosstalk

The basic method used for measuring chrominance–luminance crosstalk is given in reference 1. For automatic measurement, the 14 µs chrominance bar section of the i.t.s. is passed through a low-pass filter to remove the chrominance and the difference in level between the mean value of the sub-carrier bar and the luminance pedestal can then be measured; a circuit similar to the one being developed for bar waveform distortion is being considered for this purpose.

6.7 Noise

To measure noise the signal on one of the 'quiet' lines in the field-blanking interval is gated into an amplifier whose output is fed to an amplitude detector similar to that already described. If, during the quiet line, a noise pulse occurs which is of greater amplitude than the fed-back signal from the pump it will cause the output to be pumped up until it reaches an equilibrium value. Because of the statistical nature of noise the output cannot reach the theoretically infinite peak value. It will instead settle around a voltage which bears a constant ratio to the r.m.s. value as long as the noise is random. The value of this constant may be less than the 18 dB normally used for the conversion of peak-to-peak to r.m.s. continuous random noise and further study of this subject is required. With the time-constant chosen the output fluctuations are of the order of $\pm 2\%$. The typical range of measurement extends from -55 to -28 dB (p p picture/r.m.s. unweighted noise) with an accuracy of ± 1 dB.

A fundamentally different approach to the problem of noise measurement is given by Barbieri and d'Amato.[5]

7. Experimental Results

Automatic monitoring equipment using some of the techniques described in this paper and equipped with a digital output display has been undergoing field-trial during the past few months. The results so far obtained tend to indicate that the accuracy of measurement is

considerably higher than can be achieved with conventional oscilloscope measurements and the speed which the measurements can be made is a considerable operational advantage.

An experimental alarm and control unit operating on the output signals from the monitor has given 'caution' or 'urgent' warnings when one or more of the measured distortions or impairments has exceeded preset limits.

8. Conclusions

The automatic measurement of insertion test signals is becoming an important factor in the automation of high quality broadcasting networks. Automatic devices can carry out continuous surveillance of the essential performance characteristics at strategic points in a transmission chain and can be used to initiate alarms, operate correctors and take executive action when significant deviations from normal are detected.

It is to be hoped that the measuring techniques described in this paper will serve as both a guide and a stimulus to the further rapid development of the use of i.t.s. for both national and international television transmissions.

9. Acknowledgments

The authors wish to thank the Director of Engineering of the BBC for permission to publish this paper. They are also indebted to Mr. M. G. Nutt for his work on the measurement of waveform distortion and delay inequality and to other colleagues in the BBC Designs Department who have given advice and assistance.

10. References

1. Savage, D. C. and Carter, D. A., 'Application of insertion test signal techniques to television chain operations,' *The Radio and Electronic Engineer*, 41, No. 4, April 1971 (To be published) I.E.R.E. Joint Conference on Television Measuring Techniques, May 1970. (I.E.R.E. Conference Proceedings No. 18).

2. Weaver, L. E., 'Sine-squared Pulse-and-bar Testing in Colour Television'. BBC Monograph No. 58, August 1965.

3. Coles, D. A., 'A set for annulling gain and delay inequality'. I.E.R.E. Joint Conference on Television Measuring Techniques, May 1970. (I.E.R.E. Conference Proceedings No. 18.)

4. Voigt, K., 'A new method for measuring differential phase distortions with test line signals and without transmitting a reference signal ', *ibid.*

5. D'Amato, P. and Barbieri, G., 'Signal-to-noise ratio automatic measurement in the blanking interval of the video signal', *ibid.*

STANDARD FREQUENCY TRANSMISSIONS—February 1971

(Communication from the National Physical Laboratory)

Feb. 1971	Deviation from nominal frequency in parts in 10¹⁰ (24-hour mean centred on 0300 UT)			Relative phase readings in microseconds N.P.L.—Station (Readings at 1500 UT)		Feb. 1971	Deviation from nominal frequency in parts in 10¹⁰ (24-hour mean centred on 0300 UT)			Relative phase readings in microseconds N.P.L.—Station (Readings at 1500 UT)	
	GBR 16 kHz	MSF 60 kHz	Droitwich 200 kHz	*GBR 16 kHz	†MSF 60kHz		GBR 16 kHz	MSF 60 kHz	Droitwich 200 kHz	*GBR 16 kHz	†MSF 60 kHz
1	− 300·1	− 0·1	+ 0·1	668	662·4	15	− 299·7	+ 0·1	− 0·1	661	660·0
2	− 300·0	0	+ 0·1	668	662·6	16	− 299·9	0	− 0·1	660	660·8
3	− 300·0	0	+ 0·1	668	662·9	17	− 299·9	+ 0·1	0	659	659·6
4	− 299·8	0	+ 0·1	666	662·9	18	− 299·9	+ 0·1	0	658	658·0
5	− 300·1	+ 0·1	+ 0·1	667	662·3	19	− 300·0	+ 0·1	0	658	657·2
6	− 300·2	+ 0·1	+ 0·2	669	661·8	20	− 300·1	+ 0·1	0	659	656·5
7	− 299·8	0	+ 0·2	667	661·7	21	− 300·0	+ 0·1	0	659	655·7
8	− 299·9	0	+ 0·1	666	661·3	22	− 299·8	+ 0·1	+ 0·1	657	655·2
9	− 300·3	0	+ 0·1	669	661·3	23	− 299·8	+ 0·1	+ 0·1	655	654·2
10	− 299·7	0	+ 0·1	666	661·5	24	− 299·9	+ 0·1	+ 0·1	654	652·8
11	− 300·1	0	+ 0·1	667	661·9	25	− 299·8	+ 0·2	+ 0·1	652	651·1
12	− 299·8	+ 0·1	+ 0·1	665	660·5	26	− 299·9	+ 0·1	+ 0·1	651	650·3
13	− 299·7	+ 0·1	+ 0·1	662	659·3	27	− 299·8	+ 0·1	+ 0·1	649	649·3
14	− 300·2	+ 0·2	0	664	657·7	28	− 299·9	+ 0·1	+ 0·1	648	648·1

All measurements in terms of H.P. Caesium Standard No. 334, which agrees with the N.P.L. Caesium Standard to 1 part in 10¹¹.

* Relative to UTC Scale; (UTC$_{NPL}$ — Station) = + 500 at 1500 UT 31st December 1968.

† Relative to AT Scale; (AT$_{NPL}$ — Station) = + 468·6 at 1500 UT 31st December 1968.

Contributors
to this issue

Mr. I. J. Shelley (M. 1959; A. 1946; S. 1943) is Head of Monitoring and Control in the Engineering Designs Department of the B.B.C. After obtaining his early training and experience with the Post Office he joined the B.B.C. in 1946. During the past 25 years he has been concerned with theoretical and practical studies covering many aspects of television and sound transmission. In 1959 he was a member of the team which developed 'Cable Film' and in 1964–65 he visited the Soviet Union to assist with comparative tests on various colour television systems.

Mr. Shelley is Chairman of the E.B.U. Working Party dealing with the Eurovision Satellite Project, and is a member of C.C.I.R. Study Group 4 (Space Communication Systems) and the C.C.I.R./C.C.I.T.T. Joint Study Group for Television Transmissions (C.M.T.T.).

Dr. V. J. Phillips graduated with first class honours in electrical engineering in 1955 from Imperial College, London. Following a period of research work at the College, he was awarded the degree of Ph.D. in 1959. From 1958 to 1960 he worked at the G.E.C. Research Laboratories (now Hirst Research Centre) at Wembley, Middlesex, and he took up his present lecturing post at the University College of Swansea in 1960.

Mr. M. H. Lee commenced his technical education as an engineering apprentice with British Rail. After obtaining the Ordinary National Certificate, he won a Technical State Scholarship and graduated with first class honours in electrical engineering at the University College of Swansea in 1967; he was awarded the Isaacs prize for the best undergraduate thesis in that year. After carrying out research leading to the degree M.Sc., he obtained his present post as lecturer in computing science in the School of Mathematics, Computing and Statistics, City of Leicester Polytechnic in 1969.

Mr. J. E. Thomas studied electrical engineering at the University College of Swansea, graduating with honours in 1970. He is at present working for G.E.C. (Telecommunications) Ltd. at Coventry.

Mr. M. L. Meade is a research assistant in the J. J. Thomson Laboratory, University of Reading. A fuller note of Mr. Meade's career was printed in the August 1970 issue of The Radio and Electronic Engineer.

Mr. G. E. Williamson-Noble obtained a B.A. degree in natural sciences from New College Oxford in 1943. For the next three years he was with the transmitters section of the development department at the Marconi Wireless Telegraph Co. and from 1946 to 1947 he worked on v.h.f. television link test equipment at the G.E.C. Research Laboratories. During 1948 Mr. Williamson-Noble formed Isis Records and was its technical director until 1952. For the next three years he was in charge of the radar test equipment laboratory at the Decca Radar Research Laboratory. Since 1955 he has been in the designs department of the British Broadcasting Corporation, being concerned with sound recording, television studio equipment and automation and control.

Mr. N. J. Keen (Fellow 1970) spent four years at the Services Electronic Research Laboratory, Baldock, and from 1952 to 1954 was an air radar mechanic in the R.A.F. In 1957 he obtained a B.Sc. degree in physics at the University of Nottingham. For the next two years he worked in the steel industry and in 1959 took up an appointment as assistant lecturer at Paddington Technical College. In 1960 he joined the staff of the Twickenham College of Technology as a lecturer and two years later went to the National Radio Astronomy Observatory, Green Bank, U.S.A., where he designed and coordinated the phase-coherent interferometer, and made the first radio-astronomical observations. In 1966 he joined the space group of the Observatoire de Paris, France, designing receiver systems for rocket- and satellite-borne radio astronomy. Since March 1968 he has been with the Max-Planck-Institut für Radioastronomie, Bonn, and in December 1968 he was appointed leader of the receiver systems group.